Print ISSN 2436-1550
Online ISSN 2436-2034

Okhotsk Sea and Polar Oceans Research

Volume 5 (2021)

Okhotsk Sea and Polar Oceans Research Association

Mombetsu City, Hokkaido, Japan

Vol. 5

General Information for OSPOR

(July 2020)
for OSPOR Vol. 5 (2021)

1. Aims and Scope

Okhotsk Sea and Polar Oceans Research (OSPOR) is published by the Okhotsk Sea and Polar Oceans Research Association (OSPORA).

Since 1986 the Okhotsk Sea and Cold Ocean Research Association (OSCORA) has held the International Symposium at Mombetsu, Hokkaido, in Japan every February and has released its proceedings over 30 years. In 2017 OSCORA changed to OSPORA, because the Symposium scope was broadened to include the polar oceans (the Arctic and Antarctic Oceans), the Arctic passages, global warming, and environmental change in Polar Regions.

OSPORA started a reviewed papers system from the 2017 Symposium. The papers are refereed by multiple reviewers, published in the proceedings of the Symposium with a title of “Article”, and opened on the OSPOR web site.

2. Subjects covered by OSPOR

1) Environment of Okhotsk Sea
2) Meteorology and oceanography in polar regions
3) Cold region engineering
4) Arctic sea routes
5) Global warming and environment change
6) Remote sensing
7) Snow, ice and human life
8) Other topics about Okhotsk Sea and Polar Oceans

3. Editorial Policy of OSPOR*

We intend to publish three types of papers;

1) **Article**, containing original scientific materials and results, not submitted for publication elsewhere,
2) **Review**, containing an overview of previous activities, projects and workshops with an outlook of a specific category.

Each of them will be peer-reviewed.

4. Editorial Board

5. OSPOR website*

Temporal website: http://okhotsk-mombetsu.jp/okhsympo/top-index.html
E-mail: momsys(at)okhotsk-mombetsu.jp

Okhotsk Sea and Polar Oceans Research (OSPOR)

Contents

Volume 5 (2021)

Okhotsk Sea and Polar Oceans Research 5 (2021) 1-6

https://doi.org/10.57287/ospor.5.1

Review

Arctic warming amplification and warming suppression in East Antarctica - Contribution of MOC to north-south asymmetry -

Takashi YAMANOUCHI [1, 2]

[1] *National Institute of Polar Research, Japan*
[2] *SOKENDAI (The Graduate University for Advanced Study), Japan*

(Received October 3, 2020; Revised manuscript accepted November 20, 2020)

Abstract

Warming amplification in the Arctic and warming suppression in the Antarctic are seen. What makes this great contrast under global warming? Several mechanisms to make this contrast have already been discussed; however, one of the most effective is ocean circulation, called meridional overturning circulation (MOC). Here, we will review the progress of studies in the recent decade of how MOC contributes to the large North-South asymmetry in warming.

Key words: Arctic amplification, Antarctic, warming suppression, asymmetry, meridional overturning circulation

1. Introduction

Under global warming, extreme warming occurs in the Arctic, more than twice the global average since 1970, and we call this increase as "Arctic amplification." Also, strong warming is seen in the Antarctic Peninsula, comparable to the Arctic. However, the surface air temperatures in East Antarctica show no clear warming trends, and we call this "warming suppression." This great contrast in the surface air temperature (SAT) trends between the Arctic and East Antarctica, even in the polar regions, is of great concern and the target of the present review.

Many ideas – theories – are introduced in the recent to explain this contrast or extreme phenomena in the one side of the polar region. The famous hypothesis in atmospheric science is the warming suppression by the ozone hole proposed by Thompson and Solomon (2002). Since the ozone hole seems to recover within a few decades (~ 2060), this hypothesis would be verified. Another idea is the difference in the surface topography between the Arctic and Antarctica. The high surface topography of the Antarctic ice sheet prevents the intrusion of air from the lower latitude. In comparison, the Arctic ocean's sea level allows the intrusion of warm-moist air from the lower latitude, which contributes to warm the Arctic (Yamanouchi, 2019). Also, the Antarctic ice sheet's high surface elevation makes the surface temperature much colder than the Arctic surface. It makes the outgoing longwave radiation (OLR) smaller in the Antarctic compared to the Arctic (Salzmann, 2017).

Another mechanism that derives the different warming trends is the difference in the area where the ice albedo feedback is effective (Goose and others., 2018). In the Arctic, ice albedo feedback works in most areas over the sea ice in the Arctic Ocean or over the land area where snow covers the surface in vast latitude regions. On the other hand, in the Antarctic, the area where ice albedo feedback is effective is limited to the sea ice area, which is restricted to 55 to 70° south, and not over the Antarctic ice sheet, where the surface snow cover could not change in the short time scale.

In addition to the many components responsible for the asymmetry of warming as introduced above, ocean circulation is another strong agent to make this asymmetry. It was found in the recent that meridional overturning circulation (MOC) is the most significant source to make the warming difference in both polar regions (e.g., Chylek and others., 2010; Marshall and others., 2014). Here, we will introduce and review these recent findings of MOC to contribute to the asymmetry of warming in the Arctic and Antarctic. This mechanism is in the analogy with the millennial seesaw of temperature found in the paleo ice core records (e.g., Blunier and others., 1998; EPICA community members, 2006), but with a rather short time scale.

2. Twenty century bipolar seesaw of the Arctic and Antarctic surface air temperatures

Cheylek and others. (2010) identified bipolar seesaw patterns in the 20th century the Arctic and Antarctic temperature records for the first time. It is a great surprise that the detrended annual averaged temperatures from meteorological stations north from 64°N and south of 64°S are anti-correlated, as seen in Fig. 1. We could also find a typical "Early 20th century warming pattern" in the Arctic temperature anomaly shown in Fig. 1 top (Yamanouchi, 2011). Cheylec and others. extracted a linear trend (which greenhouse gases

increase must be responsible for) and residual variability (with an 11 year or a 17 year running average), as shown in Fig. 2a. It was found that the residual detrended series were highly anti-correlated, just as the seesaw pattern. The correlation coefficients were r = -0.76 for the 11 year averages and r = -0.89 for the 17 year average. The higher trend of temperature increase in the Antarctic (~2 °C/century) compared to the Arctic (~ 1°C/century) in these hundred years was one point difficult to understand.

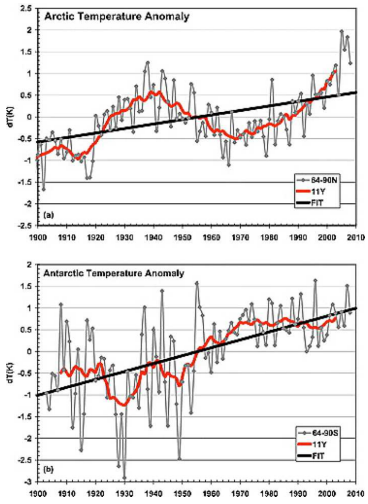

Fig. 1 Temperature anomaly with respect to the 1903-2008 average, its 11 year running mean (red line) and the least square linear fit (thick black line) for the (a) Arctic and (b) Antarctic region. Temperature data used are from the NASA GISS compilation (Chylek and others., 2010).

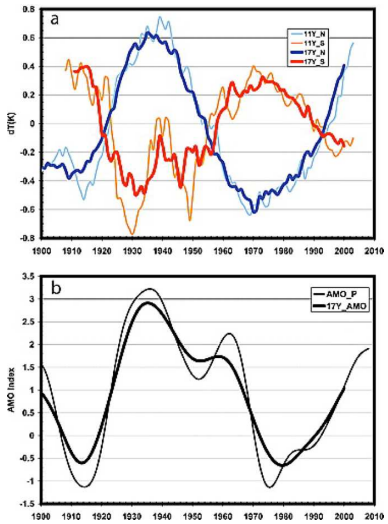

Fig. 2 (a) De-trended Arctic (blue) and Antarctic (red) temperature time series smoothed by a 11 year running average (thin lines) or 17 year running average (thick lines), and (b) the AMO index annual values (thin line) and 17 year running average (thick line) (Chylek and others., 2010).

Cheylec and others. (2010) imagined that the strong anti-correlation of the multidecadal temperature anomalies in the Arctic and Antarctic regions must be due to the ocean, and moreover, the Atlantic Ocean through the high correlation of the residual temperature time series with the Atlantic Multidecadal Oscillation (AMO) index. Knight and others. (2005) explained the AMO to be originated by the variability of the Atlantic Meridional Overturning Circulation (AMOC).

The AMOC is the large scale thermohaline circulation in the world ocean, driven mainly by temperature–salinity buoyancy forces, starts sinking in the North Atlantic, Greenland Sea, and pass through as a deep current through the Southern Ocean (SO) and upwelling in the Pacific. Knight and others., from a 1400 year control run of the coupled climate model, showed that the AMO was strongly related to the variations in the overturning circulation on a near century time scale. Here, a schematic diagram of the overturning circulation called the "Great Ocean Conveyor Belt," published by Wallace Broeker (1987), are shown in Fig. 3, as a popular image that explains the inter-connected ocean circulation and the northward flux of heat in the Atlantic (Richardson, 2008). The AMO index analyzed by Parker and others. (2007) was shown in Fig. 2b. The correlation coefficient with the Arctic temperatures (Fig. 2a) was r = 0.71 for the 11-year AMO index average (r = 0.72 for the 17-year average), while the corresponding anti-correlations with the Antarctic temperature were r = -0.69 (r = -0.80 for the 17-year).

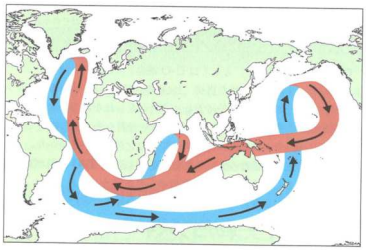

Fig. 3 The great ocean conveyor belt logo shown by Broeker (1987) as illustrated by Joe Le Monier, Natural History Magazine.

3. Asymmetric Arctic and Antarctic responses to greenhouse gas and ozone forcing

We are greatly surprised at the similarity of the sea surface temperature (SST) anomalies distribution by ocean-only model and coupled climate model (15 CMIP5 models) 100 years after an abrupt quadrupling of CO_2 demonstrated by Marshall and others. (2014) in Fig. 4. In both experiments, distinct asymmetries with SSTs in both hemispheres or polar regions were clearly seen. So, the temperature perturbations must be attributable to ocean circulation. It was so striking that this similarity in spatial patterns were mostly a consequence of the underlying ocean circulation rather

than the atmosphere processes under global change. Marshall and others. (2014) discussed these processes using climate response functions (CRFs), the response of the climate to step changes in anthropogenic forcing in which greenhouse gas (GHG) and/or ozone-hole forcing was abruptly turned on.

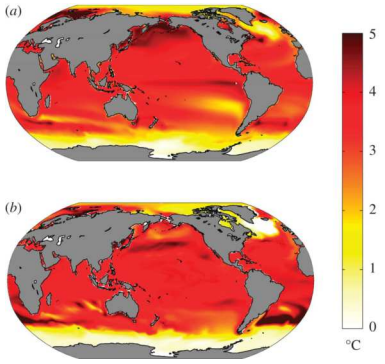

Fig. 4 (a) Ensemble-average SST anomalies 100 years after an abrupt quadrupling of CO_2 in 15 CMIP5 models. (b) SST anomalies after 100 years of an ocean only configuration of the MITgcm induced by a uniform downwelling flux of 4 W m^{-2} and damped at a uniform rate of 1 W m^{-2} K^{-1}, as described (Marshall and others., 2014).

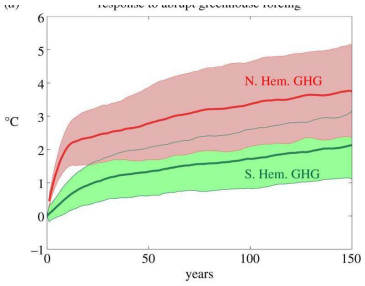

Fig. 5 Sea surface temperature CRFs for GHG forcing computed from an ensemble of 15 CMIP5 models under quadrupling of CO_2. The Arctic is defined as north of 50°N (in red) and the Antarctic between 50°S and 70°S (in green). Thick lines denote the ensemble mean and the shaded area spans 1 s.d. (Marshall and others., 2014)

Fig. 5 shows the response to abrupt GHG forcing. Variations of SST were drawn in the Arctic north of 50°N and the Antarctic between 50° and 70° S under the quadrupling of CO_2. We could find significant differences between the Arctic and the Antarctic. To understand the processes for these responses, heat fluxes and interior temperature structure were examined in Fig. 6. An apparent interhemispheric asymmetry with anthropogenic temperature signal (T_{anthro}) was much larger in the Arctic than in the Antarctic. In Fig. 6a, the time-integrated anomalous air-sea fluxes over hundred years (energy accumulation) is plotted and reveals that most of the energy is fluxed into the ocean around Antarctica due to delayed warming there; however, not stored around Antarctica, but transported to the north and, keeping the Antarctic water cool (Fig. 6b, c). The situation in the Arctic was reversed, and the ocean carried heat into the Arctic, increasing its temperature and then some heat was lost to the atmosphere (Fig. 6a). The advective process was mainly due to the upper cell of the ocean's meridional circulation. This ocean circulation cell, MOC, was a major cause for the interhemispheric asymmetry of the global climate.

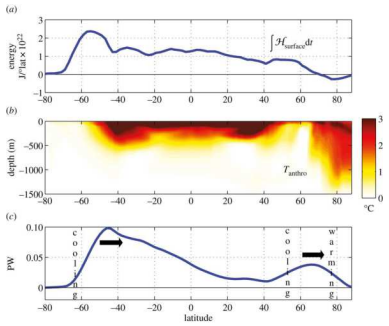

Fig. 6 (a) Surface energy accumulation integrated over 100 years in J/°lat x 10^{22}. (b) Meridional section of zonal-average T_{anthro} after 100 years from the ocean-only configuration of MITgcm whose SST_{anthro} is shown in Fig. 4b. (c) Anomaly in meridional ocean heat transport (in PW) after 100 years relative to control integration. Latitudinal bands of implied ocean warming and cooling are marked (Marshall and others., 2014).

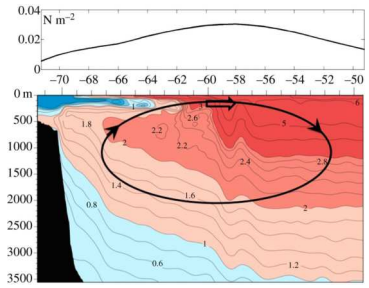

Fig. 7 Meridional hydrographic section of temperature (WOCE section P19) stretching up to Antarctica on the left. The longitude range of the section is 85°-90°W. The region of seasonal sea ice is coincident with cold water (blue tongue) at the surface overlying warmer water (red) below. Superimposed is the sense of the anomalous meridional overturning circulation associated with a positive SAM anomaly, with upwelling around Antarctica and downwelling further equtorward. This acts to warm the ocean just beneath the surface layer. The black line in the top panel shows the SAM-induced zonal wind stress anomaly (Marshall and others., 2014).

The direct effect of ozone-hole forcing on the ocean's surface was due to the surface winds related to Southern Annular Modes (SAM). SST anomaly pattern with cooling around Antarctica and warming

further north was seen firstly. This anomaly could be the direct response of SST to anomalous advection brought by Ekman currents induced by SAM forcing. However, over time, subsurface warming appeared in the top few hundred meters of the ocean and then impacted surface temperatures. So, a cooling came at first, and then came a prolonged warming trend. When the summertime SAM was in its positive phase, upwelling was induced around Antarctica, and downwelling was in further north (Fig. 7). In the upwelling region, a temperature inversion was seen as a consequence of the melting/freezing and export of ice, and resulting freshening of the surface waters appeared. In response to a positive SAM forcing, widespread warming of the ocean was seen just below the mixed layer.

Here, Marshall and others. (2014) clearly explained the mechanism of warming asymmetry in the Arctic and Antarctic derived by ocean circulation, MOC, assumed by Cheylec and others. (2010). The differences in ocean circulation, with sinking in the North Atlantic and upwelling around Antarctica strongly affected the SST response to the GHGs forcing.

4. Delayed warming of Southern Ocean

The SO has shown little warming over the recent decades, in contrast to the rapid warming observed in the Arctic. Armour and others. (2016) presented analyses of oceanographic observations and general circulation model simulations showing fundamentally shaped by the SO's meridional overturning circulation. Fig. 8 showed the observed trends over 1982-2012 when both in situ and satellite observations were available. It was seen that rapid surface warming occurred in zonal bands along the northern side of the Antarctic Circumpolar Current (ACC), and slower warming and cooling appeared to the south. It was clear that these SST patterns were influenced by trends in zonal mean ocean temperature and depth-integrated heat content (Fig. 8c, d). It was found that regions that had warmed strongly had increasingly lost heat to the atmosphere, whereas regions that had warmed less (or cooled) had increasingly taken up the heat. The regions of greatest surface heat uptake showed the least amount of heat storage (Fig. 8b, c). The Southern Hemisphere warming pattern was derived by the meridional ocean heat transport changes. In the south of the ACC, most of the heat taken up had been transported northwards with only a small amount stored locally, and converged along the northern side of ACC. Consequently, it was clearly suggested from observations that the MOC's anomalous heat transport had damped warming south of the ACC and enhanced warming to the north.

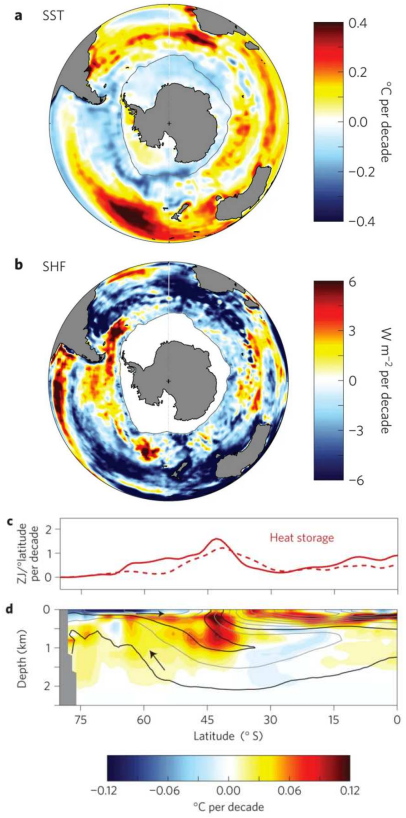

Fig. 8 Observed trends over 1982–2012. **a**, Annual-mean SST trend. **b**, Net SHF trend (positive into ocean). **c**, Zonally and depth-integrated ocean heat content trends from two different subsurface temperature data sets: EN4 (solid; Good and others., 2013) and Ishii (2009; dashed). **d**, Zonal-mean ocean potential temperature trend from EN4, with contours of climatological ocean salinity in intervals of 0.15 practical salinity units (psu) (grey lines). Arrows indicate the orientation of the residual-mean MOC following Karsten and Marshall (2002), along 34.4 and 34.7 psu contours (black lines). Grey line in **a** and **b** shows maximum winter sea-ice extent from Yu and others. (2007) (Armour and others., 2016; Permission for this figure was granted by Springer and Nature).

To quantitatively study the mechanisms driving delayed SO warming, Armour and others. (2016) focused on numerical climate model simulations. The CMIP5 models (GCMs participating in phase 5 of the Coupled Model Intercomparison Project) broadly captured the observed changes over 1982-2012, with little surface warming poleward of the ACC and rapid warming bands along the northern side. Heat storage and warming near the ACC and less warming in the southern side were clearly shown by the models. The 60% of hemispheric surface heat uptake was seen in the region of delayed SO warming, poleward of 50°S, with only 23% of hemispheric heat storage (Fig. 9a). Most of the heat taken up at the surface was transported northwards, by the increase in northward ocean heat transport across the ACC (Fig. 9b), and only a small

portion was stored locally. The heat stored on the equatorward side of the ACC (40° - 50°S) was mainly due to the convergence of heat by the ocean and only less than half from local surface heat uptake. These model results were mostly consistent with the observations (Fig. 8). Delayed SO warming, which was driven by anomalous northward ocean heat transport, seemed to be a fundamental ocean response to GHG forcing. The observed cooling of the SO as seen in Fig. 8a was not explained enough; however, the delayed SO and its driving mechanisms were clarified against a background GHG-induced warming, compared to the rapid warming in the Arctic.

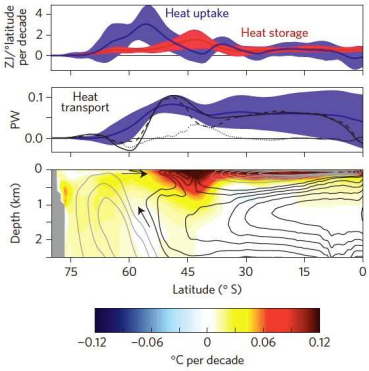

Fig. 9 CMIP5-mean trends over 1982–201. **A**, Zonally integrated average SHF (blue) and full-depth ocean heat content trend (red). **B**, Anomalous OHT for CMIP5-mean (blue) and CCSM4 (black; solid, dashed and dotted lines show total, residual-mean advection and diffusion, respectively). **C**, Zonal-mean ocean potential temperature trend, with contours showing the MOC from CCSM4 (black contours show positive circulation in 4 Sv increments, grey contours show negative circulation in 4 Sv increments) (Armour and others.,2016; Permission for this figure was granted by Springer and Nature).

Now, Armour and others. (2016) verified the mechanism of MOC within the SO from observations and CMIP5 modeling to enhance heat transport to the north and bring the SAT or SST variations, especially in the SO, which Marshall and others. (2014) outlined by the model results.

5. Recent recognitions of MOC

We have followed the role of MOC to enhance north-south asymmetry in the climate, then, what is the actual condition of MOC. There was already long history of discussions of MOC. Richardson (2008) had shown the discussion based on the history of MOC schematic diagrams before and after Blocker's simple schematics (Fig. 3). Lozier (2010) pointed out the over simplified image of ocean conveyor-belt (Fig. 3), and indicated the importance of wind and eddy field as the forcing. Marshall and Speer (2012) presented a reconsideration of MOC, focusing to the SO. They presented the importance of the SO upwelling branch of the MOC circulation together with a "two-cell MOC," one was a southward deep flow counter back to northward shallow flow, and another was a southward deep flow with counter back as deep water.

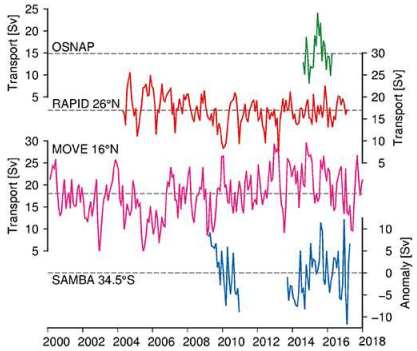

Fig. 10 Monthly values of *MOCz* transport from four observing arrays: OSNAP (green), RAPID 26◦N (red), MOVE 16◦N (magenta) and SAMBA 34.5◦S (blue). For SAMBA, the transports are shown as anomalies. The respective means are given by the black dashed line (zero in the case of SAMBA) (Frajka-Williams, E. and others., 2019).

Actual observations of transport and variability of MOC are limited only to the recent activities. Frajka-Williams and others. (2019), based on the meridional cross section of salinity and ocean circulation originally drawn by Lozier (2012) just as similar to the two cell MOC by Marshall and Speer (2012), presented many observational amounts of MOC transport. Even though a long data set showed a decline in AMOC, this data set was assumed to be biased due to the seasonal variability of single hydrographic measurements at each timing. Continuous measurements have been made already by six active observing arrays in the Atlantic. One cross-section, OSNAP (Overturning in the Subpolar North Atlantic Program), was launched to provide an observational basis for a slowing AMOC in the 21st century (Lozier and others., 2019). From their 21-month records, no clear trend could be derived. Frajka-Williams and others. (2019) showed four records including OSNAP as Fig. 10, but still the long record was limited, and a long term trend was not clear but records were fairly stable. The mean strength of AMOC was about 15 to 18 Sv (10^6 m^3/s). So, from these results, inter decadal variability as proposed by Cheylec and others. (2010) shown in Fig. 1 could not be confirmed simply by the data of MOC yet. We need to obtain these observational data for a long duration.

6. Conclusion

We have reviewed the progress of studies in the recent decade of how MOC contributes to the large

North-South asymmetry in warming. The variation of MOC could clearly explain multidecadal SAT variations in the Arctic and Antarctic. MOC strongly influenced the sea surface temperature response to anthropogenic GHG forcing, accelerating warming in the Arctic while delaying it in the Antarctic. Anomalous transport of heat by the MOC was shown to damp warming in the SO and enhance warming to the north. MOC was an effective source to make the warming difference in both polar regions; however, the contributing ratio compared to the other agent is a future subject. In the 1990s and 2000s, AMOC was observed as about 15 to 18 Sv (Frajka-Williams and others., 2019); however, no direct comparison in multidecadal time scale with damping effect was made yet.

References

Armour, K. C., Marshall, J., Scott, J. R., Donohoe, A. and Newsom, E. R. (2016): Southern Ocean warming delayed by circumpolar upwelling and equatorward transport. *Nature Geo.*, **9**, 549-554. http://dx.doi.org/10.1038/ngeo2731.

Blunier, T. and 11 others (1998): Asynchrony of Antarctic and Greenland climate change during the last glacial period. *Nature*, **394,** 739-743, doi: 10.1038/29447.

Broecker, W.S. (1987): The biggest chill. *Natural History Magazine,* **97**, 74–82.

Cheylek, P., Folland, C. K., Lesins, G. and Dubey, M. K. (2010): Twentieth century bipolar seesaw of the Arctic and Antarctic surface air temperatures. *Geophys. Res. Lett*., **37**, L80703. doi:10.1029/2010GL042793.

EPICA community members (2006): One-to-one coupling of glacial climate variability in Greenland and Antarctica. *Nature*, **449**, 195-198, doi:10.1038/nature05301.

Frajka-Williams, E. and 40 others (2019): Atlantic meridional overturning circulation: observed transport and variability. *Frontiers Marine Sci.*, **6**, 260, doi: 10.3389/fmats.2019.00260.

Good, S. A., Martin, M. J. and Rayner, N. A. (2013): EN4: quality controlled ocean temperature and salinity profiles and monthly objective analyses with uncertainty estimates. *J. Geophys. Res.,* **118,** 6704_6716.

Goose, H. and 13 others (2018): Quantifying climate feedback in polar regions. *Nature Comm.*, DOI: 10.1038/s41467-018-04173-0.

Hansen, J., Sato, M., Kharecha, P. and von Schuckmann, K. (2011): Earth's energy imbalance and implications. *Atmos. Chem. Phys.,* **11**, 13 421–13 449. doi:10.5194/acp-11-13421-2011.

Ishii, M. and Kimoto, M. (2009): Reevaluation of historical ocean heat content variations with time-varying XBT and MBT depth bias corrections. *J. Oceanogr.* **65,** 287_299.

Karsten, R. H. and Marshall, J. (2002): Constructing the residual circulation of the ACC from observations. *J. Phys. Oceanogr.*, **32,** 3315_3327.

Knight, J. R., R. J. Allan, C. K. Folland, M. Vellinga, and M. Mann (2005): A signature of the persistence natural thermohaline circulation cycle in observed climate. *Geophys. Res. Lett.,* **32**, L20708, doi:10.1029/2005GL024233.

Lozier, M. S. (2010): Deconstructing the conveyer belt. *Science*, **328**, 1507-1511.

Lozier, M. S. (2012): Overturning in the North Atlantic. *Ann. Rev. Mar. Sci*. **4**, 291–315. doi: 10.1146/annurev-marine -120710-100740.

Lozier, M. S. and 37 others (2019): A sea change in our view of overturning in the subpolar North Atlantic. *Science,* **363**, 516-521,

Marshall, J. and Speer, K. (2012): Closure of the meridional overturning circulation through Southern Ocean upwelling. *Nature Geosci.* **5,** 171_180.

Marshall, J., Armour, K. C., Scott, J. R., Kostov, Y., Hausmann, U., Ferreira, D., Shepherd, T. G. and Bitz, C. M. (2014): The ocean's role in polar climate change: asymmetric Arctic and Antarctic responses to greenhouse gas and ozone forcing. *Phil. Trans. R. Soc.* **A 372**, 20130040. hdoi.org/10.1098/rsta.2013.0040.

Parker, D. E. and 7 others (2007): Decadal to interdecadal climate variability and predictability and the background of climate change, *J. Geophys. Res.*, **112**, D18115, doi:10.1029/2007JD008411.

Richardson, P. L. (2008): On the history of meridional overturning circulation schematic diagrams. *Prog. Oceanography*, **76**, 466-486. doi:10.1016/j.pocean.2008.01.005.

Salzmann, M. (2017): The polar amplification asymmetry: role of Antarctic surface height. *Eath Syst. Dynam*., **8**, 323-336, doi:10.5194/esd-8-323-2017.

Thompson, D.W.J. and Solomon, S. (2002): Interpretation of recent Southern Hemisphere climate change. *Science*, **265**, 895-899, doi:10.1126/science.1069270

Yamanouchi, T. (2011): Early 20th century warming in the Arctic: A review. *Polar Science*, **5**, 53-71, doi:10.1016/j.polar.2010.10.002.

Yamanouchi, T. (2019): Arctic warming by cloud radiation enhanced by moist air intrusion observed at Ny-Ålesund, Svalbard. *Polar Science*, **21**, 110-116, doi.org/10.1016/j.polar.2018.10.009.

Yu, L. and Weller, R. A. (2007): Objectively analyzed air-sea heat fluxes for the global ice-free oceans (1981_2005). *Bull. Am. Meteorol. Soc.* **88,** 527_539.

Summary in Japanese

和文要約

北極温暖化増幅と東南極温暖化抑制
－ 子午面逆転循環（MOC）の南北非対称への寄与 －

山内　恭[1,2]

[1]国立極地研究所、[2]総合研究大学院大学極域科学専攻

北極では温暖化増幅が、南極では温暖化抑制が見られる。地球温暖化の下でこの大きなコントラストをもたらすものは何だろうか？ このコントラストをもたらすいくつかのメカニズムについては既に議論されているが、最も効果的なものの 1 つが、海洋循環、特に子午面逆転循環（MOC）と呼ばれるものだろう。ここでは、MOC が温暖化における南北の大きな非対称性をどのようにもたらしているかについて、過去 10 年間の研究の進捗をレビューした。

Correspondence to: T. Yamanouchi, yamanou@nipr.ac.jp

Okhotsk Sea and Polar Oceans Research 5 (2021) 7-14

https://doi.org/10.57287/ospor.5.7

Review

The *Belgica* Antarctic Expedition, 1897-1899 – A view, 120 years later

Hugo DECLEIR[1] and Gaston R. DEMARÉE[2]

[1]*Free University of Brussels, Brussels, Belgium*
[2]*Royal Meteorological Institute of Belgium, Brussels, Belgium*

(Received October 27, 2020; Revised manuscript accepted December 13, 2020)

Abstract

In 1897-1899 the Belgian captain Adrien de Gerlache, carried out - on board of their ship the *Belgica* – a historic scientific Antarctic expedition. This expedition, a stepping-stone in Antarctic research and exploration, claims many first finds as well in the field of geographical exploration, its scientific results, its international staffing and achieving the first wintering in Antarctica.

Key words: *Belgica*, Antarctic, expedition, wintering, geographical discoveries, meteorological observations

1. Introduction

In the beginning of the 1890's, Adrien de Gerlache, a young Belgian naval officer, surprised the world by announcing his plans for a small (with respect to logistics and funding) scientific expedition to Antarctica. Such an initiative was rather expected to come from one of the larger countries with respect to polar research (e.g.; United Kingdom, Germany, …). Indeed, in July 1895 the Sixth International Geographical Congress[1] met in London and passed unanimously a resolution which stated that '*the exploration of the Antarctic regions is the greatest piece of geographical exploration still to be undertaken… and this work should be undertaken before the close of the century'*.

But, already in October 1894, thus one year before the London resolution, de Gerlache had presented with success a memoir to the council of the *Société royale belge de Géographie* (Royal Belgian Geographical Society), entitled '*Project for the Organization of a Belgian Expedition for the Exploration of the Antarctic Ocean*'.

After having obtained the intellectual and moral support of the *Société royale belge de Géographie* and of important Belgian scientists and industrialists (e.g. Ernest Solvay), de Gerlache appealed to the *Société royale belge de Géographie* to launch in January 1896 a national subscription fund to raise the draft budget of 250 000 Belgian francs for the expedition. Having collected in that way, the amount of 100 000 Belgian francs in only four months, de Gerlache knowing that this wasn't sufficient, contacted the government who intervened for 60% of the total costs of the expedition so that de Gerlache could finally leave in August 1897. Notwithstanding difficulties in the funding, the project sparkled enthusiasm in the entire Belgian population. (Cabay, 2001; Barr, 2007)

Adrien de Gerlache participated from March to August 1895 on board of the Norwegian vessel *Cantor* in a seal and whale hunting campaign in the Arctic Ocean close to Jan Mayen and East Greenland. He experienced the navigation under icy conditions, learned Norwegian, selected Norwegian sailors because of their Arctic expertise and looked out for a suitable ship for his own expedition.

He returned to Norway in June 1896 where he bought the sealing vessel *Patria,* 30 meters long, 6.50 m wide at the main beam and weighing 244 tons, which was actually a very small but strong building. The vessel, renamed *Belgica*, had to be adapted for its future scientific mission, adaptations which were carried out under the direction of de Gerlache at the shipyard Framnoes in Sandefjord, Norway.

2. The remarkable men of the *Belgica*

2.1 The final crew of the Belgica

The final crew of the *Belgica* consisted of 19 members : Board Personnel: Adrien de Gerlache (Commander), Georges Lecointe (Captain), Roald Amundsen (Second Officer); Scientific Personnel: Émile Danco (Geomagnetician, deceased on June 5, 1898), Henryk Arctowski (Meteorologist, Geologist and Glaciologist), Emile Racovitza (Naturist, Biologist), Antoni Bolesław Dobrowolski (assistant Meteorologist), Frederick Cook, (Surgeon, Photographer, Anthropologist); Other Board Personnel: Jules Melaerts (Third Officer), Henri

[1] Among the Belgian participants of the international congress, Albert Lancaster and Jean Vincent belonged to the meteorology department of the Royal Observatory of Belgium (ROB). The Royal Observatory had a leading role in the scientific aspects of the *Belgica* Antarctic expedition among other by providing scientific training. At the return of the *Belgica* several crew members were integrated in the ROB.

Somers (Chief Engineer), Max Van Rysselberghe [2] (Second Engineer), Louis Michotte (Steward), Jan Van Mirlo and Gustave Dufour (Sailors); Norwegian Crew : Adam Tollefsen, Ludvig-Hjalmar Johansen, Johan Koren, Engelbret Knudsen, Carl-Auguste Wiencke (deceased on January 22, 1898) (Sailors).

The scientists belonged to 5 nationalities: Belgian, Norwegian, American, Polish and Rumanian. Several like Arctowski (1903), Cook (1900), de Gerlache (1902), Dobrowolski (1899, 1950, 1962), Lecointe (1902, 1903, 1904), Racovitza (1998) and Amundsen (see Decleir, 1998b) kept diaries which were printed and hence available for the general public. For their publishing details, see the reference list at the back of this paper.

2.2 Adrien de Gerlache de Gomery

Adrien Victor Joseph de Gerlache de Gomery (1866-1934) (Fig. 1) started engineering studies at the *Université Libre de Bruxelles* but, being more attracted to maritime life, he went as a ship boy on intercontinental travel during his vacations. He graduated at the Nautical College of Ostend and sailed extensively in the North Sea. He became captain at the same Nautical College on August 22, 1894. De Gerlache dreamed of a more adventurous life and developed interest in polar regions with the Belgica expedition (1897-1899) as result. After his successful expedition to Antarctica, Adrien de Gerlache participated in several other scientific expeditions to the Arctic as well as being the reorganizer of the Belgian Maritime Administration. (Verlinden, 2001)

Fig. 1 Adrien de Gerlache de Gomory.

2.3 Georges Lecointe

Georges Lecointe (1869-1929) (fig. 2) entered the *École Royale Militaire (ERM)* at Brussels in 1886 and in 1891 he was appointed second lieutenant of artillery. The Belgian government detached him in 1894 to the French Navy, where he was ultimately promoted to ship-of -the-line lieutenant in 1897. Lecointe got reckoning of his degree in the Belgian army. In 1897, Lecointe was attached to the Observatory of the *Bureau des Longitudes* at Montsouris, located in the south of Paris. At the request of the Belgian Government he returned to Belgium end of June 1897. In October 1900, he became the scientific Head of the Astronomical service of the Royal Observatory of Belgium and from August 1913 till May 1925 its Director.

Fig. 2 Georges Lecointe

[2] Max Van Rysselberghe (1878-1952), son of François Van Rysselberghe (1846-1893), meteorologist at the Royal Observatory in Brussels and later professor in Applications of Electricity at the University of Ghent, Belgium. (Courtesy Hilde Langenaken, ROB)

2.4 Roald Amundsen

Roald Amundsen (1872-1928) (Fig. 3) already interested at early age in polar exploration contacted de Gerlache during his stage in Sandefjord, Norway. He was accepted as second mate. As a matter of fact, the *Belgica* expedition was a training ground for all Amundsen's later successful explorations. Amundsen was the first to navigate the Northwest passage and with his Antarctic expedition to reach the South Pole in 1911. Tragically, Amundsen disappeared in a plane crash in the Arctic Ocean in June 1928, while on a rescue mission for Umberto Nobile.

Fig. 3 Roald Amundsen.

2.5 Henryk Arctowski

Henryk Arctowski [Artzt] (1871-1958) (Fig. 4), studied at the University of Liège (Belgium) and at Paris (France) and, while working with prof. Walthère Spring at Liège, found himself strongly recommended to de Gerlache. Arctowski also requested de Gerlache to recruit his countryman, Antoni Bolesław Dobrowolski (1872-1954) who joined the expedition at the last moment. After the *Belgica* expedition, Arctowski started to work at the Royal Observatory of Belgium under the direction of Albert Lancaster, Head of the Meteorological Service. Besides operational tasks in the Meteorological Service, he mainly devoted himself to the research and analysis of the meteorological, oceanographic, geological, glaciological, optical and aurora material collected in the Antarctic expedition. His stay at the Royal Observatory was a turbulent stopover on a road to an international scientific career as he left to become Head of the division of natural sciences at the New York Public Library. After World War I, he became a well-known scientist in Poland, his home country. (Demarée, Decleir & Orvanová, 1995)

Fig. 4 Henryk Arctowski

2.6 Frederick Albert Cook

Frederick Albert Cook (1865-1940), became the surgeon of the *Belgica* expedition, after having joined Robert E. Peary's expedition to Northern Greenland.

The polar experience he collected in the Arctic was extremely useful for the *Belgica* expedition during the long winter conditions in Antarctica. His medical expertise helped several members of the expedition to overwin psychological diseases and the prevention and treatment of scurvy. His claim to have discovered the North Pole in 1908 made him a controversial figure.

3. The Odyssey of the *Belgica*

3.1 The travel route of the Belgica

The Odyssey of the *Belgica* can be split up into 6 parts: (i) from August 16 till October 22, 1897: crossing the Atlantic Ocean from Antwerp to Rio de Janeiro; (ii) from October 22 till January 14, 1898: different stops in South America and slow progress through the channels of Tierra del Fuego; (iii) from January 14 till February 27, 1898: geographical discoveries at the western side of the Antarctic Peninsula; (iv) from February 27, 1898 till January 7, 1899: first wintering in the Antarctic pack ice of the Bellingshausen Sea; (v) from January 7 till March 14, 1899: deliverance from the pack ice; (vi) from March 14 till November 5, 1899: home journey to Antwerp (Decleir, 1998a) (Fig. 5)

3.2 Crossing the Atlantic

On August 16, 1897, in the morning, the *Belgica* left Antwerp, heavily loaded with the deck barely some 50 centimeters distance from the waterline. Sailing a few miles in the North Sea, a problem occurred with the machine. It was decided to go back and repair it in Ostend. There, two men asked to disembark. Fortunately, the Polish researcher, Antoni Bolesław Dobrowolski, could be embarked, making the crew more complete.

Continuing their voyage, the *Belgica* anchored in front of Funchal, the main port of the Madeira Islands on September 11, 1897.

3.3 Stops in South America and through the channels of Tierra del Fuego

On October 22, 1897, the *Belgica* entered the harbor of Rio-de-Janeiro. Here, Dr. Frederick Albert Cook, who had been invited by de Gerlache to serve as surgeon of the Antarctic expedition joined the expedition. The expedition was heartily welcomed by the authorities, the Brazilians and the Belgian colony, among them Luís Cruls[3].

As the crossing from Rio (Brazil) to Punta Arenas (Chile) took at least several weeks and Emil Racovitza had been suffering a lot from seasickness during the crossing of the Atlantic, he was allowed to travel with the fast steamer *Oravia* of the Pacific Steam Navigation Company in order to study the fauna and flora of Patagonia and Tierra del Fuego. He departed from Rio de Janeiro on October 27, made a brief stop at Montevideo, Uruguay, and arrived at Punta Arenas, Chile, on November 3, 1897. Here he travelled to various places in the area waiting for the *Belgica* which arrived only on December 1, 1897, at Punta Arenas.

At Punta Arenas, de Gerlache had to drop four sailors for disciplinary reasons, as well as the Swedish cook. Afterwards, the *Belgica* traveled through the channels of Tierra del Fuego, visiting Ushuaia, Argentina. Special ethnographical and anthropological interest was shown in the tragic situation of the Amerindian tribes of Tierra del Fuego. Coal provision was completed at the Argentine coal deposit of Lapataia while the embarkation of water was carried out at San Juan del Salvamento, Isla de los Estados (Staten Island), Argentina. On January 14, 1897, the *Belgica* left that last place pushing into the mysterious South (de Gerlache, 1902).

3.4 Geographical discoveries at the western side of the Antarctic Peninsula

The *Belgica*, with a crew of nineteen, among them seven sailors, was heading for South Shetland Islands and Hughes Bay. It is possible, due to this reduced crew, that de Gerlache changed his sailing programme for the *Belgica.*

Henryk Arctowski made the first bathymetric soundings in the Drake Passage. On the second day of sailing (January 15, 1898), as well as on the following

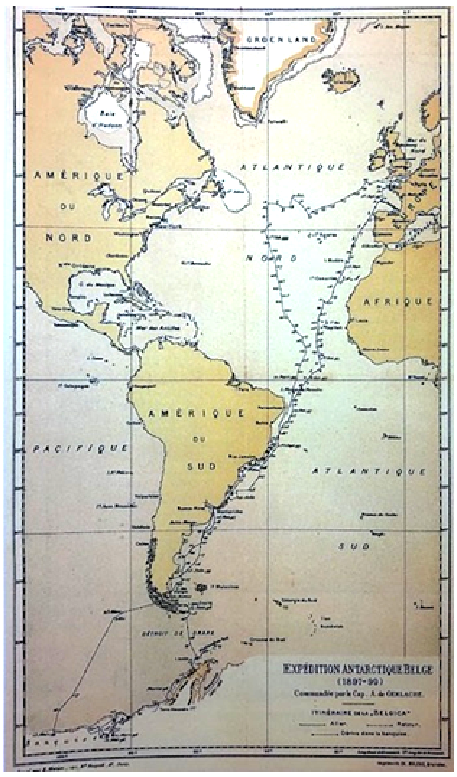

Fig. 5 Travel route of the *Belgica* from Antwerp to Antarctica and its home journey to Antwerp

[3] Luís Cruls, Belgian-Brazilian astronomer (1848-1912) who helped Lecointe with the calibration of his instruments.

days, depths of around 4000 meters were measured indicating deep water lying close to the Andes mountain chain, which was unexpected. The South Shetland Islands, as well as seeing the first icebergs, were reached on January 19, 1897. On January 22, 1898, with a view to Low Island, South Shetland Islands, the Norwegian sailor Auguste-Karl Wiencke (born at Oslo in 1877), having fallen overboard, perished despite the courageous rescue trial by Georges Lecointe.

On January 23, 1898, the *Belgica* entered the Brialmont Cove, at the south-eastern end of Hughes Bay. Next, the *Belgica* sailed crisscross through the strait, which later would be called de Gerlache Strait, situated between Danco Land (West coast of Graham Land) and the Palmer archipelago (Anvers and Brabant Island) and this in order to investigate more thoroughly the Antarctic Peninsula.

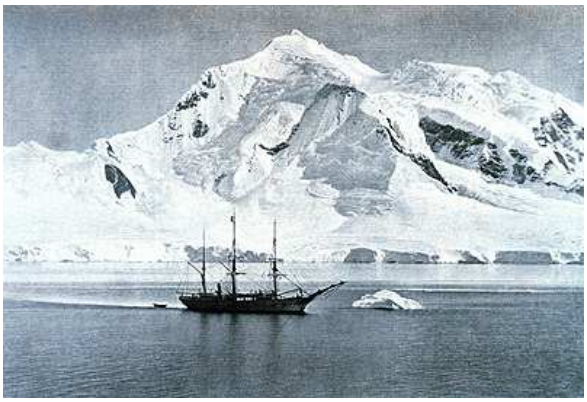

Fig. 6 The *Belgica* anchored at 'Mount William' near the south extreme of Anvers Island.

The only existing maps, but differing rather fundamentally, were the British Admiralty Chart No. 1238 and the German Friedrichsen's Map (1895). It became immediately clear that the existing maps were inadequate and, under the direction of Lecointe, they started to take bearings for an improved mapping of the region. The initiative to undertake not less than 20 landings provided fixed positions for the hydrographic work but also for the scientific task of the expedition. De Gerlache numbered these 20 landings by a Roman numeral. On a landing, Lecointe and Dobrowolski could make astronomical observations (Latitude & Longitude), Danco magnetic observations, Arctowski geological observations while Racovitza searched for plants (mostly mosses and lichens) and animals, among which the *Belgica antarctica*, the largest purely terrestrial animal native to the continent, a flightless midge (Fig. 8).

However, at the Xth landing, on Sunday, January 30, 1898, in the Buls Bay, a party consisting of de Gerlache, Danco, Amundsen, Cook and Arctowski was organized equipped with two Nansen sledges, sleeping bags, a silk shelter tent, a little aluminum stove, Norwegian ski, Canadian snow-shoes, ice-axes, a 40-foot rope for a seven days' excursion. Arctowski considered that there was too much baggage, and indeed the sledges were horribly heavy. The original idea of Danco and de Gerlache was to land on Brabant Island and try to climb one of the mountains where a levee by the method of Admiral Mouchez would be done. However, the observations carried out with a theodolite Brunner by Danco and de Gerlache did not give the expected results due to the bad weather conditions and the geographical obstructions (Derwael, 2013).

On Sunday, February 6, 1898, the party got on board of the *Belgica* again. Meanwhile the *Belgica* had sailed through the South and South-West of the de Gerlache Strait with Lecointe as captain. Lecointe and Racovitza had also made meanwhile the landings XI and XII. On February 10, 1898, the *Belgica* sailed into Flanders Bay noting that it wasn't a gateway to the Weddell Sea and discovered the Moureau Islands. On February 12, 1898, they entered Lemaire Channel between the Antarctic continent and the Dannebrog Islands and sailed again in the Pacific Ocean. Under bad weather conditions and severe pack ice, the *Belgica* sailed skirting the pack ice and on February 16, 1898, they saw the Alexander I Island, the last piece of coast to be seen in more than 17 months to come. (Arctowski, 1901; de Gerlache, 1902; Decleir, 1998)

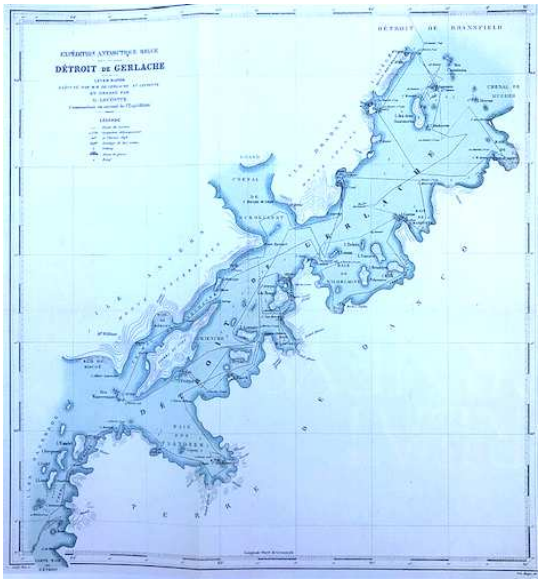

Fig. 8 Lecointe's map of de Gerlache Strait with the route of the *Belgica* and the landings

3.5 First wintering in the Antarctic pack ice of the Bellingshausen Sea

From 17 February till 28 February, 1898, the *Belgica* sailed along the edge of the pack ice. The depth soundings showed that the *Belgica* had left the continental plateau. Entering then the pack ice on

February 28, 1898, and on March 4, 1898, it became obvious that the *Belgica* was become beset in the pack ice at 71° 22' S 84° 55' E and a wintering became reality (Fig. 9 and 10). Cook, Arctowski and Amundsen thought that the wintering, was not originally planned, but secretly wished by de Gerlache and Lecointe for various reasons.

Fig. 9 The *Belgica* in the ice

Fig. 10 The *Belgica* in moonlight during wintering.

The *Belgica* drifted from about 85° to 103° W and between 70° and 71°30' S. In March and April 1898, the *Belgica* drifted westerly to 92° 25' W on April 25, 1898, while from May to October 1898 drifting backwards to a place near the starting point. From October 31, 1898, to February and March 1899, the *Belgica* drifted rapidly westward. The Antarctic winter drift is eastward and the Antarctic summer drift is westward. The farthest point south, 71° 36' 05'' S, was reached on May 31, 1898 (see figure 11).

Being trapped in the ice and as a long and tedious wintering became inevitable, the interior of the *Belgica* was developed as comfortably as possible and isolating the vessel by a layer of snow to limit the energy losses. De Gerlache installed a strict time-schedule on board of the *Belgica.* The bi-hourly meteorological observations were carried out by Arctowki (1904b) and Dobrowolski (1903), magnetic observations by Danco, cloud, snow and frost observations by Dobrowolski, the organisms collected by depth soundings by Racovitza.

By May 19, 1898, the sun disappeared and a long Antarctic night of another 63 days till July 22, 1898, started. Imbalance in the food consumption caused signs of scurvy to start. In the long and harsh conditions of isolation, dark and bitterly cold, stormy weather and high humidity, several sailors began to show signs of mental illnesses. Fortunately, the ship's surgeon, Dr. Cook, took the necessary steps. Émile Danco fell ill from his heart condition and, cried by everyone, died on 5 June.

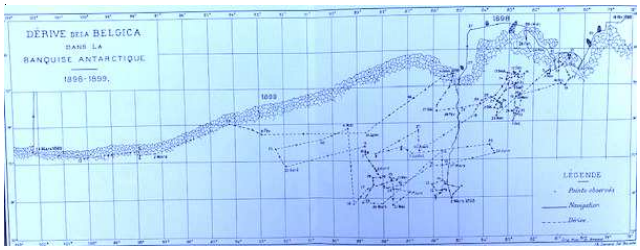

Fig. 11 Drift of the *Belgica* in the Antarctic pack ice.

3.6 Deliverance from the pack-ice and home journey

In the Antarctic spring the *Belgica* was still ice-bound. At the suggestion of Cook, two trenches were cut and sawn to open water so that the *Belgica* could emerge from its frozen-in position on February 14, 1899. It still took another month to reach open water at 103° W, 70° 45' S, on March 13, 1899. The *Belgica* reached Punta Arenas on March 28, 1899, at 6 o'clock in the morning.

However, de Gerlache did not want to waste precious time for the scientific collaborators: it was agreed that Racovitza, Arctowski and Dobrowolski would return directly to Europe, where they could usefully work, upon their return, on the classification of the collections that had been collected and on the coordination of certain observations. In 1899, Arctowski and Dobrowolski were appointed members of the *Belgica Commission* Editorial Board. In fact, Arctowski and Dobrowolski started to work at the Meteorological service of the Royal Observatory of Belgium while Racovitza officially became attached to the Sorbonne, as deputy director of the Arago Laboratory in Banyuls-sur-Mer in the *Pyrénées-Orientales* department in southern France. Lecointe, for his part, started to explore the Andes in Patagonia. Amundsen left the *Belgica* returning home with a passenger ship in order to be at home before the end of the holidays. Finally, Cook continued his studies on the Amerindian tribes in Tierra del Fuego before returning to the United States.

Lacking coal and funds, the *Belgica* crossed the Atlantic only on its sails. The crossing took a long time (see its route on figure 5) and was tedious but the *Belgica* expedition was enthusiastically welcomed in Antwerp on 5 November, 1899.

5. Meteorological observations in the wintering period

The most interesting meteorological results are of course those that span an entire annual cycle including the polar winter in Antarctica. In the early publications on his meteorological data carried out on the *Belgica,*

Arctowski (1899, 1900)[4] lists: the monthly mean temperature and the monthly minima and maxima of the temperature (in °C and in °F), the monthly means of the atmospheric pressure and the monthly minima and maxima of the atmospheric pressure (in mm Hg) with their day of occurrence. Arctowski presents further: a monthly table of wind expressed in 16 directions, the monthly number of days of continuous fog or overcast sky, the monthly number of days with sky partially clear, the monthly number of days on which fog was observed, the monthly number of days on which snow was recorded, the monthly number of days on which rain was observed, the number of days of calm, or of wind not exceeding wind force 1, and the number of days with wind force less than 4 (Fig.12).

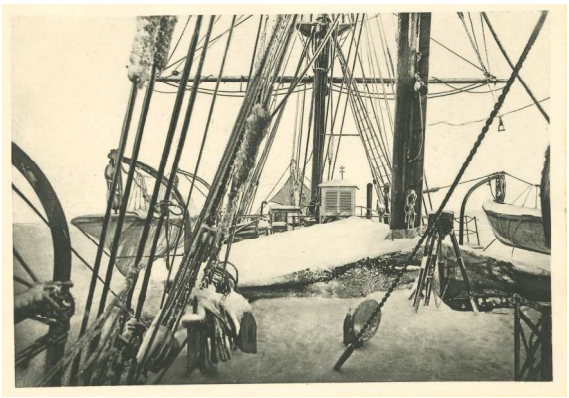

Fig. 12 The deck of the *Belgica* during the wintering with the thermometric screen in the background.

As shown in Fig.13, the month of February 1899 was the warmest month with a mean temperature of -1 °C and a minimum temperature of -9.6 °C while July 1898 was the coldest month with a mean temperature of -23.5 °C and a minimum temperature of -37.1 °C. The extreme minimum of temperature was observed on 8 September 1898, at 4 a.m., with -43.1 °C. The maximum temperature is between -1 °C to 1 °C, the Antarctic winter months of June, July and August included. Arctowki's monthly temperature data clearly indicate a warm period in August 1898 where the monthly mean temperature raised to -11,3 °C. Such episodes of mid-winter warm periods have been regularly detected in temperature time-series of Antarctic stations and have been coined as '*coreless winter (CW)*'. In a first instance, a CW can been recognized by the simple formula $t_{m-1} < t_m$ and $t_m > t_{m+1}$ where t is the monthly mean temperature for the succeeding months m-1, m and m+1.

These time series could therefore be compared with the observations during the First International Polar Year (1882-1883) in the Arctic region. Noteworthy were not so much the low winter temperatures measured on the *Belgica* which are comparable to those of the Arctic, but rather the cold summer temperatures which rarely rise above zero degrees (Fig. 13).

The atmospheric pressure observations were carried out with a marine barometer and with an aneroid barometer. Arctowski (1899) lists the tables:

- monthly (approximate) means expressed in 0.1 mm only and without corrections to these observations. For February 1898 the atmospheric pressure observations concern only the latter half of the month;
- monthly minimum and maximum atmospheric pressure data, expressed in 0.01 mm, with their data of occurrence and reduced to freezing point and the latitude correction to 45° according to the contemporaneous International Meteorological Tables.

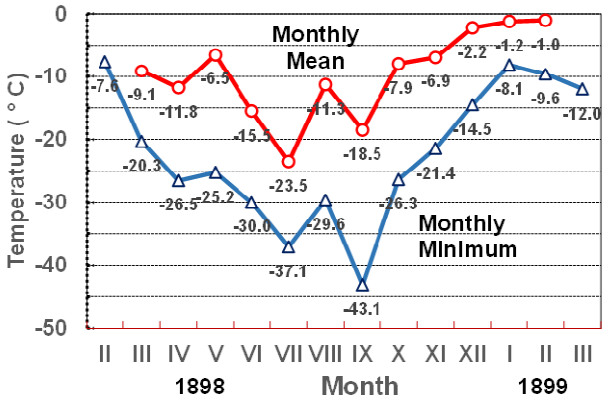

Fig. 13 Monthly mean (upper) and monthly minima temperature (lower) for the months February (II) 1898 till the month of March (III) 1899. The Roman numerals indicate the number of the month.

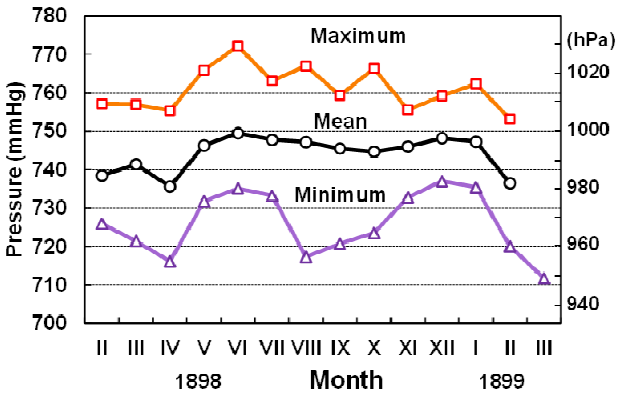

Fig. 14 Atmospheric pressure observations expressed in mm Hg and in hPa during the stay in the pack ice of the *Belgica*: monthly average (approximate) observations (middle), monthly maximum observations (upper) and monthly minimum observations (lower). The Roman numerals indicate the number of the month.

[4] The figures represented in this paper are based upon the earliest published data in Arctowski (1899). Later on more elaborated data were published (Arctowski, 1904a, b).

From May 1898 through January 1899 the average values are between 990 and 1000 hPa while its values for February through April 1898 and February 1899 lay between 980 and 990 hPa (Fig. 14). It is noteworthy that none of the monthly average values and even 7 of the monthly maxima values do not reach the value of the standard atmospheric pressure of 1013.25 hPa.

The wind force data expressed in the Beaufort scale are given as follows: the number of days of calm, or with wind not exceeding wind force 1, and the number of days with wind force less than 4. The Fig. 15 represents the monthly ratio of wind force according to the Beaufort scale; the blue represents the number of days with wind force [0-1], calm and light air, with wind speed < 1.5 m s^{-1}; the green represents the number of days with wind force [2-3], light breeze and gentle breeze, with wind speed < 5.5 m s^{-1}; the yellow represents the number of days with wind force 4 and stronger.

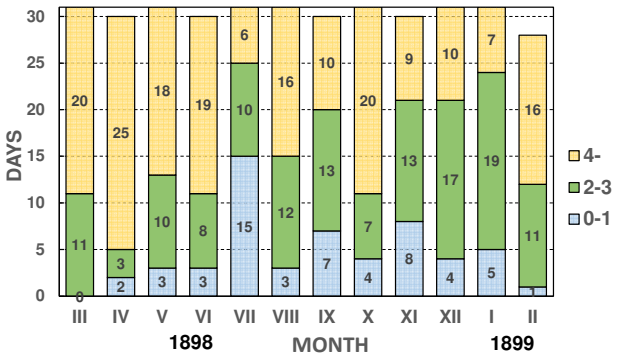

Fig. 15 Monthly Ratio of wind force scale. Wind force [0-1] means calm and light air, [2-3] means light and gentle breeze, [4-] means moderate breeze and more strong wind.

The wind direction observations betrayed the existence of a polar semi-permanent anticyclone[5]. Arctowski (1899) showed how the *Belgica* was under the influence of this anticyclone during the Antarctic summer (wind directions north-east to south-east from November to February), but in the Antarctic winter (June, July and August) it came under the grip of the circumpolar westerly wind.

[5] The Norwegian cyclone model was introduced by a group of meteorologists led by Vilhelm Bjerknes just after WWI. The model explains the generation, intensification and decay of mid-latitude cyclones, and introduced the idea of fronts. At the Royal Meteorological Institute of Belgium, Jacques Van Mieghem (1905-1980) collaborated in the early 1930s with Jacob Bjerknes and introduced the frontal model in the daily weather forecasts at the Institute.

5. Conclusion

The *Belgica* expedition is notable for its first wintering in Antarctica, for its purely scientific nature and for its internationally staffing (Machowski, 1998; Barr, 2007; Decleir, 2011, 2012). The *Belgica Commission* published the *Rapports Scientifiques* volumes (see e.g. Arctowski (1904b) and Dobrowolski (1903) for meteorology). Later on, these volumes gave rise to numerous scientific publications.

In this review the numerous interactions between the *Belgica* Antarctic expedition and the Royal Observatory of Belgium are highlighted.

The *Belgica* expedition was special remembered in the *Belgica Centennial Symposium* in May 1998 at Brussels (Decleir & De Broyer, 2001). However, 120 years later, it would be highly interesting to confront the original scientific findings of the expedition with the view of climatic and environmental Antarctic science under present-day Climatic Change conditions.

Acknowledgements

The lead author H.D. of this article wishes to thank all people who were helpful during his stay in the Sør Rondane (JARE 28, JARE 31, JARE 32): K. Hirakawa, K. Shiraishi, H. Motoyama, N. Matsuoka and former NIPR director Okitsugu Watanabe for his overall support.

G.D. has been motivated in co-authoring the review article because of the numerous interactions of the scientific staff of the *Belgica* with the Meteorological service of the Royal Observatory of Belgium which was the institution preceding the founding of the Royal Meteorological Institute of Belgium as an independent research institute.

The authors express their sincere thanks to prof. Shuhei Takahashi for his positive and constructive help and suggestions in numerous aspects of the elaboration of this paper. The authors also thank the Library of the *Académie Royale de Belgique* (ARB) for making readily available *Belgica* literature.

References

Arctowski, H. (1899) The Antarctic Climate. *The Geographical Journal*, **14**, 413-420.

Arctowski, H. (1900) *The Antarctic Climate*. Appendix No. II. In: Cook, F.A. *Through the first Antarctic Night 1898-1899. A Narrative of the Voyage of the Belgica among Newly Discovered Lands and over an Unknown Sea about the South Pole*. New York, Doubleday & McClure Co. and London, Heineman, 425-435.

Arctowski, H. (1901) Exploration of Antarctic Lands. *The Geographical Journal*, Vol. **17**, No. 2 (Feb., 1901), 150-180.

Arctowski, H. (1903) Die antarktischen Eisverhältnisse. Auszug aus meinem Tagebuch der Südpolreise der Belgica 1898-1899. *Petermanns Geographische Mitteilungen*. Gotha, Ergänzungsheft, 144, 121 p.

Arctowski, H. (1904a) Aperçu des résultats météorologiques de l'hivernage antarctique de la *Belgica*. *Annuaire météorologique pour 1904* publié par les soins de A.

Lancaster, Observatoire Royal de Belgique. Bruxelles, Hayez, 267-305, 1 Planche.

Arctowski, H. (1904b) *Météorologie sur les observations météorologiques horaires.* Rapports scientifiques publiés aux frais du Gouvernement belge, sous la direction de la Commission de la *Belgica*. Anvers, Buschmann. Météorologie sur les observations météorologiques horaires faites pendant l'hivernage antarctique de la *Belgica*, 1-51, Tableaux d'observations, 1*-150*, XXII Planches.

Barr, W. (2007) *Belgian Antarctic (Belgica) Expedition (1897-1899).* In: Riffenburgh, Beau (Ed.) *Encyclopedia of the Antarctic*, Volume 1, Routledge, 136-137.

Cabay, A. (2001) *The funding of the Belgian Antarctic expedition 1897-1899*. In: Decleir, H. & De Broyer, C. (eds) The *Belgica* Expedition Centennial: Perspectives on Antarctic Science and History. VUB Brussels University Press, 83-92.

Cook, F.A. (1900) *Through the first Antarctic Night 1898-1899. A Narrative of the Voyage of the Belgica among Newly Discovered Lands and over an Unknown Sea about the South Pole*. New York, Doubleday & McClure Co. and London, Heineman, 478 p.

Decleir, H. (1998a) The discoveries of the *Belgica* expedition. *Noesis*, Travaux du Comité Roumain d'Histoire et de Philosphie des Sciences, XIII, Editura Academiei Române, 33-46.

Decleir, H. (ed.) (1998b) *Roald Amundsen's Belgica Diary. The First Scientific Expedition to The Antarctic.* Hadewijch, 224 p.

Decleir, H. & De Broyer, C. (eds) (2001) *The Belgica Expedition Centennial: Perspectives on Antarctic Science and History.* VUB Brussels University Press, 327 p.

Decleir, H. (2011) Van '*Belgica*' tot *'Princess Elisabeth'* station. Belgisch wetenschappelijk onderzoek met betrekking tot Antarctica. *Monumenten en Landschappen*, **30**(2), 40-62. [in Dutch]

Decleir, H. (2012) Belgian Expedition: World's first wintering in Antarctic Circle by Ship *Belgica*. JARE OB Magazine, No. **16**, 10-11. [In Japanese]

Demarée, G.R., Decleir, H. and Orvanová, E. (1995) *Henryk Arctowski at the Royal Observatory of Belgium – A turbulent Stopover on the Road to an International Scientific Career.* In: Abstracts of 'Climate Dynamics and the Global Change Perspective', International Conference, 17-20 0ctober 1995, Cracow, Poland, 18-19.

Derwael, J.-J. (2013) Méthode de l'amiral Mouchez (1821-1892). *Revue XYZ*, N° **134**, 61-66.

Dobrowolski, A.B. (1899) Belgijska wyprawa antarktyczna [The Belgian Antarctic Expedition]. *Atheneum*, Warsaw, **95**, 240-272. [in Polish]

Dobrowolski, A. (1903) *La neige et le givre [Snow and Frost]*. Rapports scientifiques publiés aux frais du Gouvernement belge, sous la direction de la Commission de la *Belgica*. Anvers, Buschmann, 79 p.

Dobrowolski, A. (1950) *Wspomnienienia z wyprawy polarnei*. [Memoirs from the polar expedition]. Warsawa, Wydawnictwo Prasa Wojskowa. [In Polish]

Dobrowolski, A.B. (1962) [Edited by I. Lukaszewska & J. Ostrowski] *Dziennik wyprawy na Antarktyde (1897-1899)* [*Journal of the Antarctic expedition, 1897-1899*]. Wroclaw-Warszawa-Krakow, Zaklad Narodowy Imienia Ossolinskich, 332 p. [In Polish]

de Gerlache, A. (1902) *Voyage de la Belgica. Quinze mois dans l'Antarctique* Par le Commandant de Gerlache. Préface par Elisée Reclus. Bruxelles, Imprimerie Scientifique Ch. Bulens, Editeur, 303 p., 1 Carte.

Lecointe, G. (1902) Vers le Pôle Sud. Impressions éprouvées à bord de la *Belgica*. *Revue des questions scientifiques* publiée par la Société scientifique de Bruxelles, Série 3, Tome 2, 173-212 ; 492-553.

Lecointe, G. (1903) Vers le Pôle Sud. Impressions éprouvées à bord de la *Belgica*. *Revue des questions scientifiques* publiée par la Société scientifique de Bruxelles, Série 3, Tome 3, 164-208 ; 516-559 ; Tome 4, 140-210 ; 440-461.

Lecointe, G. (1904) *Au Pays des Manchots. Récit du Voyage de la Belgica [In Penguin Country, Story of the Voyage of the Belgica]*. Bruxelles, Société belge de librairie, Oscar Schepens & Cie, 368 p.

Machowski, J. (1998) Contribution of H. Arctowski and A.B. Dobrowolski to the Antarctic Expedition of the *Belgica* (1897-1899). *Polish Polar Research*, **19**(1-2), 15-30.

Racovitza, E. (1998) *Le Rameau d'Or Belgica (1897-1899) [The Golden Branch Belgica (1897-1899]*. Emile Racovitza, le naturaliste de l'expédition antarctique *Belgica*. Lettres, Journal antarctique, Conférences. Fondation culturelle roumaine, Nr. **2**(7) – 1998, 207 p.

Report of the Sixth International Geographical Congress, held in London, 1895. Edited by the Secretaries, 1896, London, John Murray, 806 p.

Verlinden, J. (2001) *Adrien de Gerlache and the Belgica expedition*. In: Decleir, H. & De Broyer, C. (eds) The *Belgica* Expedition Centennial: Perspectives on Antarctic Science and History. VUB Brussels University Press, 95-102.

Summary in Japanese

和文要約

1897–1899 南極探検船ベルジカ号の越冬記録 — 120 年後の視点から

Hugo DECLEIR[1] and Gaston R. DEMARÉE[2],

[1]ブラッセル自由大学, [2]ベルギー王立気象研究所

1897–1899 にかけてベルギーの Adrien de Gerlache 船長はベルジカ号で歴史的な南極科学探検を行った。この探検は, 南極での科学調査としての探査を飛躍的に高めるものであり, 国際的な隊員によって初めて南極海域での越冬を行い, 地理的調査や各種科学観測など多くの成果をもたらした。その歴史的経緯を解説し, 科学成果の一部を紹介する。

Correspondence to: G. R. Demarée, gdemaree@meteo.be

Okhotsk Sea and Polar Oceans Research 5 (2021) 15-22

https://doi.org/10.57287/ospor.5.15

Review

Economic feasibility of Arctic shipping from multiple perspectives: a systematic review

Chathumi Ayanthi KAVIRATHNA[1] and Ryuichi SHIBASAKI[1]

[1]*Resilience Engineering Research Center, The University of Tokyo, Tokyo, Japan*

(Received September 24, 2020; Revised manuscript accepted January 3, 2021)

Abstract

The emerging interest in Arctic shipping driven by global warming results in a growing number of related academic publications. Considering the need for a systematic review that incorporates multiple perspectives of Arctic shipping on evaluating its economic feasibility, this study summarizes 60 selected publications made after 1999 that focus on eleven different aspects of the Arctic shipping including cost comparison of Arctic and conventional routes, environment concerns for navigating via Arctic routes, operational aspects, route choice modelling, feasibility of NSR (Northern Sea Route)/SCR (Suez Canal Route) combined service, criteria for choosing Arctic routes, navigation speeds, required freight rate, effects of Arctic shipping on other economics, engineering aspects of Arctic shipping, and Russian Arctic policy. Further, this review discusses their focused geographical markets, commodities, methodological aspects, factors for model developments, navigable periods, vessel sizes and types, sailing speeds, routing geometry, fuel types, and the feasibility of Arctic shipping. This review also highlights the limitations in previous studies especially due to the simplified assumptions made with transport cost models on fuel consumption, navigation speed, and vessels' engine specifications, among others if analyzing the economic feasibility of Arctic shipping.

Keywords: Arctic shipping, multiple perspectives, systematic review, economic feasibility

1. Introduction

The retreat of Arctic sea ice driven by global warming led to an emergent interest on Arctic shipping among researchers especially during the last decade (Theocharis and others, 2018) due to the potential cost and time saving of shipping via Arctic routes than the conventional routes (Pierre and Olivier, 2015; Stephenson and others, 2013; Xu and others, 2011). Apart from original research articles, several review articles (Lasserre, 2014; Meng and others, 2017; Theocharis and others, 2018) appeared although their scope was limited mainly to the comparative studies between the Arctic vs conventional routes and the commercial aspects of Arctic shipping. Owing to the high potential of Arctic shipping in the future, there is a need for a systematic review that focuses on the economic feasibility of Arctic shipping considering multiple perspectives that are summarized in a single article. Thus, this review aims to provide a better understanding of the economic feasibility of Arctic shipping by summarizing previous studies that focused on eleven different aspects.

As the remainder of this paper, Section Two explains the review method, and the results and discussion are given in Section Three. Finally, Section Four concludes the paper.

2. Review Method and Selection of Studies

Since this paper presents a systematic review of Arctic shipping, 60 research publications were selected for the review. To maintain quality, the majority of publications were selected from refereed international journals. First, we made a collection of studies using keywords such as Arctic shipping, Northeast Passage (NEP), Northwest Passage (NWP), and Northern Sea Route. Thereafter, we grouped the selected studies into eleven categories based on their main focus as explained in Section 3.1. Several publishers and databases including Scopus, Elsevier, Emerald Insight, and Taylor & Francis, among others were considered. The selected 60 papers were published in 33 international journals, two refereed international conferences, and one research organization as given in Table 1. Regarding their publication years (Fig. 1), the papers published on or after 1999 were selected and the majority were selected from the years 2017-2020 to provide a more updated review than the previous review articles.

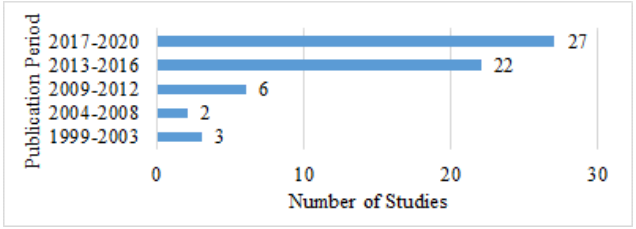

Fig. 1 Publication period of selected articles

Table 1. Sources of selected articles

Journal/Conference/Organization	No of Studies
Maritime Policy and Management	7
Journal of Transport Geography	5
Transportation Research Part A	5
Asian Journal of Shipping and Logistics	3
International Journal of Naval Architecture and Ocean Engineering	3
Climatic Change	2
International Journal of e-Navigation and Maritime Economy	2
International Northern Sea Route Programme (INSROP)	2
Maritime Economics and Logistics	2
The Polar Journal	2
Transport Policy	2
Arctic Review on Law and Politics	1
Canadian Journal of Remote Sensing	1
Geographical Review	1
Geophysical Research Letters	1
International Journal of Geographical Information Science	1
International Journal of Scientific & Technology Research	1
International Association of Maritime Economics Conference	1
Journal of Cleaner Production	1
Journal of Risk and Reliability	1
Journal of Ship Research	1
Maritime Business Review	1
Marine Policy	1
Ocean Engineering	1
Ocean Development and International Law	1
Polar Research	1
Polar Record	1
Port and Ocean Engineering under Arctic Conditions Conference	1
Research in Transportation Economics	1
Research in Transportation Business & Management	1
Safety Science	1
Scientific Reports	1
Ship Technology Research	1
The Cryosphere	1
Transportation Research Part D	1
Transportation Research Part E	1

3. Results and Discussion

This section discusses the results of the systematic review considering several subsections as follows.

3.1 Classification of Studies

Since this paper discusses the economic feasibility of Arctic shipping from multiple perspectives, selected 60 studies can be grouped into eleven categories as given in Table 2. Although a few studies focused on multiple aspects simultaneously, the categorization was done based on their main focus such that each study belongs to only one category. Accordingly, eight studies were selected on the cost comparison between Arctic routes and conventional routes. Among them, a majority focused on the comparison between NSR and SCR and a few on NWP, Panama Canal route, Cape route, and the Trans-Siberian railway. The environment and climate concerns for navigating through the Arctic sea were discussed by seven studies. They also focused on emission level, and impacts of global warming and climate change on the retreat of Arctic sea ice, among other issues.

Furthermore, eight studies focused on the operational aspects of Arctic shipping such as additional cost due to ice-water navigation, fuel types, and choice of ice-class, among others. The route choice between the Arctic and other routes were analyzed by five studies and some incorporated choice models to estimate the market share. Moreover, four studies focused on the feasibility of NSR/SCR combined service, which assumed the use of NSR during its navigable period and the SCR for the rest of the year. They focused on the network design for the combined service, scenario analysis with different navigable periods of NSR, vessel sizes, transit fees, and bunker price, among others. Further, the criteria for choosing Arctic shipping were discussed by two studies and they highlighted the significance of economic (e.g. time and distance saving), safety, and technical factors. Further, navigation speeds on Arctic routes were analyzed by three studies, and two studies calculated

Table 2. Categorization of previous studies

Category	Selected Studies
Cost comparison of Arctic routes and conventional routes	Cariou and others (2019), Ding and others (2020), Lasserre (2014), Otsuka and others (2013), Pruyn (2016), Shibasaki and others (2018), Theocharis and others (2018), Zhang and others (2016)
The environment and climate concerns for navigating through the Arctic sea	Chang and others (2015), Faury and Cariou (2016), Lindstad and others (2016), Meng and others (2017), Stephenson and others (2013), Yumashev and others (2017), Zhang and others (2018)
Operational aspects of Arctic shipping	Afenyo and others (2017), Erikstad and Ehlers (2012), Eguíluz and others (2016), Konygin and others (2015), Solakivi and others (2019), Tseng and Pilcher (2017), Wang and others (2018), Wang and others (2019)
Route choice models for the Arctic and conventional routes	Lasserre and Pelletier (2011), Lee and Song (2014), Wang and others (2018), Wang and others (2020), Zeng and others (2020)
Feasibility of NSR/SCR combined service	Furuichi and Otsuka (2014), Liu and Kronbak (2010), Xu and others (2018), Zhao and others (2016)
Criteria for choosing arctic shipping over other routes	Moon and others (2015), Tseng and Cullinane (2018)
Navigation speed on Arctic routes	Cariou and Faury (2015), Löptien and Axell (2014), Xu and others (2011)
Required freight rate on Arctic routes	Theocharis and others (2019), Somanathan and others (2009)
Effects of Arctic shipping on other economics	Ha and Seo (2014), Hong (2012), Rahman and others (2014), Sur and Kim (2020)
Engineering aspects of Arctic shipping	Aksenov and others (2017), Goerlandt and others (2017), Howell and Yackel (2004), Hu and Zhou (2015), Kamesaki and others (1999), Montewka and others (2019), Nam and others (2013), Overland and Wang (2007), Patey and Riska (1999), Spencer and Jones (2001), Wang and others (2020)
Russian Policy on Arctic Shipping	Bognar-Lahr (2020), Bognar (2016), Gritsenko and Kiiski (2015), Moe and Brigham (2017), Sevastyanov and Kravchuk (2020), Solski and others (2020)

the required freight rate for Arctic shipping services to cover all associated costs. Moreover, four studies analyzed the effects of Arctic shipping on other economics such as China and Korea, and they considered international cargo flows via Arctic routes for the analysis.

Due to the navigation via ice water, the economic feasibility of Arctic shipping is affected by its related engineering aspects. Although numerous studies are available on engineering aspects, only 11 studies were selected to highlight their focused issues. Accordingly, several studies analyzed the deforming of sea ice cover to examine the Arctic routes' navigability, sailing time with ice conditions, implications of ice-numerals on safe navigation, and the risks for vessels caused by ice drift and convoy collisions. Sea ice resistance and vessel's propulsion power were modeled incorporating vessel's specifications and hull-ice friction coefficient. Moreover, navigation speed reduction at environmental conditions such as ice concentration, ridge, and current direction was modeled. A few studies focused on route planning considering ice conditions, resistance, and net thrust provided by the ship and the effect of multiyear ice and various ice cover states on energy consumption.

Finally, the feasibility of Arctic shipping is greatly influenced by the Russian Arctic policy as summarized from six selected studies. They discussed the policy to develop NSR's transport-logistics aspects, the changes in Russian ice-breaking tariff, and Russian policy on building NSR's infrastructure by cooperating with other countries. They highlighted the conflict of interests with Russia in promoting independent navigation vs their income from icebreaker escorting, Russian policy to move their natural resources to global markets, and the competition between Russian state and private service providers on NSR activities. Several studies discussed the Russian policy on liberalizing the use of NSR by foreign actors vs increasing NSR's traffic by ships of Russian investors. Lastly, studies discussed the positions of Russia and Canada when negotiating the Polar code, and Russian jurisdictional claims on controlling the navigation of vessels via NSR.

Therefore, studies were selected covering multiple perspectives that influence the economic feasibility of Arctic shipping, which makes a significant contribution to the existing literature. The next few sub-sections discuss several important aspects of Arctic shipping which were summarized from all 60 studies.

3.2 Focused Geographical Markets, Shipping Routes, and Types of Commodities

Since the Arctic routes have different influences on individual markets, previous studies focused on various geographical markets as summarized in Fig. 2. Accordingly, that the majority of studies (14) included Japan or China as the origin/destination for shipping via Arctic routes could be due to their strategic locations in East Asia. Besides, Netherland (Rotterdam), German (Hamburg), and Russian ports were mainly included for the analysis. However, compared to Asian and European commercial ports, most Russian ports have a slightly different role as exporting ports of natural resources and some of them pursue becoming a hub of cargo transshipment. A few studies discussed the impacts of Arctic shipping on different regions such as Asia and Europe in general as their focused markets.

Fig. 2 Major countries/regions focused by studies

If considering the Arctic shipping routes focused by previous studies (Fig. 3), a majority of studies considered NSR/NEP (40) including the studies on Russian Arctic policy, and a few focused on NWP (6). However, 15 studies considered all Arctic routes in general. A comparatively less number of studies focused on the Trans-polar route could be due to the consistent presence of sea-ice and less developed ports and logistics infrastructure along this route.

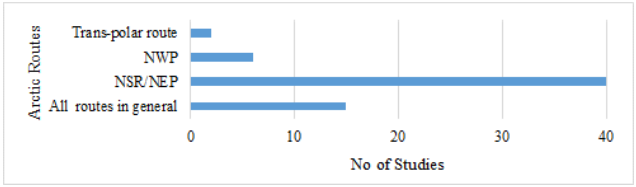

Fig. 3 Arctic shipping routes focused by studies

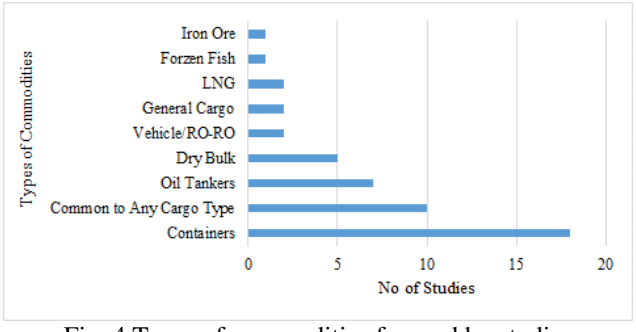

Fig. 4 Types of commodities focused by studies

As the types of commodities (Fig. 4), studies mainly focused on container cargo (18), implying the interests on Arctic routes from the liner shipping industry. The

oil tankers and dry bulk cargo were focused by a few studies possibly with the discovery of natural resources along the Arctic coast. However, several studies (10) discussed Arctic shipping in general to any cargo types.

3.3 Methodological Aspects

For the data analysis methods (Fig. 5), the majority of studies (13) considered transport cost models to compare the costs via Arctic routes with alternatives and the optimization and simulation models especially considering engineering aspects. The macroeconomics models were used by several studies to analyze the impacts of Arctic shipping on trade patterns among countries. A few studies (4) used Multi-Criteria Decision-making (MCDM) techniques for analyzing perception-based data. The potential use of AIS (Automatic Identification System) for modeling Arctic shipping aspects was highlighted by five studies. Besides, 10 studies considered qualitative approaches mainly for analyzing expert opinions on the Arctic shipping potential and discussing the Russian Arctic policy.

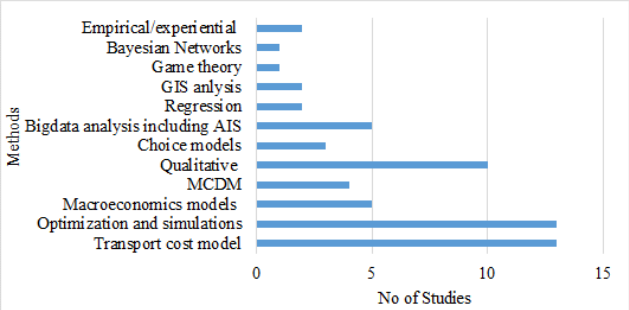

Fig. 5 Data analysis methods of previous studies

3.4 Factors Considered in Model Developments for Analyzing the Feasibility of Arctic Shipping

The feasibility of Arctic shipping was sensitive to the factors used in model development by previous studies as summarized in Table 3. Thus, the majority of studies (19) considered voyage costs including fuel cost, and a few studies considered different fuel consumption rates for arctic routes than conventional routes. Capital cost was significantly highlighted in many studies due to the higher ship-building cost (+10% by Otsuka and others (2013); +20%–30% by Zhao and others (2016)) when navigating through ice-water than the open water. Transit fees and ice-breaking fees of NSR, and canal toll of SCR were included in cost calculation with 16 studies and several studies (e.g. Liu and Kronbak; 2010; Zhao and others 2016) analyzed scenarios by changing NSR's transit fee. Besides, the insurance cost was significantly highlighted due to the risk associated with navigating through ice-water. Considering the impacts of Arctic shipping on the environment, the Carbon tax was incorporated in cost calculation by several studies (4). However, factors such as delays and waiting time, and exchange rates were incorporated by a limited number of studies.

In summarizing the factors considered in models for analyzing Arctic shipping feasibility (Table 3) and the various issues discussed from the studies that focused on engineering aspects of Arctic shipping, it is observed that most of those engineering aspects were not directly incorporated in economic feasibility analysis due to the simplified assumptions on average navigation speed for the entire route, fuel cost, and vessels' engine specifications, among others.

Table 3. Factors considered in model development

Factors Considered	No of Studies
Voyage cost, fuel cost, fuel consumption rates	19
Capital cost, depreciation cost	17
Transit fee, ice-breaking fee, canal toll	16
Insurance	12
Crew cost	12
Maintenance cost	11
Operating cost in general	10
Port charges	8
Ice condition, ice thickness	5
Carbon tax, emission	4
Load factor	3
Delays and waiting time	2
Port time	2
Exchange rates	1

3.5 Arctic Shipping Specific Considerations

3.5.1 Navigable Period

The navigable period has crucial impacts on the feasibility of Arctic shipping. Regarding the duration of the navigable period assumed by previous studies, the majority of studies highlighted the feasibility of summer navigation, although several studies (Furuichi and Otsuka, 2014; Ha and Seo, 2014; Liu and Kronbak, 2010; Shibasaki and others, 2018; Wang and others, 2018; Zhao and others, 2016) assumed multiple navigable periods as scenario analysis. Despite the ice condition, a few studies assumed all year navigation via Arctic routes. Besides, Xu and others, (2018) assumed a dynamic navigable window depending on the sea-ice extent.

3.5.2 Vessel Sizes and Types

Due to the differences in routes' geometry, the characteristics of vessels passing through Arctic routes can be different than those of conventional routes. Thus, Table 4 summarized the sizes and types of vessels used by previous studies if modeling traffic via Arctic routes. Considering the limitations with Arctic routes, the majority of studies assumed container vessels with less than 10,000 TEUs capacity, although a different range of capacities including larger vessels was assumed for scenario analysis by a few studies (3). In terms of bulk cargo vessels, Panamax vessels were used by the majority of studies including multiple vessel sizes for scenario analysis. Moreover, the majority of studies

assumed ice-classed vessels mainly 1A-class despite that a few studies did not consider ice-classed vessels. Further, the scenario analysis with different ice-classed vessels was done by a few studies (7).

Table 4. Sizes and types of vessels on Arctic routes

Study	Size	Type
Cariou and Faury (2015)	40,000 DWT Handymax	1A (IAS)
Theocharis and others (2019)	Suezmax, Aframax, Panamax, Handymax	1A (Arc4) ice class
Ding and others (2020)	9 ship sizes between 5089 - 21237 TEUs	ice-class
Erikstad and Ehlers (2012)	N.A.	Non-ice-class to 1AS ice class
Faury and Cariou (2016)	Panamax oil tanker	1A
Furuichi and Otsuka (2014)	6,500 CEU car carrier, 4,000 TEUs	Ice class
Ha and Seo (2014)	650, 4300, 5000, 8000 TEUs	DAS
Konygin and others (2015)	70 000 t DWT tanker	Arc 6
Lasserre (2014)	4500 TEU	1AS
Lindstad and others (2016)	Dry bulk (Panamax and Capesize)	N.A.
Liu and Kronbak (2010) Wang and others (2018)	4300 TEU	Ice class 1B
Otsuka and others (2013)	75,000 dwt (bulk), 147,500 m3 (LNG), 12,383GT (reefer)	Ice-class IA
Pruyn (2016)	11 ship sizes between 17,800- 289,400 DWT	ice-class 0, 1, 2, with given specifications, regular vessel with ice breaker
Shibasaki and others (2018)	147,500 m3, 172,000 m3, LNG carrier	Arc 4, Arc 7
Somanathan and others (2009)	N.A.	CAC3
Solakivi and others (2019)	7 ship sizes between 500–700 TEU, 10,000–12,000 TEU	IA and IAS Ice Class (FSCIR)
Stephenson and others (2013)	N.A.	PC3, PC6, open-water vessels with high, medium, and no ice-breaking capability
Xu and others (2011)	10,000 TEU	non-ice class
Xu and others (2018)	8000, 10 000, 12 000, 14 000 and 16 000 TEUs	ice-class 1A (Finnish-Swedish) or ARC4 (Russian)
Yumashev and others (2017)	> or < 2500 TEU, > or < 50,000 DWT (bulk)	ice-strengthened vessels in the future
Zhang and others (2016)	Panamax, Aframax	Arc 4
Zhao and others (2016)	4800 TEU	ice-strengthened ship

3.5.3 Vessel Sailing Speeds

Several studies assumed lower speed for vessels on Arctic routes than those on conventional routes (Ding and others, 2020; Furuichi and Otsuka, 2014; Lasserre, 2014; Pruyn, 2016; Shibasaki and others, 2018; Wang and others, 2018; Zhang and others, 2016). A few studies assumed multiple speed levels based on the ice-numeral (Somanathan and others, 2009; Zhang and others, 2018) or ice-thickness (Cariou and others, 2019; Xu and others, 2018; Olivier and Pierre, 2016). However, the majority of studies assumed the speed at ice water in between 10-15 knots although Pruyn (2016) assumed 9 knots with ice-breaker assistance.

3.5.4 Fuel Types for Vessels

Table 5 summarizes the fuel types assumed by previous studies for vessels navigating via Arctic routes. Accordingly, the majority assumed IFO 380 and some studies analyzed scenarios with multiple fuel types such as LFO, MGO, and LNG considering environmental aspects. Further, several studies assumed changes in fuel prices as scenarios without specifying the fuel types to understand the sensitivity of fuel price.

Table 5. Fuel types for vessels

Fuel Types	No of Studies
Intermediate Fuel Oil (IFO 380/IFO 180)	10
Marine Gas Oil (MGO)	5
Heavy Fuel Oil (HFO)	4
Liquified Natural Gas (LNG)	3
Light Fuel Oil (LFO)	2
Do not specify the fuel type	8

3.5.5 Routing Geometry

To enhance the accuracy of cost estimation, previous studies divided the entire Arctic route into different legs and zones. Studies assumed seven zones (Ding and others, 2020; Olivier and Pierre, 2016; Pierre and Olivier, 2015; Zhang and others, 2016) along the NSR based on NSR transit fee and ice pilotage fee and three legs along the NSR (Xu and others, 2011; Yumashev and others, 2017; Zhao and others, 2016) considering the sea ice condition. Chang and others (2015) assumed four zones based on the navigability along the NSR and Cariou and others (2019) assumed 49 subzones along the NSR based on ice thickness data from 2006 to 2016. Considering the NWP, Somanathan and others (2009) assumed 9 legs based on spatial and temporal variation of ice conditions.

3.6 Feasibility of Arctic Shipping

In summarizing the findings of previous studies, the majority of studies highlighted the feasibility of Arctic routes in general or under some conditions as listed in Table 6. The feasibility of Arctic routes was mainly highlighted at high fuel prices (5), with a long navigable period (4), with certain vessel sizes (4), for specific origins/destinations (4), when sea-ice diminishes (4) and with low transit fees (3). Moreover, Arctic routes were feasible with certain fuel types and with emission tax based on two studies. Significance of having a high load factor and average vessel speed was also highlighted. Considering the distance-saving effect, the feasibility of short-haul navigation was discussed. Conversely, 13 studies highlighted that Arctic routes

will not be feasible due to the number of reasons given in Table 6. Among them, the risk with weather conditions and a short navigable period (5), limited navigation speed (5), high cost of ice-class vessels (5), and ice-breaking and transit fees (5) were highlighted by the majority of studies.

Table 6. Feasibility of Arctic shipping

Feasibility of Arctic Shipping		No of Studies
Feasible in general		8
Feasible only at	High fuel prices	5
	Long navigable period	4
	Certain vessel sizes	4
	Specific origins/destinations	4
	Sea-ice diminishes	4
	Low transit fees	3
	Certain fuel types	2
	With emission tax	2
	Certain sailing speed	1
	High load factor/ cargo volume	1
	Independent sailing without ice-breaker	1
	High global emission	1
	Short-haul	1
Not feasible due to	Risk with difficult weather conditions and a short navigable period	5
	Limited navigation speed	5
	High cost of ice-class vessels	5
	Ice-breaking and transit fees	5
	Vessel size's restrictions on navigation paths	4
	High emission per unit cargo	3
	Low load factor/ cargo volume	2
	Under-developed infrastructure	2
	Supply chain risk and uncertainty	2
	Political and legal aspects	2
	Impacts of cold temperature on cargo	1
	Differences in navigational practices	1

The majority of studies quantitatively discussed the benefits of Arctic routes (e.g. 40% reduction of voyage distance with NSR than SCR according to Liu and Kronbak, 2010) and some as the reduction of sailing days and emission levels. A few studies evaluated the expert opinions on the feasibility of Arctic routes (e.g. Lasserre and Pelletier, 2011; Moon and others, 2015; Tseng and Pilcher, 2017). Several studies that concluded Arctic shipping as not feasible followed qualitative approaches, thus they could discuss negative aspects with various non-quantitative factors that were not incorporated in transport cost models. Moreover, the parameters, assumptions, input values, and target markets for cost calculations were different among studies, which could be a reason for deriving their different conclusions on the Arctic shipping feasibility. Besides, the difficulty in identifying all credible parameters to incorporate with model development might lead to diverse conclusions from previous studies. Thus, it is challenging to make a unified conclusion on the Arctic shipping feasibility from previous studies.

3.7 Limitations of Previous Studies and Future Research Directions

As the limitations of previous studies, the feasibility of Arctic routes was sensitive to the parameters used in their models. Some studies analyzed the feasibility for a single voyage, which did not consider the factors such as the number of possible round trips that can be made and a reduction in capital cost by reducing the number of vessels. Studies excluded important stakeholders such as shippers, port operators, and vessel owners. They barely considered the operational challengers with NSR/SCR combined service when changing routes twice a year, just-in-time operations in liner shipping, and the loss caused by excluding strong intermediate markets (e.g. Singapore, India) when using Arctic routes. The diseconomy of scale with small vessel sizes, opportunity cost with heavy vessels which limit the cargo-carrying capacity, and changes in load factors with Arctic routes were not highlighted by many studies. Studies on economic feasibility analysis barely incorporated detailed engineering aspects of sea-ice navigation such as multiyear ice and sea-ice resistance, among others discussed by related previous studies. Therefore, these limitations highlight the directions for further research.

4. Conclusion

This paper presents an updated review on Arctic shipping based on 60 selected articles published after 1999, that focus on cost comparison of Arctic vs. other routes, environmental and climate concerns, operational aspects of Arctic shipping, route choice, NSR/SCR combined service, criteria for choosing Arctic routes, sailing speed, required freight rate, effects on other economics, engineering aspects and Russian Arctic policy. Studies were summarized by highlighting their focused geographical markets, commodities, methodological aspects, factors for model developments, navigable periods, vessel sizes and types, sailing speeds, fuel types, routing geometry, the feasibility of Arctic shipping, and the limitations highlighted by them. Accordingly, Arctic routes were feasible mainly at high fuel prices, with a long navigable period, with certain vessel sizes, for specific origins/destinations, when sea-ice diminishes, and with low transit fees. However, the risk with weather conditions and a short navigable period, limited navigation speed, high cost of ice-class vessels, and ice-breaking and transit fees were highlighted as the main reasons for concluding the infeasibility of Arctic shipping. Studies mainly focused on container cargo, including Japan or China as origins/destinations, and considered summer navigation mostly with 1A-class vessels. Most studies used transport cost models for the feasibility analysis. However, apart from some operational aspects that were not incorporated by

previous studies, it is also important to incorporate sea-ice resistance, ships' propulsion systems, and variations of ice-thickness, among others if analyzing economic feasibility because they were highlighted as the important engineering aspects of Arctic shipping by related previous studies. Moreover, to confirm the economic feasibility, the Russian Arctic policy should promote the NSR's attractiveness regardless of their monopolistic features because the NSR is one alternative that is compared with other routing options in the global shipping market. Hence, this review develops a better initial understanding of Arctic shipping from multiple perspectives simultaneously. As the limitations, this review did not discuss the regulatory and political agreements of Arctic states which also influence the economic feasibility of Arctic shipping, thus they can be incorporated in further studies.

References

Afenyo, M., F. Khan and 2 others (2017): Arctic shipping accident scenario analysis using Bayesian Network approach. *Ocean Eng*. 133, 224-230.

Aksenov, Y., E.E. Popova and 5 others (2017): On the future navigability of Arctic sea routes: high-resolution projections of the Arctic ocean and sea ice. *Mar. Policy*. 75, 300–317.

Bognar-Lahr, D (2020): In the Same Boat? A Comparative Analysis of the Approaches of Russia and Canada in the Negotiation of the IMO's Mandatory Polar Code. *Ocean Dev. Int. Law*. 51(2), 143-161.

Bognar, D (2016): Russian Proposals on the Polar Code: Contributing to Common Rules or Furthering State Interests? *Arct. rev. law polit*. 7 (2), 111-135.

Chang, K.Y., S.S. Hea and 3 others (2015): Route planning and cost analysis for travelling through the Arctic Northeast Passage using public 3D GIS. *Int. J. Geogr. Inf. Sci*.

Cariou, P., A. Cheaitou., O. Faury and S. Hamdan (2019): The feasibility of Arctic container shipping: the economic and environmental impacts of ice thickness. *Marit Econ Logist*.

Cariou, P. and O. Faury (2015): Relevance of the Northern Sea Route (NSR) for bulk shipping. *Transp. Res. Part A*. 78, 337–346.

Ding, W., Y. Wang., L. Dai and H. Hu (2020): Does a carbon tax affect the feasibility of Arctic shipping?. *Transp. Res. Part D*. 80: 102257.

Eguíluz, V., Fernández-Gracia, J. and 2 others (2016): A quantitative assessment of Arctic shipping in 2010–2014. *Sci Rep*. 6, 30682.

Erikstad, S.O. and S. Ehlers (2012): Decision Support Framework for Exploiting Northern Sea Route Transport Opportunities. *Ship Technol. Res*. 59 (2).

Faury, O. and P. Cariou (2016): The Northern Sea Route competitiveness for oil tankers. *Transp. Res. Part A*. 94, 461-469.

Furuichi, M. and N. Otsuka (2014): Economic feasibility of finished vehicle and container transport by NSR/SCR-combined shipping between East Asia and Northwest Europe. *International Association of Maritime Economics*, July 15-18, Norfolk, VA, USA.

Goerlandt, F., J. Montewka and 2 others (2017): An analysis of ship escort and convoy operations in ice conditions. *Saf. Sci*. 95, 198–209.

Gritsenko, D. and T. Kiiski (2015): A review of Russian ice-breaking tariff policy on the northern sea route 1991–2014. *Polar Rec.* 52 (263), 144-158.

Ha, Y.S. and J.S. Seo (2014): The Northern sea routes and Korea's trade with Europe: Implications for Korea's Shipping Industry. *Int. J. e-Navigation and Marit. Econ.* 1: 73-84.

Hong, N. (2012): The melting Arctic and its impact on China's maritime transport. *Res. Transp. Econ.* 35(1), 50-57.

Howell, S.E.L. and J.J. Yackel (2004): A vessel transit assessment of sea ice variability in the Western Arctic, 1969–2002: implications for ship navigation. *Can. J. Remote Sensing*, 30 (2), 205–215.

Hu, J. and L. Zhou (2015): Experimental and numerical study on ice resistance for icebreaking vessels. *Int. J. Nav. Archit. Ocean Eng*. 7, 626~639.

Kamesaki, K., S. Kishi and Y. Yamauchi (1999): Simulation of NSR shipping based on year round and seasonal operation scenarios. INSROP Working Paper No. 164.

Konygin, A., S. Nekhaev and 4 others (2015): Oil tanker transportation in the Russian arctic. *Int. J. Sci. Technol. Res.* 4, 03.

Lasserre, F (2014): Case studies of shipping along Arctic routes. Analysis and profitability perspectives for the container sector. *Transp. Res. Part A*. 66: 144–161.

Lasserre, F. and S. Pelletier (2011): Polar super seaways? Maritime transport in the Arctic: an analysis of shipowners' intentions. *J. Transp. Geogr.* 19, 1465-1473.

Lee, S.W. and J.M. Song (2014): Economic possibilities of shipping though Northern Sea route. *Asian J. Shipping Logist*. 30 (3), 415-430.

Lindstad, H., R.M. Bright and A.H. Strømman (2016): Economic savings linked to future Arctic shipping trade are at odds with climate change mitigation. *Transp. Pol.* 45: 24-30.

Liu, M and J. Kronbak (2010): The potential economic viability of using the Northern Sea Route (NSR) as an alternative route between Asia and Europe. *J. Transp. Geogr*. 18, 434–444.

Loptien, U. and L. Axell (2014): Ice and AIS: ship speed data and sea ice forecasts in the Baltic Sea. *The Cryosphere*. 8, 2409–2418.

Meng, Q., Y. Zhang and M. Xu (2017): Viability of transarctic shipping routes: a literature review from the navigational and commercial perspectives. *Marit. Pol. Manage.* 44(1), 16-41.

Moe, A. and L. Brigham (2017): Organization and Management Challenges of Russia's Icebreaker Fleet. *Geogr. Rev.* 107 (1), 48-68.

Montewka, J., F. Goerlandt and 3 others (2019): Toward a hybrid model of ship performance in ice suitable for route planning purpose. *J. Risk and Reliability*. 233 (1), 18–34.

Moon, D.S., D.J. Kim and E.K. Lee (2015): A Study on Competitiveness of Sea Transport by Comparing International Transport Routes between Korea and EU. *Asian J. Shipping Logist.* 31 (1), 001-020.

Nam, J.H., I. Park and 4 others (2013): Simulation of optimal arctic routes using a numerical sea ice model based on an ice-coupled ocean circulation method. *Int. J. Naval Archit. Ocean Eng*. 5, 210-226.

Otsuka, N., K. Izumiyama and M. Furuichi (2013): Study on Feasibility of the Northern Sea Route from Recent Voyages. *22nd International Conference on Port and Ocean Engineering under Arctic Conditions.* June 9-13, Espoo, Finland.

Overland, J.E. and M. Wang (2007): Future regional Arctic sea ice declines. *Geophys. Res. Lett*. 34, L17705.

Patey, M. and K. Riska (1999): Simulation of Ship Transit Through Ice, INSROP Working Paper No.155.

Pruyn, J.F.J (2016): Will the Northern Sea Route ever be a viable

alternative?. *Marit. Pol. Manage.* 43(6), 661-675.
Rahman, N.S.F.A., A.H. Saharuddin and R. Rasdia (2014): Effect of the Northern Sea Route Opening to the Shipping Activities at Malacca Straits. *Int. J. e-Navigation and Marit. Econ.* 1, 85-98.
Sevastyanov, S. and A. Kravchuk (2020): Russia's policy to develop trans-arctic shipping along the Northern sea route. *The Polar Journal.*
Shibasaki, R., T. Usami and 3 others (2018): How do the new shipping routes affect Asian liquefied natural gas markets and economy? Case of the Northern Sea Route and Panama Canal expansion. *Marit. Pol. Manage.*
Solakivi, T., T. Kiiski and L. Ojala (2019): On the cost of ice: estimating the premium of Ice Class container vessels. *Marit Econ Logist.* 21, 207–222.
Solski, J.J., T. Henriksen and A. Vylegzhanin (2020): Introduction: regulating shipping in Russian Arctic Waters: between international law, national interests and geopolitics. *The Polar Journal*.
Somanathan, S., P. Flynn and J. Szymanski (2009): The Northwest Passage: A simulation. *Transp. Res. Part A*. 43, 127–135.
Spencer, D. and S.J. Jones (2001): Model-Scale/Full-Scale Correlation in Open Water and Ice for Canadian Coast Guard "R-Class" Icebreakers. *J. Ship Res*. 45 (4), 249–261.
Stephenson, S.R., L.C. Smith and 2 others (2013): Projected 21st-century changes to Arctic marine access. *Clim. Change.* 118, 885–899.
Sur, J. M. and D.J. Kim (2020): Multi criteria evaluation of beneficial effect of commercializing Northern Sea Route on Europe and Asia countries. *Asian J. Shipping Logist.*
Theocharis, D., S. Pettit and 2 others (2018): Arctic shipping: A systematic literature review of comparative studies. *J. Transp. Geogr.* 69, 112-128.
Theocharis, D., V.S. Rodrigues., P. Stephen and J. Haider (2019): Feasibility of the Northern Sea Route: The role of distance, fuel prices, ice breaking fees and ship size for the product tanker market. *Transp. Res. Part E.* 129: 111–135.
Tseng, P. and N. Pilcher (2017): Assessing the shipping in the Northern Sea Route: a qualitative approach. *Marit. Bus. Rev.* 2 (4), 389-409.
Tseng, P. and K. Cullinane (2018): Key criteria influencing the choice of Arctic shipping: a fuzzy analytic hierarchy process model. *Marit. Pol. Manage.* 45(4), 422-438.
Wang, C., X. Hu and 3 others (2020): Numerical simulation of ice loads on a ship in broken ice fields using an elastic ice model. *Int. J. Naval Archit. Ocean Eng*. 12, 414-427.
Wang, Y., R. Zhang and 2 others (2018): Investigating the effect of Arctic sea routes on the global maritime container transport system via a generalized Nash equilibrium model. *Polar Research.* 37(1), 1547042.
Wang, H., Y. Zhang and Q. Meng (2018): How will the opening of the Northern Sea Route influence the Suez Canal Route? An empirical analysis with discrete choice models. *Transp. Res. Part A*, 107, 75-89.
Wang, Z., J.A. Silberman and J.J. Corbett (2020): Container vessels diversion pattern to trans-Arctic shipping routes and GHG emission abatement potential. *Marit. Pol. Manage.*
Wang, D., D. Li and 4 others (2019): Development situation and future demand for the ports along the Northern Sea Route, *Res. Transp. Bus. Manag.* 33.
Xu, H., Z. Yin and 3 others (2011): The potential seasonal alternative of Asia–Europe container service via Northern sea route under the Arctic sea ice retreat. *Marit. Pol. Manage.* 38:5, 541-560.
Xu, H., D. Yang and J. Weng (2018): Economic feasibility of an NSR/SCR-combined container service on the Asia-Europe lane: a new approach dynamically considering sea ice extent. *Marit. Pol. Manage.*. 45(4), 514-529.
Yumashev, D., K.V. Hussen and 2 others (2017): Towards a balanced view of Arctic shipping: estimating economic impacts of emissions from increased traffic on the Northern Sea Route. *Climatic Change.* 143, 143–155.
Zeng, Q., L. Tingyu and 3 others (2020): The Competitiveness of Arctic Shipping over Suez Canal and China-Europe Railway. *Transp. Pol.*
Zhang, Y., Q. Meng. and S.H. Ng (2016): Shipping efficiency comparison between Northern Sea Route and the conventional Asia-Europe shipping route via Suez Canal. *J. Transp. Geogr.* 57, 241–249.
Zhao, H., H. Hua and Y. Lin (2016): Study on China-EU container shipping network in the context of Northern Sea Route. *J. Transp. Geogr.* 53, 50–60.
Zhang, Z., D. Huisingh and M. Song (2018): Exploitation of trans-Arctic maritime transportation. *J. Clean. Prod.* 212, 960-973.

Summary in Japanese

和文要約

多様な観点に基づく北極海輸送の経済的実現性に関する体系的レビュー

Chathumi Ayanthi Kavirathna[1], 柴崎隆一[1]
[1] 東京大学

地球温暖化を契機とする北極海輸送への関心の高まりにより，最近では多くの関連研究が発表されている．本研究は，北極海輸送の経済的実現性を多様な観点から評価する体系的な研究レビューを行うことを目的に，1999年以降に出版された北極海輸送に関する60編の研究論文・報告書を整理し，その主目的に応じて11の分野に分類した．具体的には，北極海輸送と他ルートとのコスト比較，北極海航行時における環境への影響，運航に関する検討，輸送ルート選択モデル，既存ルートとの混合輸送の実現可能性，北極海輸送利用の基準，航行速度，通航料金の水準，北極海輸送利用による経済的影響，北極海輸送に関する工学的側面，そしてロシアの北極政策である．さらに，各研究の対象地域と品目，分析手法，分析において着目した要素，航行可能期間や船舶のサイズ・アイスクラス・速度に関する想定，分解能，燃料の種類，各研究において得られた北極海輸送が成立する条件についても整理した．また，特に北極海輸送の経済的実現性を検討するにあたり，多くの既存の輸送費用算定モデルにおいて燃料消費，航行速度，エンジン規格等のもたらす影響が十分に考慮されていないことなど，既存研究の限界についても明らかとした．

Correspondence to: C.A.Kavirathna,
chathumiayanthi@gmail.com

Okhotsk Sea and Polar Oceans Research 5 (2021) 23-30

https://doi.org/10.57287/ospor.5.23

Article

Impact of sea-ice cover on storm-mediated atmospheric warming over the Barents Sea: A regional modelling study

Atsuyoshi MANDA[1]

[1]*Graduate School of Bioresources, Mie University, Tsu, Japan*

(Received October 31, 2020; Revised manuscript accepted January 13, 2021)

Abstract

Sea-ice loss is believed to be one of the key processes in the recent Arctic warming. This study examines the impact of sea-ice cover on the atmospheric warming associated with cyclones. Although cyclones are an important component in the Arctic climate system, details regarding the process of heat transfer during life cycles of cyclones remain unclear. The cyclone that occurred over the Barents Sea in January 21–25, 2011 was selected as the test case given that it was well validated using in-situ data. The results of numerical simulations showed that the changes in surface heat fluxes and net long-wave radiation owing to sea-ice cover changes resulted in atmospheric warming via vertical diffusion, countered by cold advection within the atmospheric boundary layer, which corroborates earlier studies. The simulations also showed that sea ice decline intensified the advection of warm air over areas north of the sea-ice edge resulting from the southerlies associated with the cyclone and caused further atmospheric warming east of Svalbard. It was also observed that a large fraction of warmed air parcels traveled well above the top of the boundary layer. This enhanced "on-ice" flow regime and upglide of the warmed air parcels associated with cyclones could play a role in spreading out the effect of anomalous heat supply due to the sea-ice decline and contribute to further atmospheric warming in the Arctic during winter.

Keywords: cyclone; Arctic amplification; heat transport; polar WRF

1. Introduction

Over the past decades, rapidly enhanced atmospheric warming has been observed in the Arctic. This warming, a phenomenon known as Arctic amplification (AA), has been occurring at the Arctic at a much faster rate compared with the rest of the world, and it is more pronounced in the lower troposphere during the cold season than during other seasons. Sea-ice cover in the Arctic exhibits a continued and drastic decline (Fig. 1; Norwegian Polar Institute, 2020). Such decline in sea-ice cover affects the energy exchange between the ocean and the atmosphere, and this is a key factor associated with the accelerated warming observed in the Arctic (Screen and Simmonds, 2010; Dai and others, 2019). Particularly, significant sea-ice reduction that can influence cold winter extremes over the Eurasian continent have been observed over the Barents and Kara Seas (Inoue and others, 2012; Mori and others, 2019), and a recent study has shown that improving the accuracy of Arctic temperature forecasts offers potential for better prediction of Arctic-midlatitude teleconnection patterns as well as seasonal prediction in mid-latitudes during winter (Jung and others, 2020).

Several mechanisms, including the central role of sea-ice loss, have been proposed to explain the AA; however, their relative importance with respect to Arctic warming is still disputed. Both recent data analysis and numerical modelling studies have emphasized the importance of surface heat fluxes in AA (Dai and others, 2019; Kim and others, 2019). One of the interesting issues here is atmospheric heat transport. During winter, vertical temperature profiles exhibit strong stable conditions with the frequent occurrence of strong inversions in the Arctic. Such atmospheric environments prohibit vertical heat transfer across the top of the boundary layer. However, inspecting only surface fluxes cannot clarify whether the intensified vertical diffusion associated with destabilization near the surface is the sole mechanism for the vertical heat transport.

It is well known that cyclones constitute an important component of the Arctic climate system (Serreze, 1995). They can also affect the concentration and melting of sea ice (Boisvert and others, 2016). Cyclone activity largely determines the variability and changes of sea ice export from the central Arctic Ocean into the Greenland–Iceland–Norwegian Sea through Fram Strait (Wei and others, 2019). This transport comprises the largest portion of the total Arctic sea ice export (Serreze and others, 2006) and plays an important role with the drastic retreat and thinning of Arctic sea ice cover in recent years (Wei and others, 2019). Small scale cyclones in the Arctic (polar lows) affect the short-term variations of

inflow of Atlantic warm water through the Fram Strait (Sun and Gao 2018).

Cyclones can intensify surface heat fluxes via stronger surface winds. Inoue and Hori (2011) and Manda and others (2020; hereinafter referred to as M20) suggested the importance of cyclones in the storm-mediated atmospheric warming in the lower troposphere, which possibly plays a role in the recent Arctic warming. However, the effect of sea-ice cover on this process has not yet been examined.

The aim of this study is to elucidate the impact of the sea-ice cover on storm-mediated atmospheric warming. A number of numerical simulations have been performed in previous studies to examine the effect of sea-ice loss on atmospheric circulation and thermodynamic fields in the Arctic (Screen and others, 2018). However, most of these studies were focused on large scale climatological fields. Details regarding the process of heat transfer during life cycles of cyclones are still unclear. This study focuses on the cyclone that was observed in January 2011 over the Barents Sea, documented in M20. The Barents Sea is one of the areas with the highest cyclone occurrence frequency in the Arctic during winter (Raible and others, 2008). Using in-situ atmospheric soundings and surface meteorological observations, this cyclone has been realistically simulated and well validated (M20). It provides assurance regarding the reliability and suitability of the simulated results for the sensitivity experiments documented in this paper.

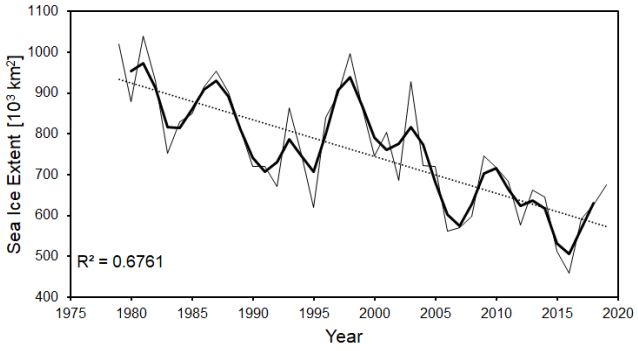

Fig. 1 Time series of changes in sea-ice extent in the Barents Sea in April, averaged over the area demarcated by latitudes 72°N and 82°N and longitudes 10°E and 60°E. The thin and thick solid lines represent monthly mean values for each year and smoothed values using the 1-2-1 filter, respectively. The dotted line represents a linear regression.

In recent studies, an increasing trend of cyclone frequency and intensity in the Arctic has been reported and a possible link with sea-ice loss has also been suggested (Rinke and others, 2017; Zahn and others, 2018; Akperov and others, 2020). The results of this study will enhance understanding regarding recent Arctic warming, and will contribute to the projection of such warming in future.

The rest of this paper is organized as follows. The data and methods used in the study are described in Section 2, and in Section 3, the results of the numerical simulations are presented. Finally, a summary and a brief discussion are provided in Section 4.

2. Data and Method

2.1 Atmospheric model

To elucidate the effect of sea-ice cover on atmospheric warming during the life cycle of a cyclone, numerical simulations were performed. For the most part, the set-up of the model was similar to those used in M20, with some minor modifications. Details regarding the model set-up can be obtained from M20. To perform the simulations, the polar-optimized Weather Research and Forecasting model (Polar WRF; version 3.7.1) developed by Hines and Bromwich (2008) was used, rather than version 3.5.1 that was used in M20. Instead of European centre for medium-range weather forecasts interim reanalysis data (Dee and others, 2011), fifth generation atmospheric reanalysis data obtained from the European Centre for medium-range weather forecasts (ERA5; Hersbach and others, 2020) was employed for the initial and boundary conditions of the prognostic variables of the model, including sea-surface temperature (SST) and sea-ice concentrations. All other set-ups, including sub-grid scale parameterizations and model grid spacings, were the same as those in M20. Only slight differences existed between the WRF models, the atmospheric data, and the oceanic data corresponding to M20 and those corresponding to this study. We also confirmed that relative to M20, the modifications described above had little effect on the life cycle of the simulated cyclone.

2.2 Numerical experiments

To examine the impact of sea-ice cover on the atmospheric warming, two ensemble experiments, namely the control (CNTL) and high ice (HICE) experiments, were conducted. The CNTL experiment was carried out to reproduce the life cycle of the observed cyclone, in accordance with M20. In the HICE experiment, the set-ups employed were almost the same as those in the CNTL experiment; however, to elucidate the impact of sea-ice cover in different years, the sea-ice cover in 1981, during which the extent of the sea-ice cover was much higher than that in 2011, was utilized. All other conditions were similar to those employed in the CNTL experiment. The only difference between the CNTL and HICE experiments was sea-ice cover. To examine the sole effect of sea-ice cover, we adopted this strategy based on previous studies (Magnusdottir and others, 2004; Higgins and others, 2009; Deser and others, 2010). Behavior of cyclones can be affected by many

processes, including low-level baroclinicity, static stability (Akperov and others, 2020), and upper-level potential vorticity (PV) anomaly (M20). They can complicate the response of the simulated cyclone and may obscure the impact of the sea-ice cover.

To evaluate the uncertainty resulting from internal model variability, each ensemble experiment consisted of 23 hindcast simulations with different initial times (Bassett and others, 2020), unlike the previous modeling study (Adakudlu and Barstad, 2011). From 01 UTC January 19, 2011, time integration of each ensemble member was started at 1-h intervals until 00 UTC January 20, 2011. From this point, all the 23 members were run for a further 5-day period, ending on 00 UTC January 25, 2011. The data corresponding to the period before 00 UTC January 21, 2011 was discarded as spin up, following the strategy used in Bassett and others (2020).

3. Results

Figure 2 shows the tracks of the simulated cyclones, which were found to be very similar to those in M20 (Fig. 6 of M20). After initiated east of Greenland, they moved eastwards towards the sea ice edge east of Svalbard.

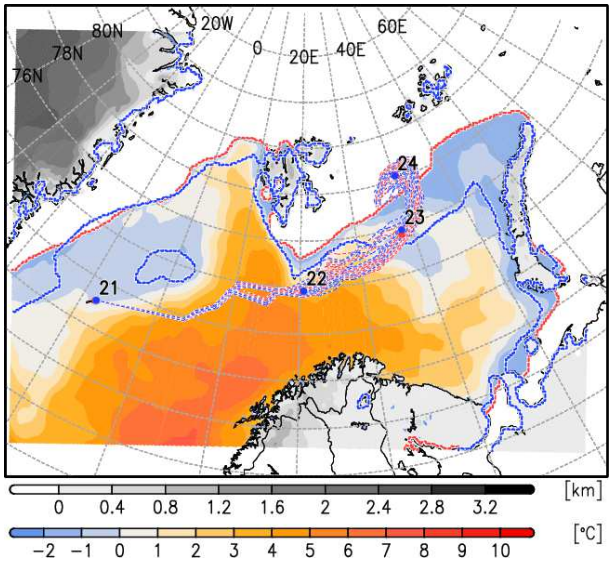

Fig. 2 Tracks of the simulated cyclones. The red and blue lines indicate the CNTL and HICE experiments, respectively. The dots indicate the location of the cyclone centers of the ensemble means at 00 UTC on the date represented by numerals. The thick dotted lines represent the sea-ice edge. Color, and black and white shades indicate SST and topography, respectively.

They were almost stationary after January 24th. The tracks in CNTL were very similar to those in HICE, indicating that differences in sea-ice cover do not have a significant impact on the track of the cyclones. This is consistent with the findings of M20, which showed that the shutting off of surface heat fluxes changed the cyclone tracks to a limited extent. This observation is partly due to the dominance of the upper-level PV anomaly with respect to cyclone development, as shown in M20, and like in M20, the CNTL also reproduced the observed wind and temperature fields well (figure not shown).

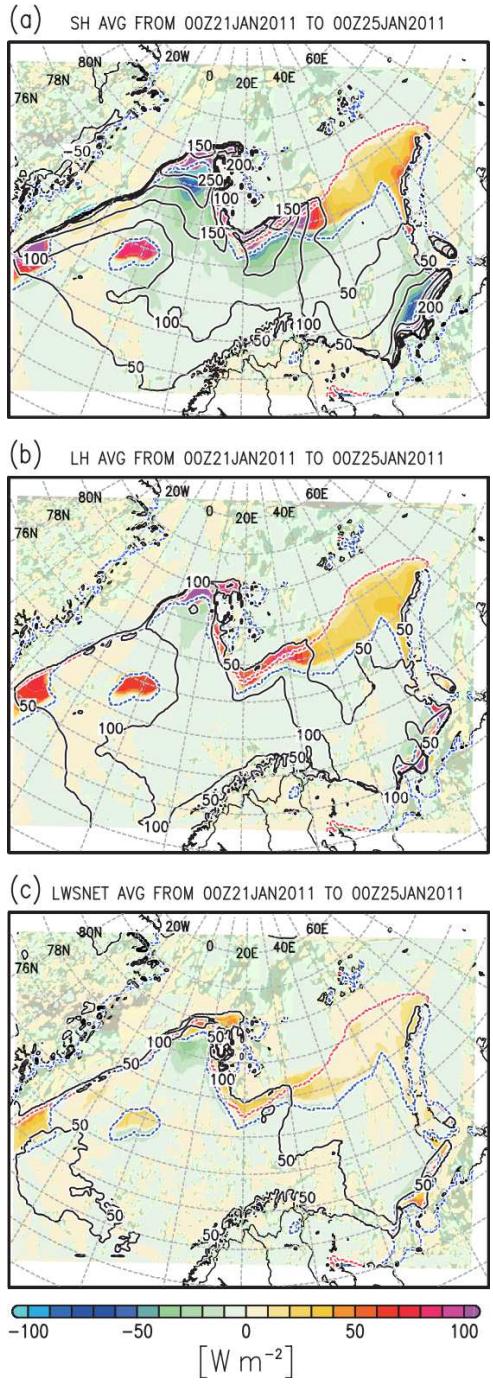

Fig. 3 Horizontal distributions of (a) SHF, (b) LHF, and (c) net LWR, averaged from 00 UTC January 21–25, 2011 (positive upward). The colors indicate differences in ensemble means between the CNTL and HICE experiments. The black contours indicate values in CNTL.

Figure 3 depicts the ensemble means of the surface heat fluxes, averaged from 00 UTC January 21–25, 2011 between the CNTL and the HICE experiments. Areas of surface heat flux change generally correspond to that of the sea ice cover. The sensible heat flux (SHF) in CNTL showed large values around the sea-ice edge west of Svalbard (Fig. 3(a)). This could be attributed to the cold air outbreak that occurred after January 22, 2011 (Fig. 5(a), M20). The latent heat flux (LHF) and net long-wave radiation (LWR) exhibited a similar tendency.

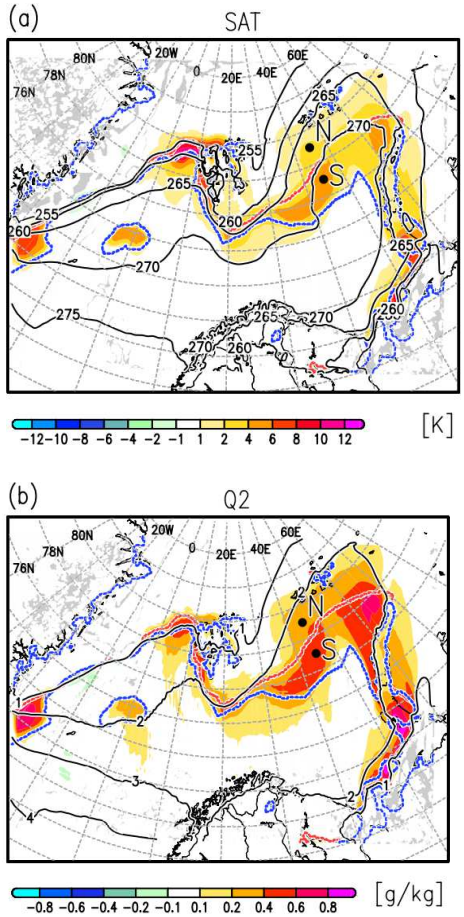

Fig. 4 Same as Fig. 3, but for (a) SAT and (b) Q2. The dots with N and S indicate the locations where the data in the time-height diagrams in Fig. 5 are sampled.

Figure 4 shows the horizontal distributions of the SAT and Q2, which is defined as the values at a height of 2 m. The areas where SAT and Q2 showed positive anomaly basically corresponded with those of the positive surface flux anomalies, e.g., the eastern coast of Greenland, an isolated sea-ice area located around 76°N, 0°E in 1981, west of Svalbard, and around the sea-ice edge from the south of Svalbard to Novaya Zemlya, suggesting the importance in local energy balance such as vertical heat transport and diabatic processes in most areas with positive SAT. On the other hand, positive SAT and Q2 anomalies farther north of the sea-ice edge east of Svalbard were found (north of 76°N and east of 30°E). These areas were found to be covered by sea ice where the surface fluxes do not heat the atmosphere directly in both the CNTL and HICE experiments, suggesting a heating mechanism other than vertical diffusion.

As expected, these surface fluxes in CNTL were larger than those in HICE over the ice-free area in CNTL. The magnitude of the positive anomaly of the LWR was relatively small, compared with those of SHF and LHF. Some areas with negative values resulted from the gaps in the location of the local maxima in these fluxes between CNTL and HICE. For example, negative SHF anomaly on the west of Svalbard is associated with the higher surface air temperature (SAT; Fig. 4b) due to the intensified SHF in CNTL north of the negative SHF anomaly.

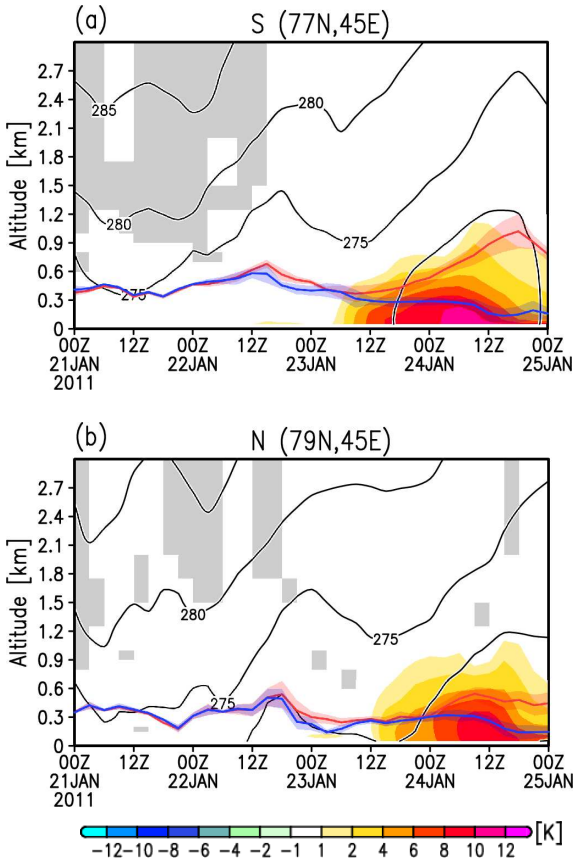

Fig. 5 Time-height diagrams of the PT in CNTL (contour) and its difference between CNTL and HICE (color) at points (a) S and (b) N shown in Fig. 4. The areas that are not gray-shaded indicate that the differences are statistically significant at a 5% confidence level. The red and blue lines indicate a boundary layer top. The transparent color shades indicate one standard deviations from the ensemble means.

Figure 5 shows the temporal evolution of the potential temperature (PT) at the points north and south of the sea-ice edge east of Svalbard, denoted "S" and "N" in Fig. 4, respectively. After 06 UTC January 23, 2011, CNTL showed higher PT in the lower troposphere at S as the boundary layer height rose. Contrarily, the boundary layer height in HICE declined gradually. On the other hand, the CNTL experiment exhibited higher PT at N after 12 UTC January 23, 2011, and the high PT anomaly appeared well above the top of the boundary layer at N, unlike the case with S. These results also indicate that the heating mechanisms at S and N are different.

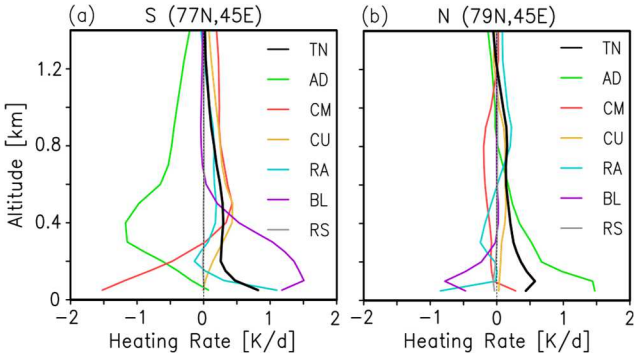

Fig. 6 Vertical profile of the difference in each term in the heat budget equation between CNTL and HICE at (a) S and (b) N, averaged within the January 23–25, 2011 period. TN represents tendency (rate of time change) of PT to change. AD, CM, CU, RA, and BL indicate heating terms due to advection, cloud microphysics, cumulus, radiation, and turbulence closure schemes, respectively. RS indicates the residual term, which is mainly due to numerical truncation errors.

Figure 6 shows the vertical profile of the difference in each term of the energy conservation (heat budget) equation between CNTL and HICE, averaged from 00 UTC January 23–25, 2011 at S and N. Positive values indicated that CNTL exhibits larger values compared with HICE. Specifically, at S, warmer air in the lower part of the troposphere was mainly caused by vertical diffusion and near surface radiation (Fig. 6(a)). The radiation term only consisted of LWR. Short-wave radiation was zero since the simulation corresponded to the polar night period. Advection counteracted this heating and cooled the air column. This advective cooling was caused by the cold air outbreak that occurred west of Svalbard and the counterclockwise circulation associated with the cyclone (Fig. 5 of M20). Near surface cooling by the cloud microphysics schemes in CNTL was presumably attributed to the upward displacement of the cloud base height associated with the destabilization of the air column. The heat balance in other areas with positive SAT anomalies was very similar to that at S, i.e., heating resulting from vertical diffusion counteracted by horizontal advection (figure not shown).

The heating mechanism at N was different from that at S (Fig. 6(b)), and the anomalous heating of the air column was predominantly caused by advection. This advective heating was counteracted by the cooling that resulted from vertical diffusion and radiation. Their roles were found to be opposite those observed at S. After January 23, 2011, the cyclone was almost stagnant and stayed close to the sea-ice edge east of Svalbard (Fig. 1). Additionally, this cyclone caused prolonged southerlies east of the cyclone center and kept conveying warm air farther northward of the sea-ice edge (Fig. 7), where SHF and LHF were shielded and could not heat the air just above the surface. The warming process over the ice-covered area is not caused by the surface turbulent heat fluxes but by the advection term. This is a typical "on-ice" flow regime when a stable internal boundary layer develops just over the ice cover (Brümmer and Thiemann 2002; Vihma and others 2003). The southerlies in the eastern sector of the cyclone in CNTL is stronger than that of HICE (Fig. 7a), indicating that the warm advection is intensified by the anomalous winds. Serreze and others (2011) show that prominent positive temperature anomaly east of Svalbard in winter during the period of 2000-2009 corresponds to the warm advection by the anomalous wind. They also suggested the anomalous winds tend to spread out horizontally the effects of the surface heat source. The sensitivity experiment in this study reveals that the enhanced on-ice flow plays a role in spreading out the effect of intensified surface heat fluxes due to the sea-ice decline.

Figure 8 shows the forward trajectories of the air parcels released at a height of 100 m close to 76°N, 45°E. Twenty-five parcels were tracked from 00 to 12 UTC January 24, 2011 in each ensemble member. Thus, a total of 575 (25 × 23) parcels were used in each ensemble experiment. In both experiments, all the parcels were transported northward by the southerlies in the eastern sector of the cyclone, with slight counterclockwise turning. The latitude-height diagram showed that the air parcels in CNTL were transported further north than those in HICE (Fig. 8(b)). Additionally, the air parcels in HICE traveled at almost constant levels close to the surface without rising. The ensemble means of the height of the air parcels were well above those of the boundary layer height north of 79.6°N, and 59% of the parcels in CNTL were at least 10 m above the top of the boundary layer at 12 UTC January 24, 2011. On the other hand, only 18% of the parcels showed satisfaction with this criterion in HICE. Thus, there was a much higher chance that the air parcels heated in the boundary layer in CNTL were transported into the free troposphere, compared with those in HICE.

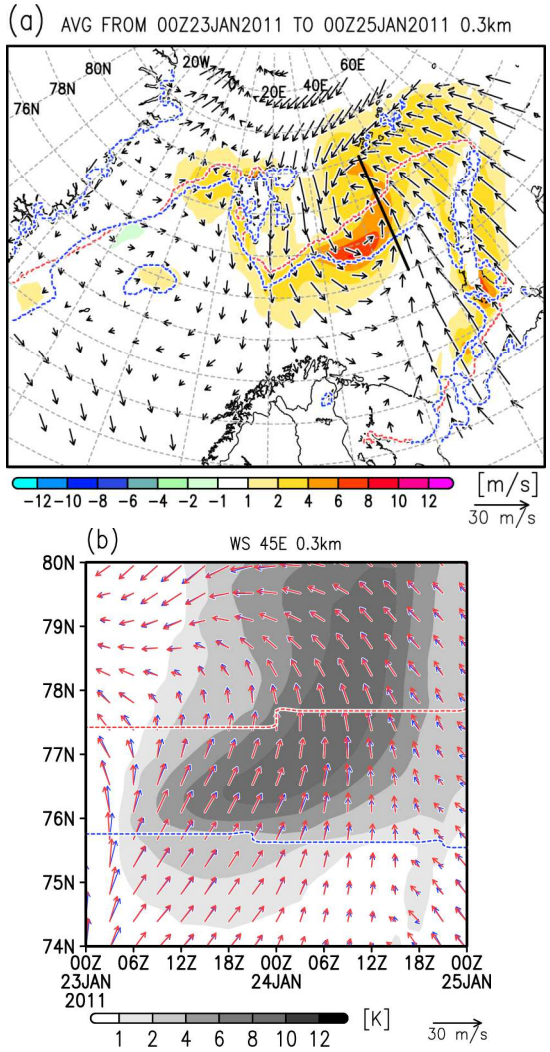

Fig. 7 (a) Horizontal wind in CNTL (vector) and difference in wind speed between CNTL and HICE (color) at a height of 300 m, averaged within the January 23–25, 2011 period. (b) Time-latitude diagram of horizontal winds and difference in PT between CNTL and HICE at a height of 300 m along the thick solid line in (a).

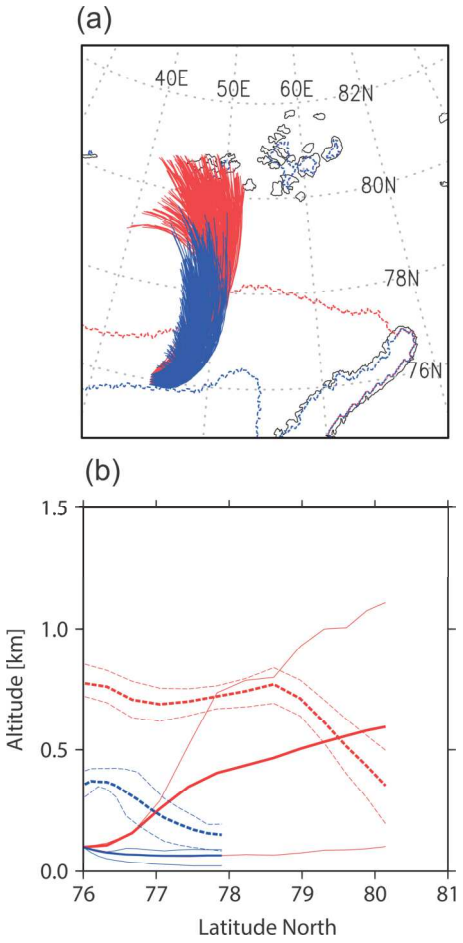

Fig. 8 (a) Forward trajectories of air parcels released at 00 UTC January 24, 2011 in the area centered at 76°N and 45°E. The dashed lines in red and blue indicate the sea-ice edge in CNTL and HICE, respectively. (b) Latitude-height diagram of the ensemble means of trajectories (thick solid lines) and boundary layer height (thick dashed lines). The thin lines indicate 25 and 75% percentiles, and the red and blues lines indicate CNTL and HICE, respectively.

The static stability in the lower troposphere is very strong during winter in the Arctic. Strong inversion in the lower troposphere tended to prohibit the transportation of heat from the boundary layer to the free troposphere. Without certain atmospheric disturbances like cyclones, the possibility of transporting warmed air in the boundary layer into the free troposphere was limited. Therefore, the upglide of the warmed air due to the cyclone demonstrated in this study possibly played an important role in the anomalous heating due to the sea ice decline during winter.

4. Summary and Discussion

In this study, the impact of sea-ice cover on storm-mediated atmospheric warming over the Barents Sea during winter was examined. As expected, SHF, LHF, and LWR in CNTL were larger than those in HICE over the area close to the sea-ice edge. These areas exhibited higher PTs within the boundary layer in CNTL than within those in HICE. The dominant mechanism that generated this temperature anomaly was anomalous heating by surface fluxes and vertical diffusion as well as radiation, counteracted by cold advection. On the other hand, the heating mechanisms farther north of the sea-ice edge east of Svalbard were quite different. The air was heated by warm advection resulting from the southerlies and cooled by vertical mixing, and in this area, anomalous heating was not limited to the boundary layer. The air parcels heated by the surface heat fluxes in CNTL traveled much higher and farther north than those in HICE. Additionally, in CNTL, there was a higher chance that the air parcels heated in the boundary layer

would be transported into the free troposphere and will travel farther north than in HICE, in which air the parcels traveled at constant levels close to the surface, without rising. The strong inversions generated in the lower troposphere during winter in the Arctic prevent the air parcels from moving above the surface boundary layer, and there is little chance for the air parcels to be transported into the free troposphere in the absence of some atmospheric disturbances. This enhanced on-ice flow regime due to sea ice decline could be an important mechanism for the anomalous heating in the free troposphere in the Arctic during winter and play a role in recent Arctic warming.

The mechanism illustrated in this study is similar to that proposed by Komatsu and others (2018), who demonstrated that atmospheric warming resulting from the upglide of humid air from Siberia initiates condensational heating in a lower part of the troposphere above the boundary layer, leading to atmospheric warming in the free troposphere during summer in the Arctic. Our numerical simulations showed that condensational heating plays a secondary role in contrast to the findings of Komatsu and others (2018). Moreover, they argued that sea-ice cover is an important contributor to the upglide of humid air and heating in the atmosphere. This argument is opposite that drawn from the results of this study, which showed that a decline in sea-ice cover enhances atmospheric warming in the Barents Sea. The enhanced on-ice flow regime demonstrated in this study could play an important role in the atmospheric warming observed during winter in the Arctic, even though the sea-ice cover showed a persistent decline as is the case with the current climate.

The impact of sea-ice cover on the frequency, intensity, and track of the cyclone is still disputed (Koyama and others, 2017) given that cyclone activities in existing atmospheric reanalysis datasets are rather different (Zahn and others, 2018). However, changes in the atmospheric environment that favor cyclogenesis were surely observed in the existing datasets (Koyama and others, 2017).

This study illustrated the importance of enhanced on-ice flow regime associated with a cyclone in spreading out the effect of the anomalous heating due to the sea-ice decline during winter. Further, the results of this study provide evidence that only changes in sea-ice cover, without any other supporting mechanisms, can intensify warm advection and vertical heat transport, which was not addressed in previous studies (Higgins and Cassano, 2010; Serreze and others, 2011). Barents Sea is one of the areas of the most frequent cyclone occurrence in the Arctic during winter (e.g., Raible et al., 2009). It is also one of the key regions of the recent AA. The results of this study imply that the better representation of heat transport due to cyclones around the sea-ice edge in the climate models contributes to a more accurate projection of future AA. A variety of cyclones occur in the Arctic and their structures and lifecycles are rather different from those of the cyclone examined in this study. Therefore, further comprehensive studies are necessary to quantify the impact of the cyclones on the Arctic climate and its change, e.g., AA.

Acknowledgements

The author thanks K. Hines and the Polar Meteorology Group, Byrd Polar and Climate Research Center, Ohio State University for providing Polar WRF. He also thanks anonymous reviewers and Editor-In-Chief H. Kitagawa for their constructive comments. This work was supported in part by the Arctic Challenge for Sustainability II (ArCS II) Project (Program Grant Number JPMXD1420318865), the Japan Society for Promotion for Science through Grants-in-Aid for Scientific Research (Grant Numbers JP17H02958 and JP19H05697), and the Collaborative Research Program of the Research Institute for Applied Mechanics, Kyushu University (Grant Number 2020 S2-6).

References

Adakudlu, M. and I. Barstad (2011): Impacts of the ice-cover and sea-surface temperature on a polar low over the Nordic seas: A numerical case study. *Q.J.R. Meteorol. Soc*., **137**: 1716–1730.

Akperov, M., V.A. Semenov and 4 others (2020): Impact of Atlantic water inflow on winter cyclone activity in the Barents Sea: Insights from coupled regional climate model simulations. *Env. Res. Lett*., **15**: 024009, doi:10.1088/1748-9326/ab6399.

Bassett, R., P.J. Young and 3 others (2020): A large ensemble approach to quantifying internal model variability within the WRF numerical model. *J. Geophys. Res. Atmos.*, **125**: e2019JD031286.

Boisvert, L.N., A.A. Petty and J.C. Stroeve (2016): The impact of the extreme winter 2015/16 Arctic cyclone on the Barents-Kara Seas. Mon. Weather Rev., **144**: 4279–4287.

Brümmer, B. and S. Thiemann (2002): The Atmospheric boundary layer in an Arctic wintertime on-ice air flow. *Boundary-Layer Meteor*., **104**: 53–72.

Dai, A., D. Luo and 2 others (2019): Arctic amplification is caused by sea-ice loss under increasing CO_2. *Nat. Commun.*, **10**: 121, doi:10.1038/s41467-018-07954-9.

Dee, D.P., S.M. Uppala and 34 others (2011): The ERA-Interim reanalysis: Configuration and performance of the data assimilation system. *Q.J.R. Meteorol. Soc*., **137**: 553–597.

Deser, C., R. Tomas and 2 others (2010): The seasonal atmospheric response to projected Arctic sea ice loss in the late twenty-first century. *J. Clim*., **23**: 333–351.

Hersbach, H., B. Bell and 42 others (2020): The ERA5 global reanalysis. *Q.J.R. Meteorol. Soc*., **146**: 1999–2049.

Higgins, M.E. and J.J. Cassano (2010): Response of Arctic 1000 hPa circulation to changes in horizontal resolution and sea ice forcing in the Community Atmospheric Model. *J. Geophys. Res*., **115**: D17114, doi:10.1029/2009JD013440.

Hines, K.M. and D.H. Bromwich (2008): Development and testing of polar weather research and forecasting (WRF)

model. Part I: Greenland ice sheet meteorology. *Mon. Weather Rev*., **136**: 1971–1989.
Inoue, J. and M.E. Hori (2011): Arctic cyclogenesis at the marginal ice zone: A contributory mechanism for the temperature amplification? *Geophys. Res. Lett*., **38**: L12502, doi:10.1029/2011GL047696.
Inoue, J., M.E. Hori and K. Takaya (2012): The role of Barents Sea ice in the wintertime cyclone track and emergence of a warm-Arctic cold-Siberian anomaly. *J. Clim*., **25**: 2561–2568.
Jung, E., J.-H. Jeong and 4 others (2020): Impacts of the Arctic-midlatitude teleconnection on wintertime seasonal climate forecasts. *Env. Res. Lett*., **15**: 094045, doi: 10.1088/1748-9326/aba3a3.
Kim, K.Y., J.Y. Kim and 5 others (2019): Vertical feedback mechanism of winter Arctic amplification and sea ice loss. *Sci. Rep*., **9**: 1184, doi:10.1038/s41598-018-38109-x.
Komatsu, K.K., V.A. Alexeev and 2 others (2018): Poleward upgliding Siberian atmospheric rivers over sea ice heat up Arctic upper air. *Sci. Rep*., **8**: 2872, doi:10.1038/s41598-018-21159-6.
Koyama, T., J. Stroeve and 2 others (2017): Sea ice loss and Arctic Cyclone Activity from 1979 to 2014. *J. Climate*, **30**: 4735–4754.
Magnusdottir, G., C. Deser and R. Saravanan (2004): The effects of North Atlantic SST and sea ice anomalies on the winter circulation in CCM3. Part I: Main features and storm-track characteristics of the response. *J. Climate*, **17**: 857–876.
Manda, A., T. Mitsui and 4 others (2020): Storm-mediated ocean–atmosphere heat exchange over the Arctic Ocean: A case study of a Barents Sea cyclone observed in January 2011. *OSPOR*, **4**: 1–9.
Mori, M., Y. Kosaka and 3 others (2019): A reconciled estimate of the influence of Arctic sea-ice loss on recent Eurasian cooling. *Nat. Clim. Change*, **9**: 123–129.
Norwegian Polar Institute (2020): Sea ice extent in the Barents Sea in April. Environmental monitoring of Svalbard and Jan Mayen (MOSJ). URL: http://www.mosj.no/en/climate/ocean/sea-ice-extent-barents-sea-fram-strait.html.
Raible, C.C., P.M. Della-Marta and 3 others (2008): Northern hemisphere extratropical cyclones: A comparison of detection and tracking methods and different reanalyses. *Mon. Weather Rev*., **136**: 880–897.
Rinke, A., M. Maturilli and 6 others (2017): Extreme cyclone events in the Arctic: Wintertime variability and trends. *Environ. Res. Lett*., **12**: 094006, doi: 10.1088/1748-9326/aa7def
Screen, J.A., C. Deser and 10 others (2018): Consistency and discrepancy in the atmospheric response to Arctic sea-ice loss across climate models. *Nat. Geosci*., **11**: 155–163.
Screen, J.A., C. Deser and I. Simmonds (2012): Local and remote controls on observed Arctic warming. *Geophys. Res. Lett*., **39**: L10709, doi: 10.1029/2012GL051598.
Screen, J.A. and I. Simmonds (2010): The central role of diminishing sea ice in recent Arctic temperature amplification. *Nature*, **464**: 1334–1337.
Serreze, M.C. (1995): Climatological aspects of cyclone development and decay in the Arctic. *Atmos.-Ocean*, **33**: 1–23.
Serreze, M.C., A.P. Barrett and 8 others (2006): The large-scale freshwater cycle of the Arctic. *J. Geophys. Res.*, **111**: C11010, doi:10.1029/2005JC003424.
Serreze, M.C., A.P. Barrett and J.J. Cassano (2011): Circulation and surface controls on the lower tropospheric air temperature field of the Arctic. *J. Geophys. Res*., **116**: D07104, doi: 10.1029/2010JD015127.
Sun, R. and G. Gao (2018): Impact of polar lows on synoptic scale variability of Atlantic inflow in the Fram Strait. *Acta Oceanol. Sin.* **37**: 42–50.
Skamarock, W.C., J.B. Klemp and 7 others (2008): A description of the Advanced Research WRF version 3. *NCAR technical note NCAR/TN-475+STR*, NCAR: Boulder, CO, USA, 113pp., doi: 10.5065/D68S4MVH.
Vihma, T., J. Hartmann and C. Lüpkes (2003): A case study of an on-ice air flow over the Arctic marginal sea-ice zone. *Boundary-Layer Meteor*., **107**: 189–217.
Wei, J., X. Zhang and Z. Wang (2019): Impacts of extratropical storm tracks on Arctic sea ice export through Fram Strait. *Clim. Dyn*. **52**: 2235–2246.
Zahn, M., M. Akperov and 3 others (2018): Trends of cyclone characteristics in the Arctic and their patterns from different reanalysis data. *J. Geophys. Res. Atmos*., **123**: 2737–2751.

Summary in Japanese

和文要約

海氷分布が低気圧を媒介とした バレンツ海の気温上昇に及ぼす影響 ー領域気象モデルを用いた研究

万田敦昌 [1]

[1] 三重大学

海氷減少は北極温暖化の主要因と考えられているがそのメカニズムには未解明の点が多い。本研究では低気圧を媒介としたバレンツ海の昇温過程に海氷分布が及ぼす影響を, 2011 年 1 月 21 から 25 日にかけてバレンツ海で観測された低気圧をテストケースとした数値実験によって調べた。海氷分布を変化させた領域の多くにおいて, 海面熱フラックスの強化に伴って乱流鉛直拡散と長波放射が強まり, これにより大気はより加熱されていた。それとは対照的に, スピッツベルゲン島東方の海氷縁よりも極側の領域では, 低気圧に伴う南風によって内部境界層がより極側に広がるとともに, 暖気移流による大気加熱が強化されていた。また, 海氷縁より南側の開水域で加熱された境界層内の気塊は, 南風によって北上しながら境界層よりも上方の自由大気に向けて輸送されていた。冬季の北極海では逆転層を伴う強い安定成層によって, 境界層と自由対流圏の熱交換が抑制されているが, 本研究で示した低気圧に伴う海氷域における暖気の北上並びに上昇過程は, 海氷減少に伴う冬季北極域における温暖化を促進する働きがあること示唆している。

Correspondence to: A. Manda, am@bio.mie-u.ac.jp

Okhotsk Sea and Polar Oceans Research 5 (2021) 31-35

https://doi.org/10.57287/ospor.5.31

Article

Large-Scale Sea Ice Divergence and Convergence Monitoring in the Arctic Ocean during Spring 2018

Mariapina VOMERO[1], Noriaki KIMURA[2], Mathias MILZ[3], Victoria BARABASH[3] and Hajime YAMAGUCHI[1]

[1] *Graduate School of Frontier Sciences, The University of Tokyo, Kashiwa, Japan*
[2] *Atmosphere and Ocean Research Institute, The University of Tokyo, Kashiwa, Japan*
[3] *Department of Computer Science, Electrical and Space Engineering, Luleå University of Technology, Kiruna, Sweden*

(Received November 2, 2020; Revised manuscript accepted January 23, 2021)

Abstract

This study investigates sea ice motion in the Arctic Ocean during the year 2018 to detect areas of ice deformation. We aim to improve the current understanding of large-scale sea ice circulation by examining ice convergence/divergence during the early melt-season. OSISAF sea ice drift data provided by EUMETSAT were used for the analysis during the months of March and April. Daily ice drifting speed and deformation parameters showed a strong correlation throughout the observed interval, while a local-scale analysis revealed different patterns for ice divergence and convergence in areas of enhanced ice drift.

Key words: sea ice drift, Arctic Ocean, OSISAF, remote sensing, ice divergence

1. Introduction

Monitoring allowed by current remote sensing systems with multi-sensor sources has led to improved analysis and a more detailed understanding of sea ice motion. Several studies investigated the variability of sea ice divergence in different regions of the Arctic from satellite records. Frey and others (2015) observed significant changes in sea ice cover across the Bering, Chukchi, and Beaufort seas of the Pacific Arctic Region. The patterns revealed were spatially heterogeneous, with significant declines in ice extent over the Chukchi and Beaufort seas. Their results suggested that some areas are experiencing rapid shifts in sea ice cover due to different drivers, being primarily wind driven in the Beaufort Sea, thermally driven in the Canada Basin, and influenced by both in the Bering Sea.

Kimura and others (2013) identified potential relationships between interannual difference in winter ice motion and ice area in the following summer using ice velocity data with a 37.5 km grid resolution from the satellite passive microwave sensor Advanced Microwave Scanning Radiometer (AMSR). Using a large-scale approach, they tracked sea ice deformation for the seasonal ice cover, which is now the dominant ice type in the Arctic. From their analysis of sea ice divergence and convergence, it was observed that the winter ice redistribution controls spring ice thickness until summer.

Kwok (2015) defined a method to study the converging motion along the Arctic coasts of Greenland and the Canadian Arctic Archipelago using satellite data for ice drift from the Special Sensor Microwave Imager (SSMI) and Advanced Scatterometer (ASCAT) data. Convergence patterns were identified along the coastal boundaries of the Arctic Basin, where pressure ridges and thicker ice are formed from the shear motion of ice floes in close contact. The ice resulting from these processes is more likely to accumulate on the multiyear ice and survive the summer months, consequentially slowing down the decline of sea ice coverage. The redistribution of the ice cover also intensifies local ice growth with resulting increased ice strength and roughness that alters the mechanical response to atmospheric and oceanic drivers.

The aim of this study is to identify both the divergence and convergence of ice motion in the Arctic Ocean during the early melt-season and to describe large-scale sea ice deformation processes during spring 2018 (60 days in total). Investigating differences in these deformation mechanisms is useful to establish an improved representation of sea ice motion for modeling studies. Spatial and temporal patterns in dispersion processes are addressed at both the periphery and interior of the ice pack to provide a global description over the whole Arctic Ocean. For this reason, the Ocean and Sea Ice Satellite Application

Facility (OSISAF) ice drift data, provided by the European Organization for the Exploitation of Meteorological Satellites (EUMETSAT), were chosen to guarantee a complete spatial coverage since it is based on low resolution (10 - 15 km) Passive Microwave instruments such as AMSR-2.

2. Data

The OSISAF low resolution ice drift dataset is daily computed from aggregated maps of passive microwave (e.g. SSMI, AMSR-2) or scatterometer (e.g. ASCAT) signals. Each map can be either derived from one sensor used as input to the processing chain (single sensor product) or from a merged (multi-sensor) dataset. Its characteristic wide ground swaths, high acquisition rates and all-weather capability ensure daily monitoring of both polar regions based on global ice drift vectors with a spatial resolution of 62.5 km.

Since these data were processed from a pair of satellite images after implementing the Continuous Maximum Cross Correlation algorithm (Lavergne and others 2010), the resulting ice drift vector describes the displacement that each ice cell observed at the initial position (lat_0, lon_0) shows at the position (lat_1, lon_1) after 48 hours. This temporal resolution limits the application of such imagery for highly variable drift speeds close to the ice edge or the coast (Williams and others, 2019), therefore these pixels were excluded from the analysis. Furthermore, due to the limited accuracy of data from summer months (defined as the period from April 30th to October 1st for the Northern Hemisphere) caused by atmospheric noise and ice surface melting (Peterson and Stanton, 2016), the present paper will only address the early melt season during the months of March and April.

3. Observation Method and Result

The deformation metrics of sea ice divergence and convergence enables the description of closure and opening processes of the ice pack. This ice deformation parameter is defined by the following equation (Tabata and others, 1980):

$$(1)\quad \dot{\nabla} = \frac{\partial u}{\partial x} + \frac{\partial v}{\partial y} = u_x + v_y$$

where u(x,y) and v(x,y) are the drift components in x- and y-direction at position (x,y). The dimension of $\dot{\nabla}$is velocity change per length unit, hence $[time]^{-1}$.

Kimura and Wakatsuchi (2004) calculated the partial derivatives of the drift vector field at a generic cell (i, j) as a rate of spatial change around the boundaries of a grid cell instead of the derivatives of the velocities as follows:

$$(2)\quad \dot{\nabla}_{i,j} = \frac{u\left(i+\frac{1}{2},j\right)-u\left(i-\frac{1}{2},j\right)}{dist} + \frac{v\left(i,j+\frac{1}{2}\right)-v\left(i,j-\frac{1}{2}\right)}{dist}$$

where *dist* is the grid resolution (62.5 km).
This formula was applied to the spatial gradients of ice motion computed from OSISAF dataset. Depending on the sign of the sum $u_x + v_y$, the final parameter is classified as divergence or convergence. As a measure of area change, a negative divergence (now defined as convergence) at a specific point indicates a converging vector field at that point, while positive values allow to identify where a diverging vector field potentially originates from. Therefore, the evaluation of ice divergence highlights characteristics not easily noticeable when using ice motion vectors only.

Daily mean values for sea ice drift, divergence and convergence were computed from OSISAF ice drift fields over 48 hours (Fig.1). Since ice convergence corresponds to negative divergence, it was plotted in Fig.1 as absolute values for comparison to positive divergence values.

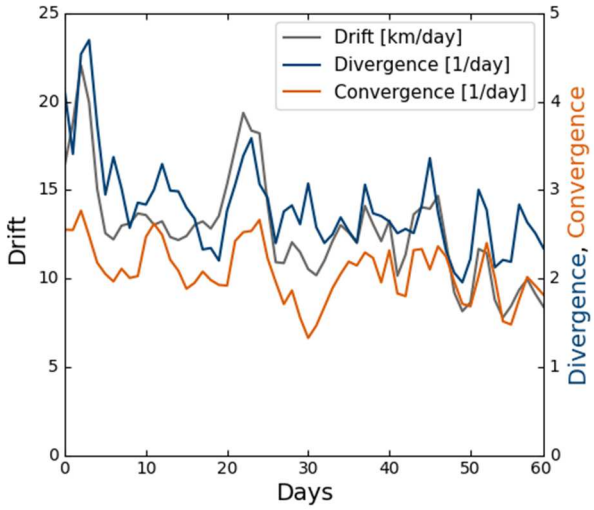

Fig. 1 Trends of sea ice drift, divergence and convergence during Spring (March – April) 2018

In order to quantify the similarity between ice drift and the other parameters, the Pearson correlation coefficient was computed using the following formula for n samples of two generic variables x and y:

$$(3)\quad \rho_{xy} = \frac{\sum_{i=1}^{n}(x_i-\bar{x})(y_i-\bar{y})}{\sqrt{\sum_{i=1}^{n}(x_i-\bar{x})^2}\sqrt{\sum_{i=1}^{n}(y_i-\bar{y})^2}}$$

Results for spring 2018 are displayed in Fig.2 and 3.

Both coefficients of about 0.78 showed a strong temporal correlation for both convergence and divergence to the ice drift trend. However, a spatial analysis allows to describe regional patterns for these deformation parameters. Therefore, vector field maps

of the Arctic Ocean were created to depict their interplay during the observed interval.

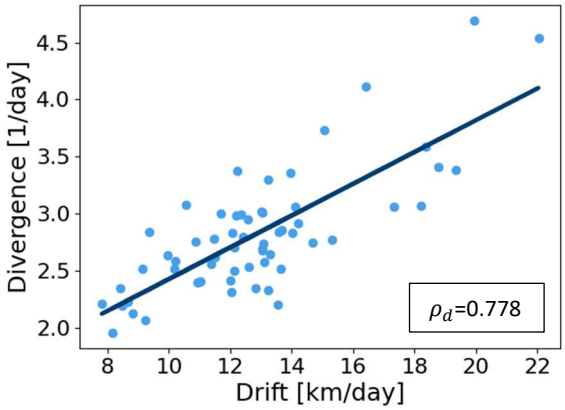

Fig. 2 Drift and Divergence scatter plot and correlation coefficient - Spring 2018

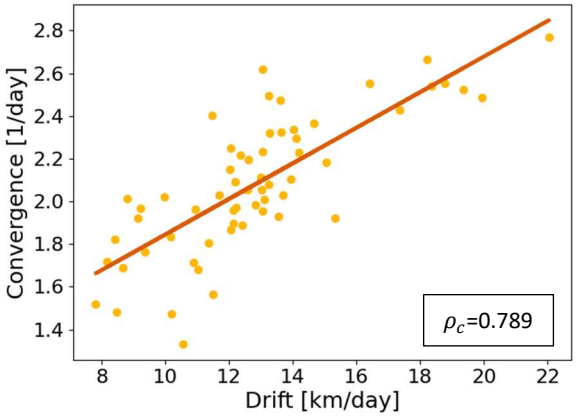

Fig. 3 Drift and Convergence scatter plot and correlation coefficient - Spring 2018

The sea-ice drift map for spring 2018 (Fig. 4) shows two distinct features: an anticyclonic motion in the Canadian basin, i.e. the Beaufort Gyre , and the Transpolar drift that drives the ice from the Laptev Sea across the Pole to the Fram Strait (Rigor and Wallace, 2004). In addition to these two dominant Arctic circulation patterns, a motion system was also identified from the Kara to the Barents Sea. The corresponding values in these areas exceeded 20 km/day.

The frequency map of intense ice motion in Fig. 5 was computed from pixels corresponding to a value higher than 10 km/day (chosen according to the study on strong drift patterns performed by Kaur and others, 2015) in order to identify areas of persistent strong sea ice speeds. This graph emphasizes the high correspondence between previously detected areas of intense and recurrent drift motion regimes. In fact, strong sea ice motion was detected in the Greenland and the Barents Seas for almost the entire length of this study.

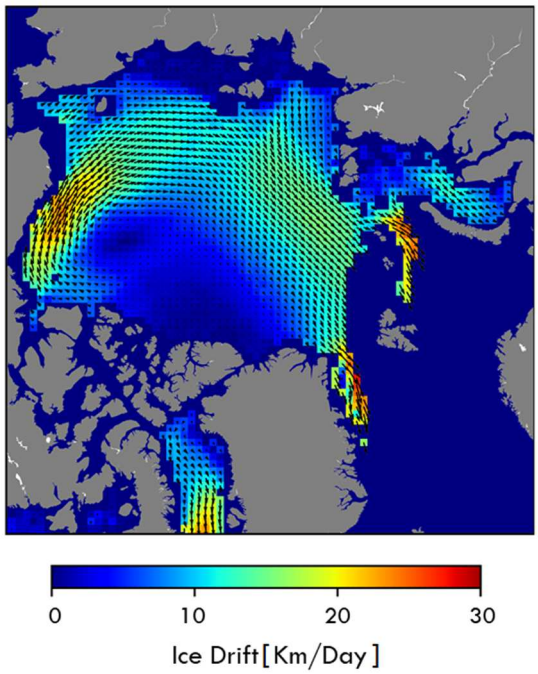

Fig. 4 Sea ice drift speed and vector map averaged for the observed interval (March - April, 2018)

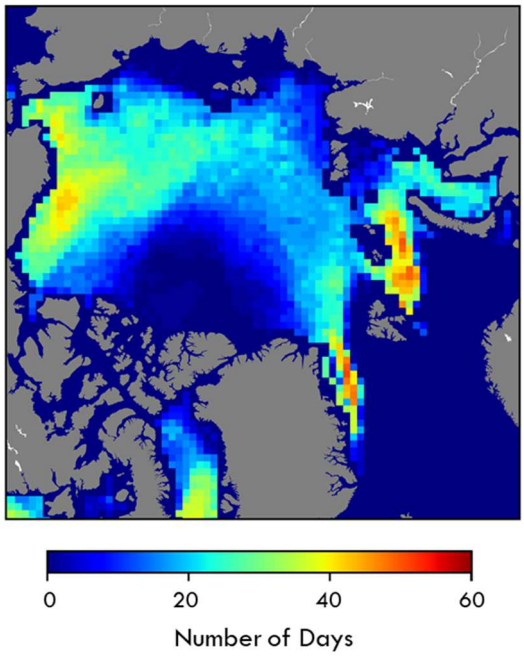

Fig. 5 Frequency map of strong ice motion for Spring 2018

The relationship between sea ice drift and divergence was further examined to identify areas for

sea ice deformation. A strong diverging pattern was identified in Fig.7 after setting a threshold to the most recurrent value of ice divergence grid cells during the observed interval (equal to 3 from the histogram in Fig. 6).

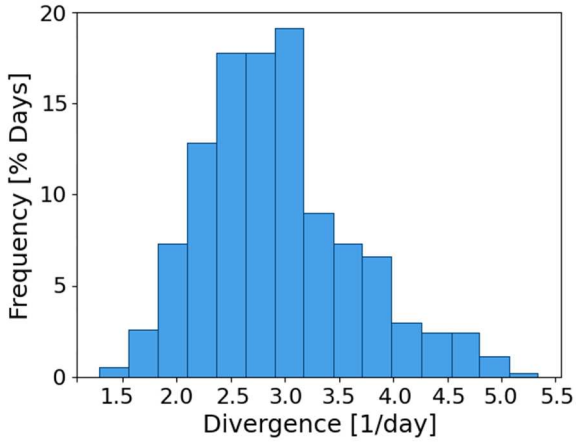

Fig. 6 Histogram of ice divergence during Spring 2018

Figure 7 shows that most of the divergent cells are located in offshore sites of the Chukchi, Laptev and East Siberian Seas. When comparing these results with the previous sea ice drift frequency map (Fig.5), areas of intense sea ice motion only overlap in the Chukchi Sea which is linked to the change in the relative strength and location of the Beaufort Gyre versus the Transpolar Drift (De Vernal *and others*, 2005).

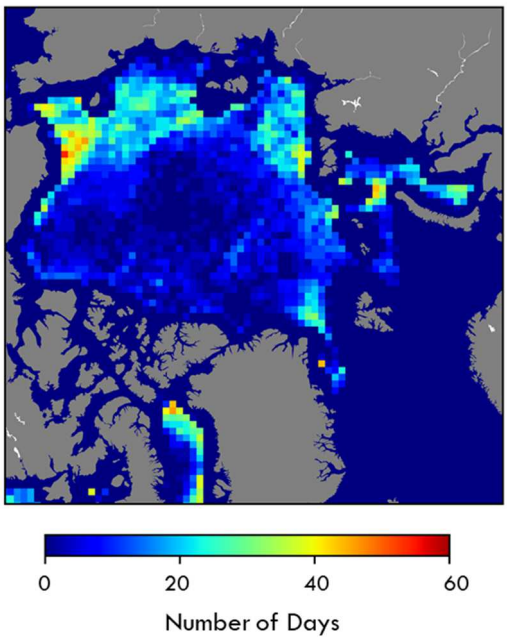

Fig. 7 Frequency map of persistent divergence - Spring 2018

Therefore, the remaining areas of strong ice motion detected in Fig.5 aren't linked to dispersing mechanisms exclusively. Values of persistent convergence (threshold set at 2 from Fig.8 for convergence grid cells) were found in the Beaufort, Kara and Greenland Seas as charted in Fig. 9.

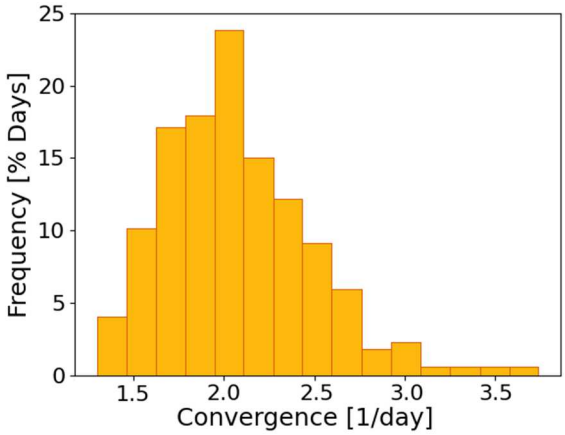

Fig. 8 Histogram of ice convergence during Spring 2018

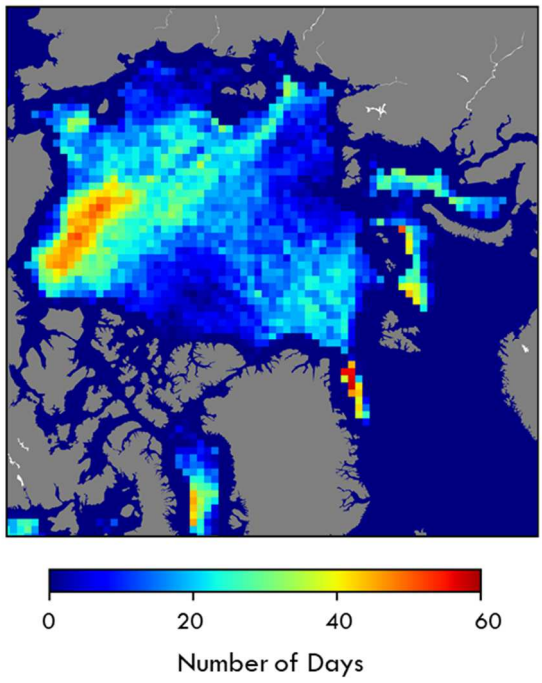

Fig. 9 Frequency map of persistent convergence - Spring 2018

This higher level of correspondence between convergence and ice-drifting speed is particularly enhanced in the Beaufort Sea, where the anticyclonic (clockwise) circulation of the Beaufort Gyre intensifies sea ice concentrations and ice ridging phenomena (Asplin and others, 2009). Off the coasts of Greenland

ice convergence is attributable to the onshore ice circulation depicted in Fig. 9 (Kwok, 2015). Lastly, the sea ice transport into the Barents Sea directed towards the Norwegian Seas represents the third noticeable area where correlation with intense convergence takes place.

4. Conclusions

In this study, three parameters for sea ice deformation were mapped over the Arctic Ocean using OSISAF data for spring 2018. The global analysis showed a noticeable correlation between the temporal change of sea ice drift and diverging/converging trends. From the analysis of the ice drift dataset, areas of strong drift patterns also confirmed the influence of the two main wind-driven ocean currents of the Beaufort Gyre and the Transpolar Drift Stream.

Values of divergence and convergence were further investigated to provide insight into the nature of motion in different areas of the Arctic sea. During the time interval considered in this paper both indicators overall showed a high correlation to intense ice drift values. Remarkable converging motion was observed in the Greenland and Barents Sea, while high diverging movements in the Chukchi Sea. Furthermore, consistent and persistent ice motion induced a widespread convergence in the Beaufort Sea.

Acknowledgments

The authors express their sincere gratitude to OSISAF and its data provider. This work was also supported by the Arctic Challenge for Sustainability (ArCS) project in Japan.

References

Asplin, M. G., J. V. Lukovich, and D. G. Barber (2009). Atmospheric forcing of the Beaufort Sea ice gyre: Surface pressure climatology and sea ice motion. *Journal of Geophysical Research: Oceans,* **114** (C1).

De Vernal A., C. M. Hillaire, and D. A. Darby (2005). Variability of sea ice cover in the Chukchi Sea (western Arctic Ocean) during the Holocene. *Paleoceanography,* **20** (4). https://doi.org/10.1029/2005PA001157

Frey, K. E., G. W. K. Moore, L. W. Cooper, and J. M. Grebmeier (2015). Divergent patterns of recent sea ice cover across the Bering, Chukchi, and Beaufort seas of the Pacific Arctic Region. *Progress in Oceanography*, **136**, 32-49.

Kaur, S., J. K. Ehn, and D. G. Barber (2018). Pan-arctic winter drift speeds and changing patterns of sea ice motion: 1979–2015. *The Polar Record,* **54** (5-6), 303-311.

Kimura, N., and M. Wakatsuchi (2004). Increase and decrease of sea ice area in the Sea of Okhotsk: Ice production in coastal polynyas and dynamic thickening in convergence zones. *Journal of Geophysical Research: Oceans*, **109** (C9).

Kimura, N., A. Nishimura, Y. Tanaka, and H. Yamaguchi (2013). Influence of winter sea-ice motion on summer ice cover in the Arctic. *Polar Research*, **32** (1), 20193.

Kwok, R. (2015). Sea ice convergence along the Arctic coasts of Greenland and the Canadian Arctic Archipelago: Variability and extremes (1992–2014). *Geophysical Research Letters*, **42** (18), 7598-7605.

Lavergne, T., S. Eastwood, Z. Teffah, H. Schyberg, and L. A. Breivik (2010). Sea ice motion from low-resolution satellite sensors: An alternative method and its validation in the Arctic. *Journal of Geophysical Research: Oceans*, **115** (C10).

Peterson, E. R., and T. P. Stanton (2016). Comparing the Accuracy of AMSRE, AMSR2, SSMI and SSMIS Satellite Radiometer Ice Concentration Products with One-Meter Resolution Visible Imagery in the Arctic. *AGUFM*, 2016, C13C-0849.

Rigor, I. G., and J. M. Wallace (2004). Variations in the age of Arctic sea‐ice and summer sea‐ice extent. *Geophysical Research Letters* **31** (9).

Tabata, T., T. Kawamura and M. Aota (1980). Divergence and rotation of an ice field off Okhotsk Sea Coast of Hokkaido. Sea Ice Processes and Models (RS Pritchard, Ed.), University of Washington Press, Seattle, Washington, 98195.

Williams, T., A. Korosov, P. Rampal and E. Ólason (2019). Presentation and evaluation of the Arctic sea ice forecasting system neXtSIM-F. *Cryosphere*. https://doi.org/10.5194/tc-2019-154

Correspondence to: M. Vomero,
mariapina.vomero@gmail.com

Okhotsk Sea and Polar Oceans Research 5 (2021) 36-40

https://doi.org/10.57287/ospor.5.36

Article

Combining UAV and satellite image for monitoring drifting ice

Kanichiro MATSUMURA[1], Susumu CHIBA[1]
Ram AVTAR[2], Sumito MATOBA[3], Toshiaki ICHINOSE[4],
Kouichi MORIKAWA[5]

[1] *A Faculty of Bioindustry, Tokyo University of Agriculture, Japan*
[2] *Faculty of Environmental Earth Science, Hokkaido University, Japan*
[3] *Institute of Low Temperature Science, Hokkaido University, Japan*
[4] *National Institute for Environmental Studies, Japan*
[5] *Oikos Co., Japan*

(Received November 10, 2020; Revised manuscript accepted January 30, 2021)

Abstract
Satellite and UAV images are widely used for ecological field analysis and interpretation. Drifting ice and Seagrass habitat are discussed. Collaborating with our Indian satellite data acquisition company, the system can acquire Normalized vegetation index (NDVI) and Normalized Moisture index (NDMI) for the targeted area. The author compared satellite obtained NDMI and UAV data, against NDVI data over grassland. The possibilities of using NDMI as a forecaster for NDVI is proposed. The possibilities applying this system for drifting ice is also proposed.

Key words: drifting ice, NDMI, NDVI, UAVs

1. Introduction

Conventional aerial imagery from UAV is increasingly used in the acquisition of high spatial resolution imagery (Pajares, 2015). The open source software (Mission Planner, 2019) makes it possible to conduct and manipulation flight waypoint. On the Mission Planner, and area is chosen and flagged. Flags are associated with coordinates and altitude above ground (not sea level) and then a flight plan is obtained. A flight plan on Mission Hub is transformed to auto pilot software (Litchi) on iOS tablet. Litchi lets the UAV fly over the pre-programmed course. Lake Notori district was study area. The Authors set a flight plan over the study area. Moba seagrass habitat is thought to be a carbon dioxide sink, and plays an important role in the carbon cycle (Nihon Keizai Newspaper, 2019).The Authors directed an UAV to fly over the study area and shot a series of pictures 100 meters above sea level. Satellite image is obtained from Sentinel-2 (Restec, 2020).

2. Drifting ice and its impacts on Seagrass

Lake Notori is situated in the eastern part of Hokkaido, Japan. The authors have been conducting surveys in this district. Identifying the distribution of seagrass patches is important to understand Hokkai shrimp habitat. Hokkai shrimp contributes fisherman. Seagrass patches are influenced by drifting ice. Small (young) individuals strongly depend on seagrass during both night and day. Large (i.e. old) individuals go out from a seagrass patch at night and return to the patch in the daytime. During winter season 2018-2019, the extremely low temperature made drifting ice thick and dense. Upon melting during warm periods, the angular blocks of crumbling ice would shred the seagrass beds are torn into smaller parches, the large juvenile-shrimp habitats would be compromised and reduced spatially. This would result in diminished Hokkai shrimp hatching populations. The authors conducted an observation at same place in 2018 and 2019 by using UAVs. A Series of pictures are transformed to three dimensional pictures by using Structure from Motion (SfM) (Inoue et al., 2014). Orthorectifying Aerial Photograph is invaluable as it offers detailed sub-meter accuracy information. Each orthorectifying aerial photograph is transformed to Google Earth KML format and compared to check the difference.

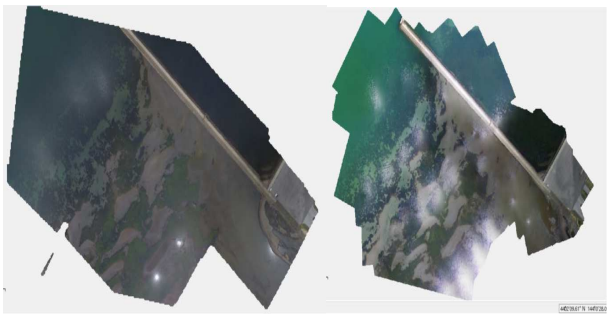

Fig. 1 Seagrass bed captured May 15rd, 2018 (Left) and May 22nd, 2019 (Right)

Circled area in Fig 2 highlights the damaged and shredded by thickened drifting ice during 2018-2019 winter season.

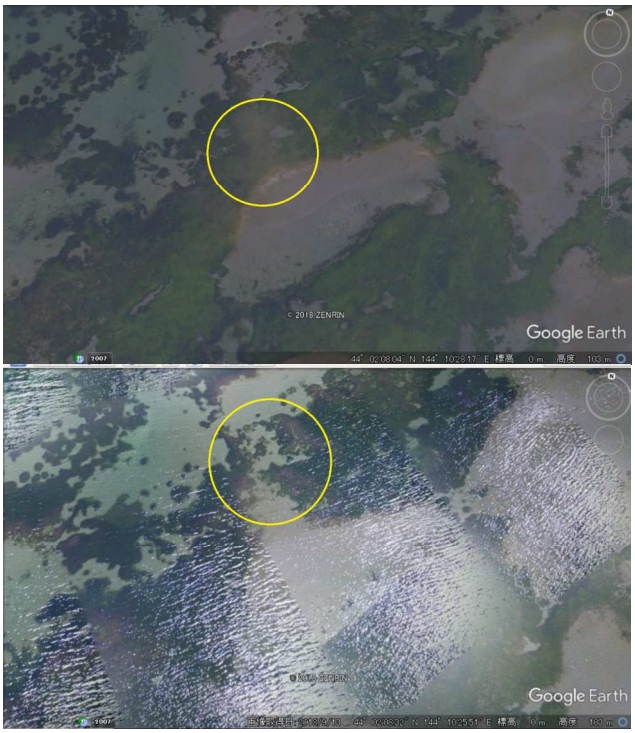

Fig 2. Highlight the place scratched by drifting ice.
The image in 2018 (Above) and 2019 (Bottom).

3. Satellite and UAV Images

One of the authors used to work for the University of Tokyo. His classes were attended by numerous foreign students. The author gave support to a proposal to create an English editing business based in India. The growth of this company has created more than 0.41 million customers (https://www.editage.com/). The CEO of Editage introduced an enterprising company and created a busines called "Agriforetell" in India (https://agriforetell.com/). These two companies joined forces. By using Copernicus: Sentinel-2-The Optical Imaging Mission for Land Services, "Agriforetell" can provide satellite images such as Normalized Vegetation Index (NDVI), Normalized Moisture Index (NDMI), and visible image values to worldwide locations. 10meter resolution is available bi-weekly. The author has been working on providing printed images derived from Agriforetell satellite analysis to farmers. Great effort is made to collect farmer feedback. The cost is an issue with many farmers; however, those concerns are allayed upon analyzing the usefulness of the data. The formula for NDMI is calculated (NIR-SWIR)/(NIR+SWIR). NIR is Near infrared and wavelength is 835.1nm (S2A) and 833nm (S2B). SWIR is short wave infrared and wavelength is 1613.7nm (S2A) / 1610.4nm (S2B). Agriforetell satellite analysis provides information by weekly. NDMI on July 27th 2020 and NDVI on September 9th obtained over the rice field in Asahikawa are shown in Fig 4. According to the owner of this rice field, NDMI image expresses NDVI one month earlier. Low moisture zone result in higher NDVI zone one month later.

Fig 4. NDMI(Left) and NDVI(Right)

The advantage of using UAVs is that data can be obtained at the time required by farmers. Sentinel satellite images restricted to the satellite flyover periods. The grassland in the eastern part of Hokkaido, NDMI on August 27th, 2020 and NDVI on October 8th (UAV obtained) are shown in Fig 5. One month later, lower NDMI zone results in higher NDVI zone.

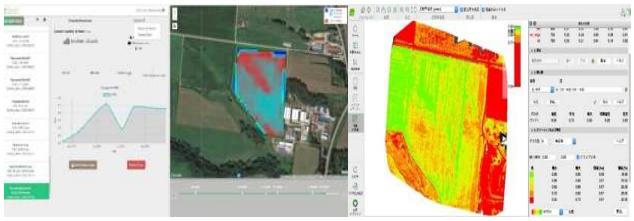

Fig 5. NDMI (Satellite) and NDVI(UAV)

Lake Notori is also famous for scallop aquaculture. At the entrance of lake, there is a chain wire preventing ice from drifting into the lake. NDMI and NDVI images on February 29th, 2020 over the entrance are shown in Fig 6. RGB shows the existence of drifting ice, however NDMI using short wave infrared detects the presence of drifting ice at the lake entrance.

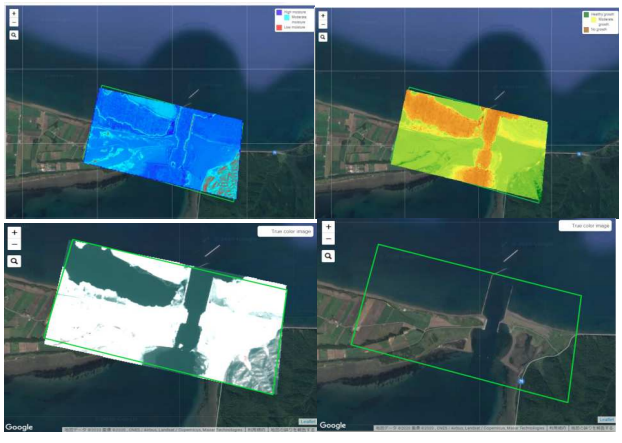

Fig 6. NDMI (Top Left), NDVI (Top Right)
RGB (Bottom Left), Base Map (Bottom Right)

Agriforetell satellite system increased the frequency of procuring data at the beginning of year 2021. Improved system is 50 times faster than the previous system and obtaining 3 to 5 images per month. During the drifting ice season, we set an observation point at Kitahama. The authors developed a drone movie here (Overtone 2015). By using Agriforetell system, NDMI and RGB images in February and March 2020 are shown below.

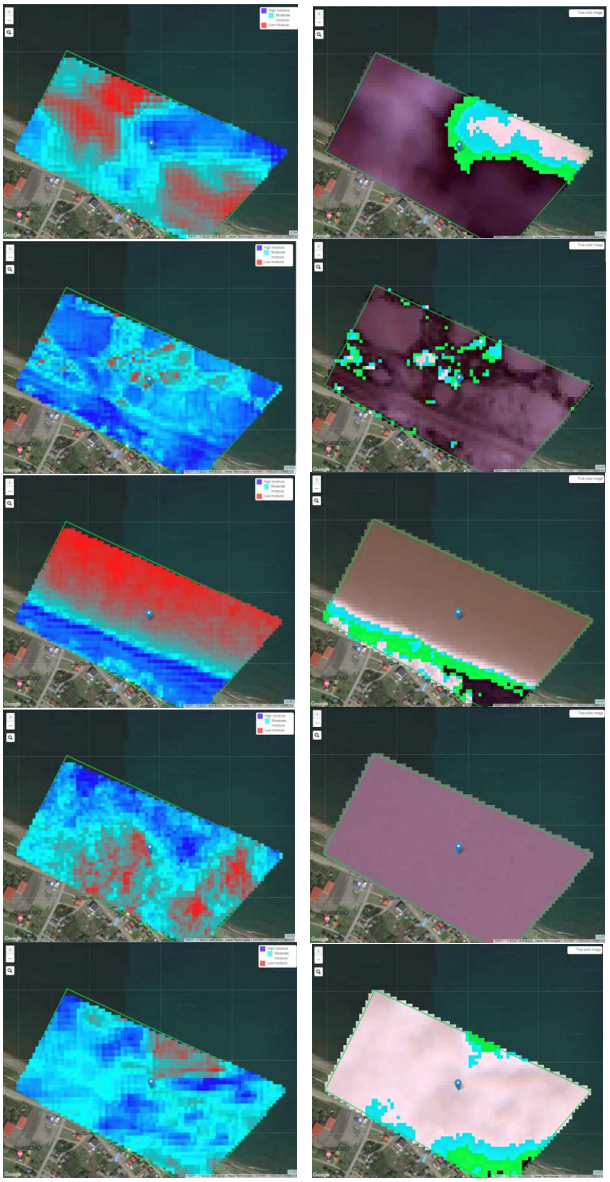

Fig 7. NDMI (left) and RGB (right) Feb 9th, Feb 14th, Feb 24th, Feb 29th and Mar 10th in 2020

Fig 8. Enlarged NDMI (left) and RGB (right) Feb 24th

NDMI shows moisture index and corresponds to open sea or thin ice. The satellite sensor is optical and is sometimes limited by cloud cover. In Figure 8, ice covered area shows lower moisture value (light blues).

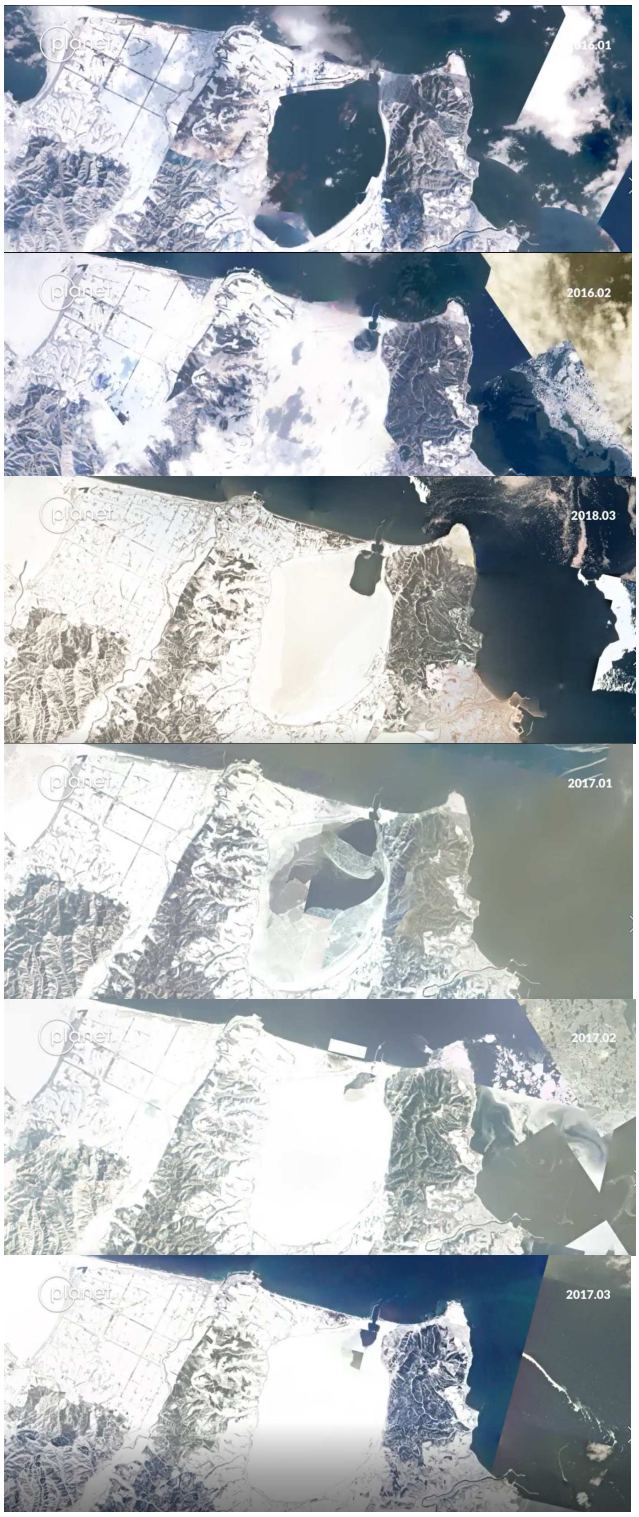

Fig 9. Planet Images over Lake Notori 2016 Jan Feb Mar and those of 2017

One of the authors has used PlanetScope images covering the study area and downloaded from the https://www.planet.com/. PlanetScope image is multispectral data comprising of 4-bands in the visible-Infrared electromagnetic spectrum. The advantage of Planet constellation satellite over other imageries is that they can capture the same location daily with 3-meter pixel size and 16-bit radiometric resolution (Marta 2018). The movement of drift ice and snow cover over Notoro lake can be clearly seen during different seasons using Planet images. The movement of drift ice can be monitored by looking into the change in position of the iceberg in the area.

Again, the advantage of using UAVs is that imagery can be obtained when necessary. Satellite image availability can be complimented by UAV fly overs as required. A balanced use of these two monitoring styles is very useful for completing analysis and interpretation. Satellite images are influenced by the cloud cover, so that combination of satellite and UAV is also useful. However, operation of UAVs is costly. Agriforetell system is expected to get not only images but also shape file format. Shape file format can be transformed to numerical values. The resolution of this satellite system is 10 meters and that of UAVs is 0.1 meter. The relationship between Satellite and UAV obtained values makes it possible to create higher resolution data by using only satellite image data (Matsumura and Ram, 2020).

The authors are using fixed wing UAVs to cover the larger area and for dealing with extreme weather conditions. A special material "Jellafin" makes it possible to develop a waterproof instrument and applying this material for fixed wing UAVs is in progress. Under the very cold conditions, batteries can not last long, reducing the power duration. This sometimes results in serious damage to the UAVs. The authors are also trying to adapt the wired system shown in Fig 8. Consulting with Helvetia Inc., the possibilities of using powered wire connected UAVs are proposed. To reduce the wire weight, a 400-volt transmitter is applied.

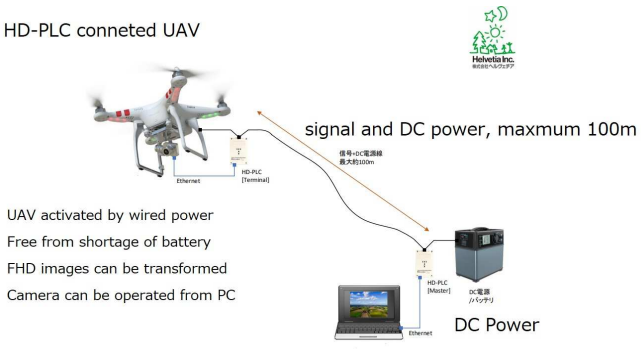

Fig 10. Wired connected UAVs

4. Conclusion and Future Prospects

Satellite and UAV obtained images are examined over seagrass patches, rice field, and drifting ice. To see the distribution of seagrass patches, the authors conducted surveys by using UAVs to understand the modification of patch morphology caused by driving ice. Orthorectifying aerial photographs in 2018 and 2019 highlights the damaged and shredded seagrass beds by thickened drifting ice in 2018-2019 winter. The Indian company is developing a system that can get NDVI, NDMI and RGB images over the targeted area in a simple way. Time series analysis of NDVI and NDMI reveal that NDMI can be used for forecasting NDVI in advance (one month earlier) for a rice field. Agriforetell system can observe drifting ice conditions by using NDMI. The possibilities of combining Satellite and UAV images are proposed.

Acknowledgement

Hasegawa Farm in Asahikawa provides detailed information related to satellite image and agricultural conditions. Supported by Joint Research Program of the Japan Arctic Research Network Center, Hokkaido University Grant, Editing assistance is provided by Mr. Robert Wener.

References

Pajares, G. (2015): Overview and current status of remote sensing applications based on Unmanned Aerial Vehicles (UAVs). Photogramm. Eng. Rem. S. 81(4): 281–329. https://doi.org/10.14358/ PERS.81.4.281

Restec, (2020): Copernicus: Sentinel-2 https://www.restec.or.jp/satellite/sentinel-2-a-2-b

Hilker, T., M.A. Wulder and N.C. Coops. (2008): Update of forest inventory data with LiDAR and high spatial resolution satellite imagery. Can. J. Remote Sens. 34(1): 5–12. https://doi.org/10.5589/ m08-004

Mission Planner (2019): available at http://plane.arudupilot.com/

Nihon Keizai Newspaper (2019), Sea forest and prevent global warming, available at: https://www.nikkei.com/article/ DGKKZO48628560W9A810C1MY1000/

Inoue, H, S. Uchiyama and H. Suzuki (2014): Multicopter Aerial Photography for Natural Disaster Research, NIED Research Report.

AgriForetell, a brand of Ignisnova Robotics Pvt. Ltd, https://agriforetell.com, accessed 2020

Overtone, Drifting ice, https://www.youtube.com/watch?v= paB119vybNY, accessed 2020

Jellafin, SEC Corporation LTD, https://seckaiyo.com/, accessed 2020

Helvetia Inc. HD-PLC wired UAVs, https://helvetia.co.jp/, accessed 2020

Marta, S. Planet Imagery Product Specifications. PLANET.COM 2018, 98.

Matsumura, K and Avtar, R, Comparison between UAV and Satellite Data and Applying Deep learning to Classify Satellite Images for Agriculture Practices in The Eastern Hokkaido, ES Journal of Agriculture and Current Research, Volume 1 Issue1, 2020

Summary in Japanese
和文要約

UAV と人工衛星を組み合わせた流氷観測の可能性

松村寛一郎 [1]，千葉晋 [1]，Ram AVTAR[2]，的場澄人 [3]，一ノ瀬俊明 [4]，森川 浩一 [5]

[1] 東京農業大学，[2] 北海道大学環境科学院，[3] 北海道大学低温科学研究所，[4] 国立環境研究所，[5]（株）オイコス

北海道の能取湖における北海エビの住処である藻場が流氷の影響による変化を UAV により捉えることができた。インド企業が開発したAgriforetellのシステムは、任意の選択地域を対象として Sentinel 衛星による NDMI, NDVI,RGB を体感的に取得できる。稲作と牧草地においてNDMI が事前にNDVI の状況を把握できる可能性を指摘し、NDMI を用いた流氷観測の可能性、さらに UAV との組み合わせによるデータ精度向上の可能性を言及した。

Correspondence to: K. Matsumura,
km205693@nodai.ac.jp

Okhotsk Sea and Polar Oceans Research 5 (2021) 41-44

https://doi.org/10.57287/ospor.5.41

Article

The first attempt of a PIV system: a case study

Vitaly KUZIN[1] and Andrey KURKIN[1]

[1]*Nizhny Novgorod State Technical University n.a. R.E. Alekseev, Nizhny Novgorod, Russia*

(Received November 7, 2020; Revised manuscript accepted February 3, 2021)

Abstract

Digital tracer imaging (Particle Image Velocimetry), which belongs to the class of non-contact optical methods, makes it possible to register instantaneous velocity fields in the measurement plane. One of its most important advantages is the absence of a disturbing influence on the flow. PIV systems can be used to observe the internal distribution of velocities in a liquid or gas flow, in particular when conducting experiments on wave propagation. This article discusses the The first attempt of a PIV system and development of the PIV system based on the LMNAD laboratory — Laboratory of Modeling of Natural and Anthropogenic Disasters (Nizhny Novgorod State Technical University na RE Alekseev, Nizhny Novgorod), the construction of the system in relation to the hydrodynamic wave tank, observation of wave effects, simulation and the development of methods of collection and visualization of experimental data.

Key words: PIV, wave tank, computer vision, remote sensing, visualization

1. What is the PIV system

PIV is an abbreviation for Particle Image Velocimetry (particle image anemometry) — a method of visualizing two-dimensional vector fields of the velocities of liquid or gas flows by digital processing of images of particles introduced into the flow. This method is applicable as a non-contact method for measuring the speed of particles in a liquid or gases, assessing the transfer of particles by the flow. The hydrodynamic wave tank described in (Rodin and others, 2018) is equipped with a PIV system, which includes an upgraded system for video recording and visualization of laboratory experiments (Kurkin and others, 2019), as well as a laser installation for illuminating the liquid and visualizing vector fields (Fig. 1).

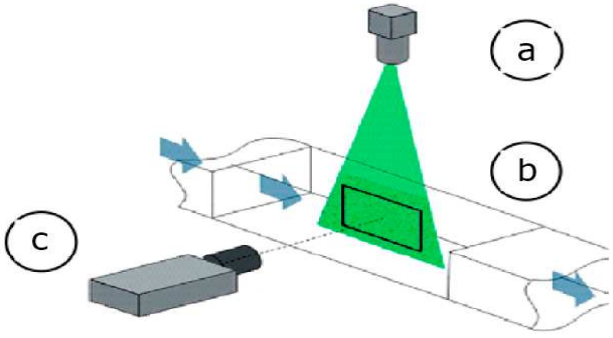

Fig. 1 PIV setup. Emitter with lens group (a), hydrodynamic pool and section with "laser knife" illumination (b), photo-video capture camera (c).

The use of the method makes it possible to register instantaneous velocity fields in the measurement plane and to observe an instantaneous flow pattern within the plane of the laser knife. The advantages of the described method include:

- no disturbing influence on the flow
- wide dynamic range of measured velocities (about 500: 1), which makes it possible to use it for studying intra-wave activity (solitons)
- the ability to register instant spatial velocity distributions
- the ability to obtain information about the dynamics of structures, their scales, calculation of differential characteristics, spatial and space-time correlations, as well as statistical characteristics of the flow.

All the described capabilities of the method impose serious restrictions on the choice of equipment for implementing the system in laboratory conditions. The use of optical sensors (cameras), the choice of a laser "knife" and their mutual synchronization is a complex engineering problem.

Methods for registering and recognizing particles in a video stream and estimating the velocities of particles in a vector field are one of the subtasks that can be solved using computer vision tools. This paper highlights approaches to solving the problems of constructing a laboratory PIV system. The following paragraphs of the article describe an approach to the first experience of building such a system based on the LMNAD laboratory.

2. Equipment description: PIV system in detail

2.1 Hydrodynamic wave tank

A hydrodynamic wave tank is installed on the basis of the LMNAD laboratory — Laboratory of Modeling of Natural and Anthropogenic Disasters (Nizhny Novgorod State Technical University na RE Alekseev, Nizhny Novgorod), which allows carrying out various experiments on the generation and propagation of both surface and internal waves. Hydrodynamic wave tank of N.N. R.E. Alekseeva has the following characteristics: length — 6.5 meters; width — 0.5 meters; height — 1 meter (figure / inset). The PIV system will not allow observing the entire pool at once, the possible coverage area of one system is about 90x90 cm. To cover a larger area, it is possible to install several laser-camera pairs, followed by stitching of a panoramic image and subsequent analysis of the combined image. This approach has a drawback, since it is not possible to ideally match the fields of view of the cameras, the final presentation of the panoramic image will be segmented, which increases the possibility of losing some of the important visual data.

A similar method was used in (Kurkin and others, 2019) to expand the area captured by cameras. The creation of the PIV system at the LMNAD laboratory (Nizhny Novgorod State Technical University na RE Alekseev, Nizhny Novgorod) will allow obtaining more information about the course of experiments by collecting data on the distribution of velocities within the fluid flow during experiments with internal waves as a non-contact method for measuring the flow rate and the rate of particle transfer by the flow both on its surface and in the depth of the liquid. To develop this system, the laboratory was modernized - special dimmers were installed on each light source, the video capture system was installed on a special guide and in order not to create glare during shooting, a special spandex curtain was used. These are minor but necessary measures to ensure the best possible image quality and to minimize the glare when reflected from the acrylic walls of the wave reservoir itself (Fig. 2).

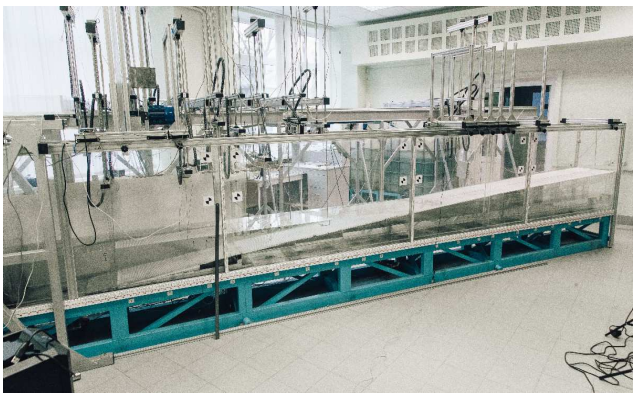

Fig. 2. Hydrodynamic wave tank

2.2 Hardware main parts

The PIV system in its simplest version consists of a laser emitter-camera pair. This version of the system uses high-speed cameras Baumer VCXU-23M (Fig. 3) with a set of wide-angle lenses, a pulsed laser and a system of cylindrical lenses to form a plane of laser radiation also called a "laser knife".

Fig. 3. Camera Baumer VCXU-23M

The main parameters of the cameras used are presented below:

- 1920 x 1200 px
- Sony IMX174
- 1/1.2" CMOS
- 159 fps
- USB 3.0 available

Cameras with such parameters allow fixing vector displacement fields with high accuracy.

The laser for this setup must be synchronized with the moment the camera takes the picture. Pulsed laser emitter with parameters — 532nm 1W 1000mW Green Dot Laser (Fig. 4) with a set of lenses is used to create a linear zone of illumination of the liquid layer in the observed section of the hydrodynamic wave tank(Fig. 1— a). A high-power green light laser is the optimal solution for creating PIV systems, since its task is to penetrate into liquid layers up to 1 meter deep and illuminate particles with maximum brightness.

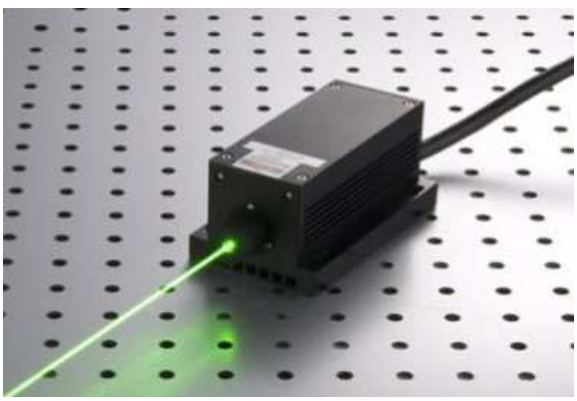

Fig. 4. Green Dot Laser (532 nm, 1000mW)

For the joint operation of the system, software is being developed that allows high-speed recording to an internal or external medium and also synchronizes the laser radiation pulse and the shutter of the camera itself in the area of the experiment.

To synchronize the hardware part of the installation and record video, photo-video data, a modified complex for registration and visualization of laboratory experiments is used (Kurkin and others, 2019). As mentioned earlier, for the post-processing of the obtained visual data of the experiment, a specially developed software package will be used, which is an add-on to the already used software package "visualization and processing of experimental data" (Kurkin and others, 2019). This software package composes of a system for recording video experiments, a synchronizer for controlling the capture of the camera shutter and a laser flash, and post-processing of data. Significant changes have been made to this complex in terms of expanding the GUI (graphical user interface), adding a new module to control the entire installation. The first version of the installation is a patented software package. In the future, after testing the entire complex, it is planned to apply for registration (patenting) of a computer program for controlling and visualizing the data obtained. Now the application is being replenished.

3. Possible applications and future scope

3.1 Particle registration. Digital image correlation method

The technology (method) of digital image correlation is used to register particles and estimate the velocities of vector fields on the final block of video data of the experiments. It is an optical technique used in image identification and tracking techniques for accurate flat and volumetric measurements on an image. The method is often used to estimate such effects as deformation of solids, displacement fields in an optical flow. Digital image correlation and tracking, (DIC / DDIT) has proven itself as a robust method for strain assessment and optical flow rate measurements in experiments using light-emitting or reflective markers in the form of specially applied toner or reflective particles (Sutton and others, 2009).

All conditions are met for the application of this method. The implementation of this method in the software package for registration and visualization of laboratory experiments is supported by the opensource power of the OpenCV library as a powerful tool for image processing using computer vision technologies, based on methods and approaches to image processing, the method for recording the displacement of the secondary fields of incoming particles in the video image is implemented. Since the output data is a video sequence or a set of frames obtained sequentially at a high speed (up to 160 fps), there is a necessary and sufficient amount of input data to accurately estimate the displacement and velocity of particles in a liquid. Among the stages of preparation for the implementation of the method are:

- sample preparation (distribution of markers in the liquid layer)
- setting, aiming and focusing cameras on the sample
- camera calibration
- test execution and image registration
- image correlation
- viewing and automatic data processing

5. Conclusion

This article describes a technique and approach to the first implementation of hardware and software parts of the PIV installation for assessing the displacement rates of particles in a fluid flow both on its surface and inside the fluid layer. The component composition and method of registration, evaluation and visualization of the final data of laboratory experiments carried out on the basis of LMNAD laboratory — Laboratory of Modeling of Natural and Anthropogenic Disasters (Nizhny Novgorod State Technical University na RE Alekseev, Nizhny Novgorod). This system is under development. The software complex for the management of the PIV system and post-processing is under testing. Also, the hardware part is undergoing modernization. Some standard parts were replaced with custom ones, fasteners were modernized using 3D modeling and printing methods. The application of this system will be tested in experiments with two-layer and three-layer fluids being conducted at the laboratory, evaluating the velocity of fluid displacement in experiments on modeling solitons, and fluid displacement in evaluating the internal propagation of a fluid when evaluating wave run-up on various types of coastal geometry. The PIV system will also be useful as the main system for registering the particle velocity, but it is planned to use it in combination with the existing equipment. Set of bottom pressure sensors, liquid columns sensors installed over the entire area of the pool bottom, as well as more than a ten string capacitive and resistive wave height sensors allows you to improve the quality of experiments (Fig. 2). The use of PIV technology for the Laboratory of Modeling of Natural and Anthropogenic Disasters (Nizhny Novgorod State Technical University na RE Alekseev, Nizhny Novgorod) opens up new possibilities in processing digital experimental data and expands the experimental basis itself, which will allow obtaining more detailed and high-quality results.

Acknowledgements

This research was funded by the grant of the President of the Russian Federation for state support of Leading Scientific Schools of the Russian Federation (grant No. NSH-2485.2020.5).

References

Rodin A., Kuzin V., Kurkin A., Likhodeev N., Zemlyanikin A. (2018) Features of the dynamics of long waves of different polarity along the flat slope: laboratory experiments and numerical experiments. *Proceedings of the 33rd International Symposium on Okhotsk Sea & Polar Oceans.* 348-351.

Kurkin A.A., Kuzin V. D. Tyugin D.Yu., Kurkina O.E. (2019) The system of video registration and visualization of the results of laboratory experiments. *Proceedings of the 34th International Symposium on Okhotsk Sea & Polar Oceans.* 287-290.

Sutton M.A., Orteu J.-J., Schreier H.W. (2009) Image Correlation for Shape, Motion and Deformation Measurements. *University of South Carolina,* 364.

Jianyong Huang, Xiaochang Pan, Shanshan Li, Xiaoling Peng, Chunyang Xiong, and Jing Fang (2011) A Digital Volume Correlation Technique for 3-D Deformation Measurements of Soft Gels. *International Journal of Applied Mechanics.* 335-354.

Sheng, J.; Malkiel, E.; Katz, J. (2008). Using digital holographic microscopy for simultaneous measurements of 3D near wall velocity and wall shear stress in a turbulent boundary layer. *Experiments in Fluids*. **45** (6): 1023–1035.

Correspondence to: V. Kuzin, chromium32@mail.ru

Submission Information for OSPOR

Reviewing processes of OSPOR

1) When manuscripts have been received by the Editor-in-Chief, an acknowledgement of receipt will be sent to the author(s) by e-mail. The Editor-in-Chief chooses an editor to handle the manuscript review.
2) The submitted manuscript will be subjected to screening review for its scope, novelty, completeness, English level, and conformation to the OSPOR policy. A manuscript not passing the screening review will immediately be returned to the authors.
3) The editor in charge will select expert reviewers to evaluate the manuscript.
4) As to results of review, if the editor decides that the paper needs revision by the author(s), the manuscript will be returned to the author(s) for revision.
5) Manuscripts returned to author(s) for revision should be resubmitted promptly. If the revision cannot be finished within a month, the manuscript will be regarded as having been withdrawn.
6) The Editor-in-Chief will finally decide whether to accept the manuscript for publication.

Paper Submission

Submission Guideline

All manuscripts should be submitted in digital format (PDF or WORD) with the OSPOR submission sheets (PDF or WORD, offered from OSPOR) by email to the OSPOR Editorial Board

OSPOR Editorial Board

Polar Oceans Research Association (OSPORA)
Address: Kaiyo Koryukan, 1 Kaiyo Koen, Mombetsu, Hokkaido 094-0031
Japan E-mail: momsys(at)okhotsk-mombetsu.jp
Phone: +81-158-26-2810 (0158-26-2810 in Japan)
Fax: +81-158-26-2812 (0158-26-2812 in Japan)

Publication Charge*

Authors of their institutions are requested to pay the publication charge according to the following rate when paper is accepted. The maximum pages are 6 pages.

1,500 Yen / page within the maximum pages
3,000 Yen / page over the maximum pages (Excess charge)

Copyright

Copyright for an article submitted to OSPOR is transferred to OSPORA when the article is published in OSPOR in any form.

Preparation of manuscripts

The manuscript should be formatted in the form of OSPOR template offered from the OSPORA office, which satisfies the following requirements. The maximum pages in printing style are **6 pages**.

1) Text
   a) The manuscript should be in the international size A4 in camera-ready style according to the form of OSPOR template.
   b) The first page should include: the title, the author(s) name(s) and their affiliations. If possible, a Japanese translation of the title and the name(s) of the author(s) should be provided in the end of manuscript. If they are not, the translation will be undertaken by the OSPOR editorial board.
   c) An abstract not exceeding 250 words must be provided.
   d) Up to five keywords that describe the content for indexing purposes must be provided.

2) References

a) A list of cited references should be arranged alphabetically. Journal abbreviations are better to use, but when the abbreviation is not known, the full title of the journal should be used in the list.

In the case of many authors, the author name can be written in short as below.

Kawamura, K., F. Parennin and 16 others (2007): Northern hemisphere forcing of climatic cycles in Antarctica over the past 360,000 years. *Nature*, **448**, 912-916.

b) References in the text will include the name(s) of the author(s), followed by the year of publication in parentheses, *e.g.* (Clark, 2003), (Li and Sturm, 2002), (Harrison and others, 2001).

3) Units

Numerical units should conform to the International System (SI).

Units should be in the form as kg m^{-3} not as kg/m^3.

4) Tables

A title and a short explanation should be located on the top of table.

They should be referred to in the text.

5) Figures

a) All Figures (illustrations and photographs) should be numbered consecutively.

b) All Figures should be of good quality and referred to in the text.

c) Figure captions should be located on the bottom of the Figures.

6) More information

For more information about manuscript instruction, please ask to OSPORA office or see OSPORA home page in http://okhotsk-mombetsu.jp/okhsympo/top-index.html

Recent information*

Resent information can be get from the following URL.

General Information: http://okhotsk-mombetsu.jp/okhsympo/artical-J/Info-artical.html
Instruction: http://okhotsk-mombetsu.jp/okhsympo/artical-J/Instruction-J.html
Template: http://okhotsk-mombetsu.jp/okhsympo/artical-J/Template-J.html
Submission Sheet: http://okhotsk-mombetsu.jp/okhsympo/artical-J/submiss-sheetJ.html

Okhotsk Sea and Polar Oceans Research, Vol. 5 (2021, February)

Published by the Okhotsk Sea and Polar Oceans Research Association (OSPORA),
Mombetsu City, Hokkaido, Japan

Executive Committee of OSPORA:

Chairman: Shuhei Takahashi (Okhotsk Sea Ice Museum of Hokkaido, Director)

Secretariat: Eriko Uematsu

Address: Kaiyo Koryukan, 1 Kaiyo Koen, Mombetsu, Hokkaido 094-0031 Japan E-mail: momsys(at)okhotsk-mombetsu.jp

Phone : +81-158-26-2810 (Japan 0158-26-2810)

Fax: +81-158-26-2812 (Japan 0158-26-2812)

http://okhotsk-mombetsu.jp/okhsympo/top-index.html

Okhotsk Sea and Polar Oceans Research

Published by the Okhotsk Sea and Polar Oceans Research Association (OSPORA)
Mombetsu City, Hokkaido, Japan

Vol. 5